SCUOLA DI DOTTORATO
UNIVERSITÀ DEGLI STUDI DI MILANO-BICOCCA

Department of School of Medicine

PhD program in Neuroscience Cycle XXXII

Curriculum in Clinical Neuroscience

An MRI-based analysis of the longitudinal progression of atrophy in amnestic and non-amnestic phenotypes of Alzheimer's disease

Da Re Fulvio

Registration number: 073768

Tutor: Prof. Carlo Ferrarese

Co-tutor: Dr. Murray Grossman

Coordinator: Prof. Guido Cavaletti

ACADEMIC YEAR 2018/2019

INDEX

Chapter 1

INTRODUCTION

1.1 Background

Worldwide, 50 million people are living with dementia according to the World Alzheimer report 2018 (https://www.alz.co.uk/research/world-report-2018), and Alzheimer's disease (AD) is the most common form of dementia, representing 60-70% of all causes (Boccardi et al., 2017). AD is a neurodegenerative disorder characterized by specific neuropathological alterations, i.e. plaques and neurofibrillary tangles, with the first formed by beta-amyloid and the latter by tau protein. The pathological mechanisms underlying AD are still not clearly understood, especially for what concerns the modality of spreading of AD across the brain; for some authors it could happen in a prion-like manner (the aggregate, once formed, could reach the adjacent cells to induce further aggregation) (Ayers et al., 2018), for others the modality is through direct neuroanatomical connections, i.e. a long-distance transmission along white matter pathways between brain areas (Guo and Lee, 2014).

Recent observations suggest that non-amnestic syndromes with underlying AD (naAD) pathology are more prevalent than previously thought, accounting for about 25 % of all AD cases (Peter et al., 2014; Dickerson et al., 2017). These non-amnestic syndromes are associated with a combination of prominent neocortical disease and relative hippocampal sparing (Galton et al., 2000; Murray et al., 2011; Whitwell et al., 2012; Mesulam et al., 2014a), and this group includes: logopenic-variant primary progressive aphasia (lvPPA), characterized by primary language deficits (Gorno-Tempini et al., 2011); posterior cortical atrophy (PCA), characterized by visuospatial deficits (Crutch et al., 2012, 2017); corticobasal syndrome (CBS), which can present with a constellation of lateralized motor and cognitive deficits (Medaglia et al., 2017); and frontal-variant Alzheimer's disease (fvAD), defined by deficits in executive function and/or social behavior (Dubois et al., 2014). A part from the relative hippocampal sparing, patients with atypical disease distributions may have different rates of clinical progression than typical amnestic Alzheimer's disease (aAD) patients (Duara et al., 2013; Byun et al., 2015; Poulakis et al., 2018). However, relatively little research has examined the

longitudinal anatomical spread of disease in non-amnestic Alzheimer's disease (naAD); what we know is mainly based on between-group comparisons in cross-sectional data, usually considering no more than two variants, thus failing to model the anatomical progression of disease over time with accuracy. Understanding this spread in naAD is critical for interpreting neuroimaging markers in diagnosis, decision-making regarding clinical trial participation, and elucidating the mechanisms by which AD pathology spreads throughout the brain. All these purposes are particularly important within a scientific scenario eager to provide useful data in order to find possible disease-modifying therapies for AD; thus, an analysis of the anatomical patterns of progression over time of different phenotypic groups, which are still sharing the same pathological profile, can be crucial to both a more precise clinical diagnosis and prediction of the longitudinal pogression of these phenotypes, and a deeper understanding of the mechanisms behind spreading of AD, and eventually which molecules or pathways to strike to stop it.

In order to answer these questions, we first created a cross-sectional model which could mimick a longitudinal one, in order to catch the possible sites of atrophy onset of each naAD variant, and its progression. Then we decided to possibly confirm this model with a real longitudinal approach, to investigate the actual spread over time and the possible implications on the connections among the involved areas.

We will start analyzing the general characteristics of AD, thus considering each of the atypical phenotypes. For each variant, a particular regard will be considered for the neuroimaging aspect, especially for MRI.

1.2 Alzheimer's disease

Alzheimer disease (AD) is the most common cause of dementia and one of the leading sources of morbidity and mortality in the aging population.

The hallmark neuropathologic changes of AD are diffuse and neuritic plaques, marked by extracellular amyloid beta deposition, and neurofibrillary tangles, comprised of the intracellular accumulation of hyperphosphorylated tau (p-tau) protein. The epidemiologic study of AD is being transformed by the availability of new biomarker technologies to measure such neuropathologic changes in vivo. Large randomized clinical trials are evaluating anti-amyloid and other disease-based therapies for the treatment and prevention of AD utilizing these imaging or cerebrospinal fluid biomarkers (Gandy et al., 2013).

1.2.1 Pathology

Essential neuropathologic changes of AD include the following:

- Neuritic plaques, associated with neuronal injury and characterized by amyloid formed from amyloid beta plus dystrophic neurites that frequently have phospho-tau immunoreactivity
- Extracellular deposits of amyloid beta peptides
- Neurofibrillary degeneration, best exemplified by neurofibrillary tangles

AD neuropathologic change is ranked along three parameters: amyloid beta plaque distribution score, neurofibrillary tangle distribution stage, and neuritic plaque density score. An overall assessment of low, intermediate, or high levels of AD neuropathologic change is obtained based on these three parameters.

In addition to these essential features, several other pathologic changes are commonly observed in association with AD, like cerebral amyloid angiopathy, inclusions of abnormal alpha-synuclein accumulation (Lewy bodies), vascular brain injury, hippocampal sclerosis (HS) and immunoreactive inclusions of transactive response DNA binding protein 43 kD (TDP-43).

The pathological progression of the typical pathological alterations was described by Braak and Braak (1991), who divided it in 6 stages: two

asymptomatic transentorhinal (stages I-II), two limbic (stages III-IV), with involvement of the entorhinal and hippocampal cortex and the subsequent onset of clinical symtpoms, and eventually two isortical (stages V-VI), with the destruction of all the isocortical association areas.

These protein aggregates are thought to generate neuronal dysfunction, directly or indirectly. The central questions are how transregional spread occurs and what underlies regional vulnerability to amyloid beta and tau pathology. Recent works have implicated cell-to-cell transmission of misfolded proteins as a common mechanism for the onset and spreading of various neurodegenerative disorders. Emerging evidence also suggests the presence of conformationally diverse 'strains' of each type of disease protein, which may be another shared feature of amyloid aggregates, accounting for the heterogeneity within each type of neurodegenerative disease (Guo and Lee, 2014). For other authors, though, clinical and mouse model research suggests both anatomic connectivity and molecular signatures of vulnerable regions, as reflected in regional gene expression profiles, might underlie transregional protein pathology progression; in particular, connectivity-based progression theories posit that spatiotemporal pathology development will follow fiber tracts (Mezias et al., 2017).

More recently, AD pathology is described in vivo through biomarkers, defining the "ATN" system, where A defines the presence of amyloidosis (analyzed through CerebroSpinal Fluid, CSF, or F-18-labelled amyloid imaging PET tracer), T is for phosphorilted Tau protein (pTau dosed in CSF), and N indicates the neudodegeneration (through total Tau protein in CSF or PET with florodesossiglucose (FDG-PET)(Jack et al., 2016)(see next paragraph for details about these proteins).

1.2.2 Pathogenesis

While the pathogenesis of Alzheimer disease (AD) remains unclear, all forms of AD appear to share overproduction and/or decreased clearance of amyloid beta

peptides. Amyloid beta peptides are produced by the endoproteolytic cleavage of mature protein translated from the amyloid precursor protein (*APP*) gene and cleaved by beta-secretase and gamma-secretase. Presenilin forms part of the gamma-secretase complex, and mutations in presenilin 1 (*PSEN1*) or *PSEN2* appear to favor production of amyloid beta overall, or more neurotoxic forms of amyloid beta. The ultimate neurotoxin in AD is debated, but experimental evidence highlights small aggregates of amyloid beta peptides called oligomers.

The pathogenesis of AD also involves a second protein, tau. Tau is a microtubule-associated protein that aids in microtubule assembly and stabilization. In AD, tau becomes hyperphosphorylated and aggregates to form paired helical filament (PHF) tau, a major component of neurofibrillary tangles within the neuronal cytoplasm. The accumulation of this altered protein is toxic to neurons in experimental models. In addition, transmission of pathologic forms of tau between neurons has been proposed to account for the spread of AD in brain, which follows a distinct progression across brain regions as AD advances (Iba et al., 2013; Medina et al., 2014).

There are several other important and potentially overlapping pathways likely involved in AD pathogenesis, many of which have been implicated by the various risk genes that have been identified. As an example, the human apolipoprotein E gene (*APOE*) is a pleiotropic lipoprotein involved in multiple cellular processes including cholesterol transport, development, synaptic plasticity, and immune regulation, among others. There are three alleles of *APOE*, called e2, e3, and e4, and their encoded isoforms also vary in several activities. At least one mechanism by which inheritance of the *APOE* e4 may increase AD risk is by impairing amyloid beta clearance from cerebrum (Castellano et al., 2011).

1.2.3 Epidemiology

AD is increasingly prevalent with advancing age, and the overall burden of AD is substantial worldwide. Worldwide, 47 million people are living with dementia according to the World Alzheimer report 2016, and AD is the most common form of dementia, representing 60-70% of all causes (Boccardi et al., 2017). The age-standardized prevalence of dementia ranges from 5 to 7 percent in most countries (Sosa-Ortiz et al., 2012). The estimated prevalence of dementia in people age 60 years and older ranges from a low of 4.7 percent in central Europe to a high of 8.7 percent in North Africa and the Middle East. Well-conducted studies have documented lower incidence and prevalence in Nigeria (1.4 percent) and rural India (1.1 percent), although rates have increased in Africa and Asia over the last six years. A large study in four areas of China reported that incidence of dementia was similar in China, the United States, and Europe. In the United States, incidence rates are highest in black Americans and lowest in Asian Americans, which could be related to racial differences in APOE4 allele frequencies as well as differences in socioeconomic status and education.

Estimates of the incidence of dementia vary across studies and depend heavily on age. In general, the incidence of dementia doubles every 10 years after age 60 years. There is very little sex difference in incidence and prevalence of dementia or AD, although by absolute numbers there are more women than men with the disease, particularly over the age of 85 years, due to differences in life expectancy.

1.2.4 Genetic Risk Factors

Aside from age, the most clearly established risk factors for Alzheimer disease (AD) are a family history of dementia, rare dominantly-inherited mutations in genes that impact amyloid in the brain, and the apolipoprotein E (*APOE*) epsilon 4 (e4) allele.

Early-onset Alzheimer disease — AD is highly heritable, even in so-called sporadic cases. The genetic basis for AD is understood most clearly in the early-onset form, which accounts for less than one percent of cases. Early-onset AD (onset of symptoms before 65 years of age) follows an autosomal dominant inheritance pattern related to mutations in genes that alter amyloid beta protein production, aggregation, or clearance, including amyloid precursor protein (*APP*), presenilin-1, and presenilin-2. Such mutations are highly penetrant, meaning that carriers have a nearly 100 percent chance of developing the disease in their lifetime.

Other early-onset cases without mutations can present clinically prior to 65 years of age. While a percentage of them have higher proportions of *APOE* e4, not all do, and this early-onset group is not fully understood.

Late-onset Alzheimer disease — The genetic basis of late-onset AD is more complex, with susceptibility likely conferred by a variety of more common but less penetrant genetic factors interacting with environmental and epigenetic influences. The most firmly established genetic risk factor for late-onset AD is *APOE*; carriers of one e4 allele are at two- to three-fold increased odds of developing AD compared with non-carriers, and those with two e4 alleles are at approximately 8- to 12-fold increased odds. The strength of the association may be modified by several factors, including gender, race, and vascular risk factors.

Family history — Family history of dementia is a risk factor for the development of AD; patients with a first-degree relative with dementia have a 10 to 30 percent increased risk of developing the disorder. Individuals in families with two or more affected siblings with late-onset AD have a threefold increased risk of AD compared with the general population.

1.2.5 Acquired Risk Factors

A variety of polygenic or acquired factors may influence Alzheimer disease (AD) risk, including hypertension, lipoproteins, cerebrovascular disease, altered glucose metabolism, and brain trauma. Many of these risk factors appear to be most relevant when they are present in midlife. In one study, individuals with two or more vascular risk factors in midlife had nearly threefold higher odds of brain amyloid deposition in late life as measured by amyloid positron emission tomography (PET) (Gottesman et al., 2017).

1.2.6 Clinical Features

Age of onset — AD is characteristically a disease of older age (Braak & Braak, 1997). Early-onset AD is unusual, and many of these patients present for evaluation due to occupation-related difficulties. Many of these patients have no clear familial pattern and thus would be considered sporadic, although some exhibit familial clustering. There are rare inherited forms of AD that routinely present before 65 years of age, and frequently in the fifth decade or earlier. These account for less than one percent of all cases of AD.

Cardinal symptoms — Memory impairment is the most common initial symptom of AD dementia. In patients with the typical form of the illness, deficits in other cognitive domains may appear with or after the development of memory impairment. Executive dysfunction and visuospatial impairment are often present relatively early, while deficits in language and behavioral symptoms often manifest later in the disease course. These deficits develop and progress insidiously. Less commonly, language deficits, visuospatial abnormalities, or even executive functions may be impaired as the most prominent initial symptom (McKhann et al., 2011).

Memory impairment — Even when not the primary complaint, memory deficits can be elicited in most patients with AD at the time of presentation.

The pattern of memory impairment in AD is distinctive (Markowitsch et al., 2012). Declarative episodic memory – memory of events occurring at a particular time and place – is usually profoundly affected in AD. This type of memory depends heavily on the hippocampus and other medial temporal lobe structures. In contrast, subcortical systems supporting procedural memory and motor learning are relatively spared until quite late in the disease. Memory for facts such as vocabulary and concepts (semantic memory) often becomes impaired somewhat later. Semantic memory is supported by neocortical temporal regions, particularly in the anterior temporal lobe.

Within episodic memory, there is a distinction between immediate recall (eg, mental rehearsal of a phone number), memory for recent events (which comes into play once material that has departed from consciousness must be recalled), and memory of more distant events (remote memory). Memory for recent events, served by the hippocampus, entorhinal cortex, and related structures in the medial temporal lobe, is prominently impaired in early AD. In contrast, immediate memory (encoded in the sensory association and prefrontal cortices) is spared early on, as are memories that are consolidated for long periods of time (years), which can be recalled without hippocampal function.

The early memory deficit in AD is most precisely described as anterograde long-term episodic amnesia. Long-term memory can encompass time frames from less than a minute to years, but because the absolute time interval over which long-term memory can fail may actually be short (eg, inability to recall a few words after a couple minutes of distraction), patients and caregivers typically describe "short-term memory" problems.

Memory deficits develop insidiously and progress slowly over time, evolving to include deficits of semantic memory and immediate recall. Impairments of procedural memory appear only in late stages of AD.

Executive function and judgement/problem solving — In early stages of AD, impairment in executive function may range from subtle to prominent (Stokholm

et al., 2006). Family members and coworkers may find the patient less organized or less motivated; multitasking is often particularly compromised. In addition to poor insight, reduced ability for abstract reasoning may be elicited. As the disease progresses, an inability to complete tasks typically emerges.

Reduced insight into deficits (anosognosia) is a common, but variable feature of AD. It is common for patients to underestimate their deficits and offer alibis or explanations for them when they are pointed out. Interviewing an informant who has known the patient over time (usually a family member) is necessary; often it is the family member, not the patient, who brings the complaint of cognitive impairment to medical attention.

Behavioral and psychological symptoms — Neuropsychiatric symptoms are common in AD, particularly in the middle and late course of disease. These can begin with relatively subtle symptoms including apathy, social disengagement, and irritability. Apathy can be difficult to distinguish from depression, which can be difficult to diagnose in the setting of dementia, and the differences should be sought diligently because of treatment implications. In some cases empirical treatment of presumed depression is a reasonable management decision.

Other signs and symptoms

Apraxia — Dyspraxia, or difficulty performing learned motor tasks, usually occurs later in the disease after deficits in memory and language are apparent.

Olfactory dysfunction — Changes in olfactory function are common in patients with AD and have been explored as a diagnostic tool.

Sleep disturbances — Sleep disturbances are common in patients with AD (Ju et al., 2014).

Seizures — Seizures occur in 10 to 20 percent of patients with AD, usually in the later stages of disease.

Motor signs — In the early stages, patients with AD generally have a normal neurologic examination except for the cognitive examination. While pyramidal

and extrapyramidal motor signs, myoclonus, and seizures do occur in patients with AD, these are typically late-stage findings. If these are clinically apparent in early to middle stages, an alternative diagnosis should be considered (McKhann et al., 1984). Myoclonus may emerge in some patients with AD, typically those with more rapid than usual decline. Similarly, primitive reflexes (grasp, snout reflexes, gegenhalten) and incontinence are late, rather than early, features of AD.

CLINICAL COURSE — AD progresses inexorably. The progress of the disease can be measured with mental status scales such as the Mini-Mental State Examination (MMSE), the Montreal Cognitive Assessment (MoCA), and the Clinical Dementia Rating Scale. An older age of onset of AD (>80 years) may be associated with a slower rate of decline compared with younger patients (Bernick et al., 2012). The average life expectancy after a diagnosis of AD ranges from three to eight years and depends in part on how impaired the person is at the time of diagnosis. Survival also relates to age at onset of symptoms. Patients generally succumb to terminal-stage complications that relate to advanced debilitation, such as dehydration, malnutrition, and infection.

1.2.7 Evaluation

Clinical assessment — A detailed clinical assessment provides reasonable diagnostic accuracy for AD in the majority of patients, although sensitivity and specificity, in particular, are limited (McKhann et al., 2011). That said, misdiagnosis is almost always another neurodegenerative or non-reversible cause. The clinical criteria for AD are based on a history of insidious onset and progressive course, exclusion of other etiologies, and documentation of cognitive impairments in one or more domains. A detailed cognitive and general neurologic examination is paramount.

Many clinicians make use of standardized mental status scales to document the presence and progression of dementia, like the Montreal Cognitive Assessment (MoCA), and the Mini-mental state examination (MMSE).

Role of neuropsychological testing — Formal neuropsychological assessment can be helpful in the evaluation of individuals with cognitive impairment and dementia. Cognitive testing under standardized conditions using demographically appropriate norms is more sensitive to the presence of impairments, especially impairments of executive function. Neuropsychological assessment can be useful in a variety of settings:

- To establish a baseline in order to follow the patient over time.
- To help differentiate among different forms of neurodegenerative dementias or between a neurodegenerative dementia and other etiologies of cognitive impairment, such as cerebrovascular disease or depression.
- To assess competencies and guide recommendations pertaining to driving, financial decisions, and need for increasing supervision.

1.2.8 Neuroimaging

Brain imaging, preferably with magnetic resonance imaging (MRI), is indicated in the evaluation of patients with suspected AD. Brain MRI can document potential alternative or additional diagnoses including cerebrovascular disease, other structural diseases (chronic subdural hematoma, cerebral neoplasm, normal pressure hydrocephalus), and regional brain atrophy suggesting frontotemporal dementia or other types of neurodegenerative disease.

Structural MRI findings in AD include both generalized and focal atrophy, as well as white matter lesions. The most characteristic focal finding in AD is reduced hippocampal volume or medial temporal lobe atrophy (Whitwell et al., 2012).

Diagnosing incipient Alzheimer disease — The key role of imaging in AD diagnosis is highlighted by the inclusion of imaging markers in proposed new criteria for earlier diagnosis of AD. These criteria build on traditional National Institute of Neurological and Communicative Disorders and Stroke–Alzheimer's Disease and Related Disorders Association criteria by keeping the requirement for objective memory deficits but removing the requirement that disability (dementia) must already be present. Instead, at least one of the following three markers is required: medial temporal atrophy, temporoparietal hypometabolism, and abnormal neuronal CSF markers (tau and/or Aβ). These criteria imply that structural imaging and other markers can reliably detect AD before dementia occurs; that is, at an MCI (Mild Cognitive Impairment) stage (see also "Diagnosis" chapter). Of all the MRI markers of AD, hippocampal atrophy assessed on high-resolution T1-weighted MRI is the best established and validated (Frisoni et al., 2010). The simplest way to assess atrophy of the medial temporal lobes is by visual inspection of coronal T1-weighted MRI. Several rating scales to quantify the degree of atrophy have been developed and are widely used. Visual rating scales provide ≈80–85% sensitivity and specificity to distinguish patients with AD from those with no cognitive impairment, and only slightly lower sensitivity and specificity levels for diagnosing amnestic MCI. These scales also have good predictive power to anticipate decline in MCI. Visual rating also correlates well with underlying pathology and has high diagnostic accuracy against a pathologically verified diagnosis of AD. Despite its convoluted structure, the boundaries of the hippocampus (and adjacent CSF spaces) are easier for human operators or automated algorithms to recognize than the amygdala, entorhinal cortex or parahippocampal gyrus. This is because the anatomical boundaries of the hippocampus are distinct on high-resolution T1-weighted MRI scans around most of the surface of this structure. Hippocampal volume measured in vivo by MRI correlates with Braak stage and neuronal counts (Bobinski et al., 2000). At the mild dementia stage of AD, hippocampal volume is already reduced by 15–30% relative to controls, and in

the amnestic variant of MCI the volume is reduced by 10–15%. A recent meta-analysis estimated that medial temporal atrophy has ≈73% sensitivity and ≈81% specificity for predicting whether patients with amnestic MCI will convert to dementia (Yuan et al., 2009). If medial temporal atrophy is measured with a continuous metric such as hippocampal volume, specificity might be increased, but at the cost of reduced sensitivity. If hippocampal atrophy is used as an inclusion criterion for clinical trials in MCI, a trade-off ensues between a relatively low proportion of screened negatives with a more-contaminated sample of screened positives and a higher proportion of screened negatives but a 'cleaner' group to treat and follow. Indeed, contamination of MCI groups with non-Alzheimer cases might in part explain the failure of some trials with cholinesterase inhibitors in patients with MCI. Enrichment of MCI groups with true AD cases in clinical trials of drugs aiming to delay the development of dementia might lead to a significant increase in study power. Despite the evidence reported above, medial temporal atrophy is not sufficiently accurate on its own to serve as an absolute diagnostic criterion for the clinical diagnosis of AD at the MCI stage. High specificity is required to minimize a false-positive diagnosis of AD, and medial temporal atrophy by itself lacks the specificity to confidently exclude other dementias. To enhance the accuracy of structural markers, other structural and nonstructural measures can be added in an algorithmic formula to diagnose AD. Studies that included pathological confirmation of the diagnosis have shown that parietal atrophy combined with medial temporal lobe atrophy on MRI carries positive predictive value for diagnosing AD. Moreover, in 59 patients with amnestic MCI, 33 of whom converted to dementia in 19 months on average, those with both medial temporal atrophy (as rated visually) and abnormal CSF biomarkers had a fourfold higher risk of progression to dementia than patients with either abnormality alone. Prediction of dementia was almost perfect (94% positive predictive value), but replication is still needed (Bouwmann et al., 2007). CSF and MRI measures provided better prediction than either measure alone, although MRI measures

were more accurate in a head-to-head comparison (Vemuri et al., 2009). Other atrophy markers have been suggested for early diagnosis of AD or to enrich MCI trials, but their validity and added value for predicting decline remains to be confirmed. These markers include analysis of whole-brain patterns of atrophy through use of support vector machines, the AD-specific structural abnormality index (STAND) score, patterns of hippocampal subfield atrophy structural changes in cholinergic nuclei of the basal forebrain, deformation-based morphometry of the gray and white matter, and measures of the lateral temporal and parietal cortex (Frisoni et al., 2010).

Atrophy as a neurodegeneration marker —MRI-based measures of atrophy are regarded as valid markers of disease state and progression for several reasons. Atrophy seems to be an inevitable, inexorably progressive concomitant of neurodegeneration. The topography of brain tissue loss correlates well with cognitive deficits, both cross-sectionally and longitudinally. Structural brain changes map accurately upstream to Braak stages (1990, 1991, 1995) of neurofibrillary tangle deposition and downstream to neuropsychological deficits. The earliest sites of tau deposition and MRI-based atrophic changes typically lie along the perforant (polysynaptic) hippocampal pathway (entorhinal cortex, hippocampus and posterior cingulate cortex), consistent with early memory deficits. Later, atrophy in temporal, parietal and frontal neocortices is associated with neuronal loss, as well as language, praxic, visuospatial and behavioral impairments. Rates of change in several structural measures, including whole-brain, entorhinal cortex, hippocampus and temporal lobe volumes, as well as ventricular enlargement, correlate closely with changes in cognitive performance, supporting their validity as markers of disease progression (Frisoni et al., 2010). The appropriate use of an atrophy marker in the clinic requires that its dynamics are known at the different stages of the disease, and that its relationship with the dynamics of other imaging and biological markers is understood. Atrophy measures change with disease progression over a wide range of AD disease severity. From MCI to well into the moderate dementia stage of AD, structural

markers are more sensitive to change than are markers of Aβ deposition (as assessed through imaging or cerebrospinal fluid [CSF] analysis). In the asymptomatic to MCI stages, however, indirect evidence indicates that amyloid markers show more-substantial abnormalities than do structural markers. Macrostructural loss (atrophy) is accompanied by microstructural (dendritic, myelin and axonal) loss and metabolite changes, all of which are measurable with other magnetic resonance-based sequences. Magnetic resonance spectroscopy, diffusion-weighted imaging (DWI), fiber tracking, and magnetization transfer imaging are all either sensitive to early change or can add complementary information to atrophy measures. Different measurements from a particular variant of the DWI, called Diffusion Tensor Imaging (DTI), help to understand the white matter disease (WMD) related to grey matter atrophy; in particular, fractional anisotropy (FA) and mean diffusivity (MD) showed alterations in the white matter close to the MTL structures (Johnson et al., 2010); these data are informative, although less precise predictors of and other MRI-based techniques, such as tissue perfusion with arterial spin labeling or functional measures of resting-state networks (particularly the default mode network), show promise as diagnostic markers, but have not yet been subjected to thorough validation. None of these techniques yet has an established role in clinical practice (Frisoni et al., 2010).

Other techniques — Functional brain imaging with [18F] FDG-PET, functional MRI (fMRI), perfusion MRI, or SPECT reveals distinct regions of low metabolism (PET) and hypoperfusion (SPECT, fMRI) in AD. These areas include the hippocampus, the precuneus (mesial parietal lobes), the lateral parietal and posterior temporal cortex. In practice, FDG-PET may be most useful in distinguishing AD from frontotemporal dementia in patients with atypical presentations (Rabinovici et al., 2011).

Amyloid PET tracers (F18-florbetapir, F18-flutemetamol, F18-florbetaben) that measure amyloid lesion burden in the brain have been developed as tools to aid in the diagnosis of AD in vivo, aid in prognosis, speed development of anti-

amyloid drugs, and differentiate AD from other causes of dementia. These tracers have been approved by regulatory agencies in the United States and elsewhere as qualitative assessments of beta-amyloid (Aβ) plaque density; such tracers are not intended for use as a diagnostic agent. Since there are issues with how much ligand binding to plaques constitutes a "positive" scan, the U.S. Food and Drug Administration (FDA) approval specifies that an amyloid PET scan that is negative decreases the likelihood that a patient with dementia has AD. In a symptomatic dementia patient, a positive scan indicates that the person has AD pathology, but it is important to keep in mind that such a finding does not rule out a co-existing pathology. More recently, F18 Tau PET tracers (flortaucipir, THK5317, and PBB3) also appeared in the scientific scenario, helping to further understand the role of this protein in AD.

1.2.9 Diagnosis

Definitive diagnosis of AD requires histopathologic examination, which is rarely done in life (Braak & Braak, 1991). The diagnosis of AD in practice depends on the clinical criteria outlined below. AD should be suspected in any older adult with insidious onset, progressive decline in memory and at least one other cognitive domain leading to impaired functioning. The role of laboratory and imaging investigations is mainly to exclude other diagnoses. Neuropsychological testing may provide confirmatory information and aid in patient management. Biomarker data can be supportive of a diagnosis of AD and is most useful in patients with atypical clinical presentations or early-onset disease.

Alzheimer disease dementia — Criteria for the diagnosis of probable AD dementia have been established by the National Institute on Aging and the Alzheimer's Association (NIA-AA) and most recently updated in 2011 (McKann et al., 2011). Probable AD dementia is a syndrome of dementia defined by the following characteristics:

- Interference with ability to function at work or at usual activities
- A decline from a previous level of functioning and performing
- Not explained by delirium or major psychiatric disorder
- Cognitive impairment established by history-taking from the patient *and* a knowledgeable informant; and objective bedside mental status examination or neuropsychological testing
- Cognitive impairment involving a minimum of two of the following domains:
    - impaired ability to acquire and remember new information
    - impaired reasoning and handing of complex tasks, poor judgment
    - impaired visuospatial abilities
    - impaired language functions
    - changes in personality, behavior or comportment

Other core clinical criteria include:

- Insidious onset
- Clear-cut history of worsening
- Initial and most prominent cognitive deficits are one of the following:
    - Amnestic presentation (ie, impairment in learning and recall of recently learned information)
    - Nonamnestic presentations include either a language presentation, with prominent word-finding deficits; a visuospatial presentation, with visual cognitive deficits; or a dysexecutive presentation, with prominent impairment of reasoning, judgment and/or problem solving
- No evidence of substantial concomitant cerebrovascular disease, core features of dementia with Lewy bodies, prominent features of behavioral variant frontotemporal dementia or prominent features of semantic or nonfluent/agrammatic variants of primary progressive aphasia, or evidence of another concurrent, active neurologic or non-neurologic disease or use of medication that could have a substantial effect on cognition.

Possible AD includes either of the following clinical scenarios:

- Atypical course – The core clinical criteria above are met in terms of the nature of the cognitive deficits, but there is either a sudden onset of cognitive impairment or insufficient historical detail or objective documentation of progressive decline.
- Etiologically mixed presentation – All of the core clinical criterial for AD dementia are met but the individual also has evidence of concomitant cerebrovascular disease, features of dementia with Lewy bodies other than the dementia itself, or evidence for another neurologic or medical comorbidity or medication that could have a substantial effect on cognition.

The Diagnostic and Statistical Manual of Mental Disorders (DSM) criteria for AD are also commonly used. Criteria for AD were revised in 2013. The DSM-5 definition of probable AD (now called major neurocognitive disorder due to AD) differs from prior versions in that the cognitive domains have been renamed and expanded to include learning and memory, language, executive function, complex attention, perceptual-motor, and social cognition. Previously, the criteria recognized five domains (memory, aphasia, apraxia, agnosia, and executive function). Like prior versions, the criteria continue to require both memory impairment and evidence of decline in at least one other cognitive domain. New to the criteria is the recognition of genetic testing results, if known, as supportive of a diagnosis of probable AD.

MCI due to Alzheimer disease — Amnestic mild cognitive impairment (MCI) refers to a state of circumscribed anterograde long-term memory impairment with preserved general cognitive and social functioning. Amnestic MCI frequently represents an early stage of AD, with a conversion rate to dementia at about 10 to 15 percent per year (Petersen et al., 1999). Non-amnestic MCI, in

which cognitive domains outside of memory are affected, is less frequently associated with prodromal AD, but may be in a significant minority of patients.
MCI may occur as a prodrome to several neurodegenerative dementias, as well as non-neurodegenerative conditions (eg, depression, medicine effects). Therefore, the specific designation of MCI due to AD is used when a biomarker associated with AD (eg, CSF testing of Aβ, tau, phospo-tau), amyloid imaging, *APOE* genotype, or functional scan consistent with AD is present in the affected subject. Using the NIA-AA criteria on a cohort of research subjects with MCI, individuals with cognitive impairment and both amyloid and neuronal injury biomarkers had an approximately 60 percent conversion rate to AD dementia over three years (Vos et al., 2015).

Preclinical Alzheimer disease — Preclinical AD refers to the stage of AD in which the molecular pathology of AD is already present in the brain but is not yet clinically expressed. Individuals are by definition asymptomatic and cognitively normal. Preclinical AD is defined by biomarker or genetic data and is primarily only recommended for use in research, in the context of clinical trials for early intervention strategies and the longitudinal study of people at risk. According to the IWG, preclinical AD encompasses two groups (Morris et al., 2014):

- Asymptomatic at risk for AD refers to cognitively normal individuals with evidence of AD molecular pathology by laboratory or imaging biomarkers. It is not currently known whether progression to symptomatic AD is inevitable in such individuals. Autopsy data revealing that people may die with normal cognition and pathological changes of AD sufficient to make a diagnosis suggest that symptomatic AD will not occur in every subject with amyloid in the brain.

- Presymptomatic AD also refers to cognitively normal and asymptomatic carriers of a dominantly inherited gene mutation that causes AD. Symptoms

of AD will almost certainly develop in these individuals over a normal lifespan.

Differential Diagnosis — The most common disorders considered in the differential diagnosis of AD are vascular dementia and other neurodegenerative dementias. The two most common neurodegenerative dementias after AD are dementia with Lewy bodies (DLB) and frontotemporal dementia (FTD).

- Vascular dementia is caused by either ischemic or hemorrhagic strokes. The most common form is due to small vessel cerebrovascular disease. Diagnosis is most specific if there is a stroke-like course of illness, neurologic signs of stroke on examination, and imaging evidence of stroke. However, the course of illness may appear smoothly progressive, and there may be no elementary neurologic signs.
- Dementia with Lewy bodies (DLB) may be the second most common type of degenerative dementia after AD. Clinical features that help distinguish this from AD include prominent early appearance of visual hallucinations, along with parkinsonism, cognitive fluctuations, dysautonomia, sleep disorders, and neuroleptic sensitivity.
- Frontotemporal dementia (FTD) is a neuropathologically and clinically heterogeneous disorder characterized by focal degeneration of the frontal and/or temporal lobes. Early alteration of personality, behavior, and executive functioning distinguish behavioral variant FTD from AD, however, it can be difficult to distinguish FTD from AD as a cause of primary progressive aphasia, especially early in the course. In addition, Alzheimer pathology is often found in patients with the logopenic variant of primary progressive aphasia.

Role of biomarkers — There are several widely investigated biomarkers for the molecular and degenerative process of AD that can be supportive of a diagnosis of AD but are not yet recommended for routine diagnostic purposes (McKhann

et al., 2011). Such testing can add incremental confidence to a clinical diagnosis of AD, however, and can be useful in certain circumstances, including early-onset dementia and atypical presentations of AD in which the differential diagnosis includes other non-amyloid neurodegenerative diseases such as frontotemporal dementia.

Molecular biomarkers of Aβ protein deposition include:

- Low cerebrospinal fluid (CSF) Aβ42 (or Aβ42:Aβ40 ratio)
- Positive amyloid PET imaging using one of the amyloid PET tracers

Biomarkers of tau deposition (a key component of neurofibrillary tangles) include:

- Increased CSF total tau and phospho-tau
- Evidence of cerebral tau using a tau-specific PET tracer

In general, the topographic biomarkers are less specific than the molecular biomarkers but correlate better with the emergence of clinical symptoms. None of these tests is valid as a stand-alone diagnostic test, but research criteria have incorporated both molecular and topographic biomarker data into the research definitions of both symptomatic and presymptomatic forms of AD, anticipating that once biomarkers become more standardized they will be incorporated into clinical diagnostic algorithms for Ad, possibly extending the current panel to other biomarkers, such as synaptic protein neurogranin in CSF or neurofilament or plasmatic tau and neurofilament light proteins (Blennow et al., 2018; Morris et al., 2014). At present, the use of biomarkers is limited primarily to investigational studies and clinical trials, and testing is not universally available or reimbursed by most insurers.

Other laboratory testing — Routine laboratory tests are not useful in the positive diagnosis of Alzheimer disease; however, some laboratory tests are indicated to

exclude contributing secondary causes. Recommended tests include screening for hypothyroidism and vitamin B12 deficiency (Knopman et al., 2001). Testing for infectious diseases (eg, syphilis, human immunodeficiency virus) should be obtained in the appropriate clinical circumstances.

Genetic testing — Genetic testing is not recommended in the routine evaluation of patients with AD. *APOE* genotyping adds marginally to the predictive value of clinical criteria for AD and may stratify risk of conversion of amnesic MCI to AD, but both false positives and negatives occur.

Genetic testing for amyloid precursor protein (*APP*), presenilin-1 (*PSEN1*) and presenilin-2 (*PSEN2*) mutations is commercially available, but should be reserved for cases in which presenile dementia occurs in the setting of a family history positive for an autosomal dominant distribution of early onset cases.

1.2.10 Treatment

Approved Pharmacological Treatment: Cholinesterease Inhibitors — There are 3 ChEIs available on the market: donepezil, rivastigmine, and galantamine. Use of these agents is based on studies showing that people with AD have defcits in ACh production leading to cortical cholinergic dysfunction (Whitehouse et al., 1982). Cholinesterase, which exists in 2 forms, BuChE and AChE, degrades ACh in the synaptic cleft. ChEIs act by inhibiting this action and optimize the levels of ACh available for postsynaptic stimulation. ChEIs improve symptoms of AD, but they do not alter its natural clinical course. Hence they are considered symptomatic treatments for AD (Bentley et al., 2009). Most common side effects are dose-dependent and generally include nausea, vomiting, diarrhea, muscle cramps, dizziness, fatigue, and anorexia.

Approved Pharmacological Treatment: Memantine — Memantine is an NMDA noncompetitive glutamate receptor antagonist Its use in AD is based on studies

showing that glutamate-related excitotoxicity is involved in the pathophysiology of the disease. A Cochrane review of memantine showed statistically signifcant treatment benefts at 24 weeks on measures of cognition, function, and global measures in pooled analyses of the 3 RCTs in moderate-to-severe AD (McShane et al., 2006). Analyses of the 3 unpublished trials in mild-to-moderate AD showed statistically signifcant treatment benefts on measures of cognition only. One study in moderate-to-severe AD showed that combining memantine to a stable dose of donepezil led to statistically signifcant additional benefts on several measures of cognition, function (Alzheimer's Disease Cooperative Study—Activities of Daily Living), and global assessment CIBIC. Memantine is usually well tolerated. Dose-limiting side effects are rare and they consist of dizziness, headache, somnolence, and confusion. Memantine is approved for the treatment of moderate-to-severe AD.

Emerging Pharmacological Treatment— Ever since Selkoe's proposal of the amyloid hypothesis 20 years ago (Selkoe 1991), and as a result of our growing understanding of the multiple genes and proteins involved in the complex pathogenesis of AD, most pharmaceuticals in the development pipeline are created to act on individual protein targets in the hope of slowing or halting disease progression (and thus are potentially disease-modifying).

Amyloid-Based Therapies. The amyloid cascade hypothesis suggests that the accumulation of Aβ is the initial trigger to the AD pathophysiological process, and that all downstream events, potentially as, or possibly even more, devastating to neuronal integrity are simply consequential. Preventing the production, increasing or promoting the removal, and reducing the effective putative toxicity of Aβ are obvious goals.

Reducing Aβ Production - β-Secretase and BACE1. β-secretase cleaves both sAPPa and, completing the amyloidogenic pathway, sAPPb. It is also involved in numerous other processes, including the notch-signalling pathway critical to cell

differentiation. Numerous candidate drugs were in various trial phases (Henley et al., 2009), but none of them showed significance results (in fact, Eli Lilly stopped the development of their inhibitor semagacestat after completing 2 phase III trials). Shifting of APP processing away from the amyloidogenic β-secretase (also called the β-site APP-cleaving enzyme 1 or BACE1) toward the nonamyloidogenic α-secretase pathway can be achieved by blocking BACE1. Inhibiting this enzyme directly may be problematic because it also cleaves numerous other substrates, including one involved in myelination, but an early candidate has completed a phase I trial (Tang 2009). Although some RCTs of these drugs in AD are still ongoing, up to now none showed positive effects (Panza et al., 2018).

α-Secretase. Shunting of APP toward nonamyloidogenesis could be achieved by stimulating a-secretase. Through a myriad of complex mechanisms, numerous agents appear to do just that, but their role in the treatment of AD is not established. No candidates, including exebryl-1, showed any positive effect up to now.

Preventing Aβ Accumulation and Promoting Clearance. Regardless of any remaining controversy concerning which of the Aβ species is most responsible for its ascribed neurotoxicity, removal of all of its forms is a legitimate objective. Numerous agents able to prevent its selfassociation and downstream aggregation or even promote disaggregation were investigated, although with no satisfying results (Nalinaeva et al., 2019).

Promoting Clearance. Approaches to enhancing clearance include both passive and active immunization. Passive immunization includes monoclonal humanized antibodies (ending with the suffx -zumab). Several candidates have been engineered in recent years, and three of them in particular are under investigation for promising results: BAN 2401 (Logovinsky et al., 2016), Aducanumab (Sevigny et al., 2016), and Gantenerumab (Ostrowitzki et al., 2017).

As for active immunization, the phase I study involving AN172 (the first vaccine used in humans) had to be prematurely terminated because of the development of aseptic meningitis in 18 patients (of 300, or 6%) (Gilman et al., 2005). This aggressive autoimmunity was attributed in part to the sensitization of cytotoxic T-cells. One patient who died of the encephalitis showed signifcant clearing of Aβ plaques; research of possible vaccines lowered down after this discouraging trial.

*Nonamyloid Strategies***.** The most salient neuropathological features present in brains of patients with AD are Aβ plaques and, as the amyloid cascade hypothesis would have it, secondary hyperphosphorylated tau-based NFTs. Other downstream fndings include inflammation, oxidative stress, and excitotoxicity. Irrespective of the validity of the hypothesis or the actual sequence of events, any implicated process amenable to pharmacological modulation represents a viable target.

Tau-Targeted Therapies. At the beginning, potential anti-tau therapies were mainly focused on inhibition of kinases or tau aggregation, or on stabilization of microtubules, but none of these approaches showed significance positive effect (some showed even toxicity). As for now, most of tau-targeting therapies in clinical trials are immunotherapies, which have shown promise in numerous preclinical studies; an exeption is represented by Leuco-methylthioninium bis(hydromethanesulfonate)(LMTM), a derivative of methylene blue, which is currently undrr investigation in phase 2/3 RCT. It is known that tau pathology correlates better with cognitive deficits rather than Aβ lesions, thus targeting of tau could be more effective than Aβ clearance, especially once the clinical symptoms are evident.

Other Downstream Processes to Target. More generalized targets, such as inflammation, oxidative stress (most often impacting mitochondria), and

excitotoxicity, are also being actively explored, but no convincing benefts have been demonstrated, including mithocondrial stabilization (Massoud et al., 2011).

1.3 Atypical variants

1.3.1 Logopenic variant Primary Progressive Aphasia

The logopenic variant (lvPPA) represents the most recently identified of the variants of primary progressive aphasia (PPA). The disorder is characterized by a unique language profile, caused by damage to specific anatomical areas, which in turn might have different probabilities of being associated with specific pathological or genetic processes. There is a growing body of research dedicated to clarifying the cognitive-linguistic, anatomical and pathological features of the logopenic variant.

PPA classification and the emergence of a third variant — PPA is characterized as a slowly progressing, relatively isolated impairment of language, which results from neurodegenerative disease (Mesulam 2001). The disorder was first described in detail in the modern literature by Mesulam and since that time has been the subject of a great deal of research aimed at clarifying its clinical phenotypes and neural and pathological bases. Whereas early reports often described PPA syndromes as being akin to aphasias resulting from stroke (e.g., Broca's and Wernicke's aphasia), it was soon recognized that the clinical presentation in PPA was both heterogeneous and distinct from vascular aphasias. Soon thereafter, efforts were made to classify PPA into clinical subtypes or variants. For more than twenty years, PPA patients were grouped broadly into two major types: nonfluent and fluent PPA. It became clear, however, that this binary classification scheme did not capture all patients adequately and a third variant was occasionally mentioned in the literature (Grossman et al., 2004). Subsequently, Gorno-Tempini et al. (Gorno-Tempini et al., 2004) described this

third clinical variant, now referred to as the logopenic variant, in detail. Since that time, it has been confirmed as a distinct clinical phenotype with unique speech and language features. Because this clinical syndrome may be associated with specific pathological and genetic markers, identification and clarification of the features of the logopenic variant may have important ramifications for therapeutic intervention.

Cognitive-linguistic features of the logopenic variant — Clinical presentation in the logopenic variant is distinct from other PPA subtypes. Recent work has identified spared and impaired cognitive and linguistic processes as well as associated behavioral characteristics.

Speech-language profile. The initial characterizations of a "logopenic" (from Greek, meaning "lack of words") presentation of PPA described an overall paucity of verbal output, with relative sparing of grammar, phonology, and motor speech. This characterization has been refined and modified in subsequent studies (Gorno-Tempini et al., 2008). Work by Gorno-Tempini and colleagues identified in the logopenic variant a fluency profile intermediate between those of patients with the semantic and nonfluent variants of PPA. Spoken language was slow in rate, with syntactically simple but accurate utterances and frequent word-finding pauses. Naming was impaired, but single-word comprehension and nonverbal semantic association were relatively spared. Patients had difficulty with comprehension and repetition of sentences, findings which have been interpreted as evidence of phonological working memory impairment. With regard to written language processing, individuals with logopenic variant have demonstrated a reading pattern conistent with phonological alexia (selective deficit in pseudoword reading). Spelling impairment has also been noted, but the precise nature of spelling deficits awaits clarification. Distinguishing the logopenic variant from the other two major PPA variants has proven challenging, and individuals with this syndrome have likely been grouped with either nonfluent or semantic variant patients in a number of early research reports.

Recent work by Wilson and colleagues (Wilson et al., 2010), however, indicates that several key characteristics of logopenic patients' spontaneous speech can be helpful in differentiating these patients from other PPA syndromes. Based on a speech sample, logopenic patients can be distinguished from nonfluent patients by a lack of speech sound distortions (although phonological paraphasias may be present) and frank syntactic errors. In addition, the maximum speech rate is typically greater in logopenic relative to nonfluent variant patients. The logopenic variant can be distinguished from the semantic variant by relatively slower maximum speech rate, presence of phonological paraphasias, and less severe impairment of lexical retrieval (as evidenced by use of lower frequence nouns and fewer pronouns). This work indicates that the logopenic variant of PPA can be differentiated from other PPA variants based on performance on a simple picture description task or other speech sample. Another study, by Mesulam and colleagues, classified PPA patients into three variants based on a 60% cutoff for scores on a measure of lexical-semantics (the Peabody Picture Vocabulary Test) and a test of syntax (The Northwestern Anagram Test) (Mesulam et al., 2009). Individuals with the logopenic variant scored above 60% correct on each of these tests, which reliably distinguished them from individuals with nonfluent/agrammatic (<60% on the NAT) and semantic (<60% on the PPVT) variants.

Underlying phonological deficit. Following their initial effort to characterize the logopenic variant as a unique PPA subtype, Gorno-Tempini and colleagues examined six previously unreported logopenic cases in order to further refine the cognitive-linguistic profile of this patient group (Gorno-Tempini et al., 2008). In particular, this study aimed to assess the status of the "phonological loop" component of verbal working memory. This aspect of working memory comprises a "store," which holds memory traces for brief periods, as well as a "rehearsal" process that helps to revive traces, which are subject to decay. Spontaneous speech in this patient group was consistent with previous

descriptions, with simple, but grammatically correct utterances and word-finding difficulty. Sentence comprehension deficits, with no effect of syntactic complexity, were again observed, as was a sentence repetition deficit, particularly for low probability sentences. Patients were noted to provide semantically appropriate renditions of repeated sentences (e.g., "The valuable watch was missing" repeated as "The watch was gone"), while failing to repeat targets verbatim, suggesting a semantic, rather than phonological, approach to the task. Several measures were included to assess the integrity of the phonological loop specifically and participants' performance confirmed a deficit in this system. In particular, their span performance for digits and short words was limited to 3, and they were unable to repeat more than a single long word. In addition, patients were only able to repeat series of 3 letters and, unlike normal subjects, showed no benefit of phonological dissimilarity in repetition of letter strings (whereas normal, healthy individuals are better able to repeat sequences of letters whose pronunciations are dissimilar, e.g., C-Y-U vs. T-P-B). Taken together, these results are indicative of phonological loop impairment; however, it remains to be determined whether the disorder affects additional aspects of phonological processing, as detailed assessments of other phonologically demanding tasks (e.g., phoneme manipulation and blending tasks) are lacking in the literature to date.

Associated cognitive and behavioral characteristics. In addition to the aforementioned speech and language characteristics, several associated cognitive and behavioral characteristics have been identified in the logopenic variant. With regard to neuropsychological profile, individuals with the logopenic variant have been observed to perform worse on tests of calculation than other PPA variants (Gorno-Tempini et al., 2004) and some cases, particularly those with Alzheimer's disease (AD) pathology, have demonstrated impaired performance on memory tasks. Impairment of limb praxis has also been noted. Studies examining abnormal behavioral characteristics associated with each variant of PPA have

identified apathy as a consistent feature in logopenic patients. Additional behavioral features include irritability, anxiety, and agitation (Roher et al., 2010).

Biomarkers in logopenic variant — Recent research examining biomarkers in the logopenic variant has led to progress in identifying how the clinical presentation relates to underlying anatomical changes as well as pathological and genetic processes.

Imaging Findings. Volumetric analyses of atrophy in the logopenic variant using voxel-based morphometry (VBM) have identified a pattern of damage primarily affecting the left temporoparietal junction, including the left posterior superior and middle temporal gyri and inferior parietal lobule with less consistent involvement of medial temporal and parietal cortex, posterior cingulate, inferior frontal cortex, and contralateral temporo-parietal cortex (Gorno-Tempini et al., 2004; Mesulam et al., 2014b). Some cases show extension of atrophy into inferior and anterior temporal regions and future studies will reveal whether this might be a marker of a specific biological process, such as a genetic mutation. White matter VBM has revealed loss of volume in long association tracts in the left hemisphere and when adding data from DTI studies, it is possible to demonstrate alterations of the fractional anisotropy (FA) within the temporoparietal component of the superior longitudinal fasciculus (SLF), a tract known to connect temporoparietal structures (Galantucci et al., 2011). Consistent with findings from structural imaging, an FDG-PET study confirmed a pattern of left temporoparietal hypometabolism in individuals with logopenic variant. The pattern of temporoparietal involvement is similar to that observed in patients with Alzheimer's disease, especially in the early-age-ofonset form. Migliaccio and colleagues (Migliaccio et al., 2009) investigated the overlap between the logopenic variant and early-age-of-onset AD by directly comparing patterns of cortical atrophy in the two clinical syndromes. The results showed a remarkable overlap between the most significantly atrophied regions in posterior temporal

and inferior parietal regions with greater involvement of the left temporal cortex in the logopenic variant. Prominent involvement of left temporo-parietal cortex is consistent with the constellation of language and non-language behaviors observed in logopenic variant patients, including phonological deficits, dyscalculia, and limb apraxia, each of which is associated with damage to this region. Molecular imaging techniques have also been a pplied to the logopenic variant. Rabinovici and colleagues [19] used PET with Pittsburgh compound B (PIB) to investigate the presence of cortical amyloid in patients with PPA in vivo. Consistent with the anatomical studies reported above, logopenic variant patients showed positivity to cortical amyloid similar to patients with AD in all cases in the small group studied.

Pathological findings. The prediction that logopenic variant is indicative of underlying AD pathology has been supported not only by observations of temporoparietal atrophy and cortical amyloid binding on PIB-PET, but also by higher than expected occurrence of the apolipoprotein E4 haplotype and CSF biomarkers consistent with AD (elevated tau and reduced Aß42) (Gorno-Tempini et al., 2004). However, pathological confirmation was lacking until Mesulam and colleagues reported that 7/11 consecutive logopenic variant cases had AD pathology at autopsy (Mesulam et al., 2008). Together, these findings provide additional evidence suggesting that the logopenic variant belongs on the spectrum of early onset AD syndromes. In fact, there is a complementary literature examining focal presentations of AD, including language-impaired patients with clinical syndromes that are sometimes, but not always, consistent with the logopenic variant. Additional support for AD as a potential pathological basis in this patient group has come from a retrospective series of PPA patients with AD pathology, in whom a pattern of temporoparietal involvement consistent with the logopenic variant was observed, even when the language syndrome was not explicitly identified as such. More recently, another retrospective study of PPA patients who had pathology or CSF biomarkers

consistent with AD identified a logopenic syndrome in all patients (N=14). Whereas there is growing evidence for an association between the clinical syndrome and AD pathology, the relationship requires continued investigation via pathologyproven series (Gorno-Tempini et al., 2011). It is well known in the field that clinical-pathological associations are probabilistic and not absolute and there are reports of individuals with logopenic variant and non-AD pathology at autopsy as well as progranulin mutations that may present with a logopenic-like syndrome (see section on genetic findings, below). In addition, the relation between AD pathology and neural and cognitive changes in the logopenic variant remains to be elucidated, as there does not appear to be a clear correspondence between distribution of pathology (neuritic plaques and neurofibrillary tangles) at autopsy and in-vivo clinical and imaging measures.

Genetic findings. There is growing evidence that progressive aphasic syndromes may, in some cases, have a genetic basis, including mutations of the progranulin (GRN) and microtubule-associated protein tau (MAPT) genes (Van Swieten & Spillantini, 2007). The phenotypes corresponding to each type of mutation have yet to be conclusively identified; however, it appears that GRN mutations may result in a logopenic-like presentation in some cases. In their recent series of nine logopenic patients, Rohrer and colleagues identified two individuals with GRN mutations (Roher et al., 2010). These individuals demonstrated speech-language characteristics and patterns of cortical involvement similar, but not identical to, a subgroup of individuals with logopenic variant and CSF biomarkers consistent with AD. The two individuals with GRN mutations demonstrated, in addition to posterior temporal involvement, damage to the left anterior temporal lobe and, accordingly, exhibited a constellation of language features consistent with semantic impairment. Detailed description of another GRN-mutation case reported, in addition to more classic logopenic variant deficits, grammatical errors, which, in the context of inferior frontal atrophy, suggests possible overlap with the nonfluent variant of PPA. These findings

indicate that individuals with GRN mutations may represent a distinct logopenic-like subtype with a partially unique behavioral and anatomical signature that may be of utility in differentiating such cases from those that result from AD or other pathological processes.

Consensus criteria for diagnosis of the logopenic variant — An international panel of experts has recently put forth a set of diagnostic criteria for PPA and its clinical variants (Gorno-Tempini et al., 2011). These criteria include both core and supporting features, as well as criteria for imaging and pathology-supported diagnoses. The diagnostic guidelines for logopenic variant include as core features both impaired single-word retrieval in spontaneous speech and impaired repetition of sentences and phrases. Additional supporting features, at least three of which must be present in order to diagnose logopenic variant, include phonological errors in speech, spared single-word comprehension and object knowledge, preservation of motor speech, and lack of agrammatic utterances. In order to reach an imaging-supported diagnosis, the aforementioned clinical features must be accompanied by imaging findings revealing atrophy, hypometabolism, or hypoperfusion of left posterior perisylvian/parietal cortex. Finally, a pathology-confirmed case of logopenic variant requires clinical diagnosis of the syndrome accompanied by histopathological data or the presence of a known genetic mutation.

1.3.2 Posterior Cortical Atrophy

Posterior cortical atrophy (PCA) is a clinical syndrome characterized by progressive loss of visual processing and other posterior brain functions (including reading, calculation, and navigational orientation) and atrophy of the parietal, occipital, and occipitotemporal cortices (Tang-Wai et al., 2004). Alzheimer disease (AD) is the most common underlying pathologic state (up to

78% of patients with PCA having pathological confirmed AD) with alternative causes including dementia with Lewy bodies (DLB), subcortical gliosis, corticobasal degeneration, and prion-associated disease. There are no epidemiologic studies of PCA, but it has been estimated that PCA may account for 5% to 10% of young-onset AD (YOAD) presentations (Snowden et al., 2007). Age at onset is usually lower in PCA than in typical (amnesic) AD, with most patients with PCA experiencing their first symptoms in their 50s or early 60s. Patients with PCA report difficulties in reading, driving, navigating, and identifying objects. In many senses these patients behave as if blind, regardless of their preserved visual acuity and absence of ophthalmologic impairment. Very often they are referred by ophthalmologists, as visual difficulties are commonly their first and main complaint. Deterioration in other cognitive domains comes over time, degrading posterior functions, such praxis, calculation, and spelling first, whereas episodic memory, insight, and anterior functions (such as attention and executive functions) are relatively preserved until later in the disease. Although research on the neurologic, cognitive, and neuroimaging characteristics of PCA have increased during the last 2 decades, the neuropsychiatric manifestations (NPM) have received little attention and are consequently poorly characterized. More than 80% of patients with typical AD have some kind of neuropsychiatric disorder over the course of the disease (Howard et al., 2001); these rates are even higher in DLB. In short, NPM have proved to be highly prevalent in patients with dementia, are a domain of great complexity, and have important implications for diagnosis, treatment, and prognosis. Studying NPM in atypical phenotypes of AD is particularly challenging because the prevalence of these forms is low and missed diagnosis common. Furthermore, in the case of syndromes in which specific clinical features are particularly salient and striking (such as visual disturbances in PCA), other regular features (eg, depression or delusions) may be overlooked.

Neuropsychiatric manifestations and clinical picture — Analyzing similarities and differences in the patterns of NPM expressed by individuals with PCA and typical AD, one pertinent factor is the older age at onset of the latter. The data regarding the prevalence of NPM in YOAD (cases with onset before 65 years of age) and late-onset AD (LOAD) are equivocal, as some studies report a higher prevalence of NPM in YOAD and others in LOAD (Van Vliet et al., 2012). The problem of interpretation is that these studies generally have small samples, and the YOAD samples are likely to include other atypical AD phenotypes (such as frontal-variant AD, which mimics frontotemporal dementia, and logopenic progressive aphasia, a form of primary progressive aphasia). Recent longitudinal studies, which have enrolled larger numbers, have described lower prevalence of depression, anxiety, apathy, and irritability in younger compared with older AD (Van Vliet et al., 2012). However, the data are ambiguous because these studies specify a diagnosis of AD but do not distinguish between typical and atypical phenotypes.

Emotional Features: apathy, anxiety, depression, and irritability — The only study to date examining the NPM of PCA reported apathy (60%), anxiety (55%), depression (45%), and irritability (35%) as the most common NPM in PCA (Isella et al., 2014). The study found differences in the rates of anxiety between PCA and AD (55% PCA, 15% AD, P<.01); there were no differences in cognition, age, education, illness duration, or severity between anxious and nonanxious patients with PCA. Depression, irritability, anxiety, and apathy were the most frequent symptoms in the PCA and AD groups. The authors found age-related differences in the levels of anxiety, with patients with YOAD having more than their LOAD counterparts, whereas there were no differences between young- and late-onset PCA. Taken together, the findings from these two studies are similar, the exception being that rates of anxiety in the authors' AD group (55%) are higher than rates in the other study (15%). Apathy and depression were the only emotional features reported in the PCA literature until recently. Apathy is a

disorder of the initiation, intensity, and persistence of goal-directed behavior and is the most common NPM in YOAD. It is the most persistent and frequent NPM in all the stages of typical AD, also the most common in PCA in one study, and the next more common after depression and irritability in another (Suàrez-Gonzàlez et al., 2015). Shakespeare and colleagues have suggested that apathy in PCA may be less severe than in amnesic AD, based on their analysis of scores derived from the Cambridge Behavioral Inventory-Revised (Shakespeare et al., 2015). Although this observation is not yet confirmed, it is consistent with other data showing associations of apathy in AD with dysfunction in the anterior cingulate and in fronto-subcortical circulates (Stella et al., 2014), all cortical regions having less degeneration in PCA than in AD. The prevalence of depressive symptoms in AD can amount to 30% to 79%, making it one of the most common NPM in PCA and amnesic phenotypes (Suàrez-Gonzàlez et al., 2015). It should be noted, however, that there are very few studies of this in PCA. A study found patients with PCA to be more prone to having depression than patients with amnesic AD (Tang-Wai et al., 2004). The conclusion was that depression in PCA reflects a reaction stemming from the patients' awareness of their handicaps, which is consistent with these patients' general preservation of insight and executive functions. This argument that greater insight in PCA regularly results in depressive reactions is not new, but it's not fully convincing. First, there is a high frequency of depression in AD; that association is well established in the amnesic phenotype whereby loss of insight is common. Although the relation between depression and risk for later development of dementia is still unclear, both disorders seem to share common neuropathologic mechanisms involving modulation of neurotransmitters (Kessing 2012). Secondly, the fact that patients with PCA seem to present with similar rates of depression as those with typical AD (in studies measuring with tools such as the Neuropsychiatric Inventory) argues against a direct (or primary) influence of insight in the development of depressive symptoms. It is, however, possible that the nature of depressive symptoms varies in individuals with PCA and other AD

phenotypes, as such insight might be indirectly involved in its modulation. Thirdly, white matter lesions may deregulate mood in late life (Alexopoulos et al., 2002) and become an added variable contributing to depressive symptoms in AD syndromes. In light of these findings, it seems reasonable at least to consider that depression in PCA has a multifactorial origin.

Psychotic Features: Hallucinations and Delusional Misidentification — Visual hallucinations (VH) have been described in up to 5% to 31% of patients with PCA (Tang-Wai et al., 2004). In a large case series, Josephs and colleagues (Joseph et al., 2006a) found that 13 out of 59 (22%) patients with PCA exhibited VH, and all patients met the criteria for DLB. This finding is consistent with findings reported by McMonagle and colleagues (McMonagle et al., 2006) in whose sample 6 out of 19 patients presented VH, and 5 of the 6 patients were diagnosed with DLB. In another study, 3 patients who presented with VH also met the criteria for probable DLB (3 out of 28); these individuals accounted for 10% of the total sample (Suàrez-Gonzàlez et al., 2015). In light of these studies, it seems that VH in PCA usually occurs in individuals fulfilling the criteria for DLB. These estimates of the relative prevalence of PCA-DLB from clinical studies are largely consistent with rates of DLB determined in the few pathologic series of. In the study by Tang-Wai and colleagues (Tang-Wai et al., 2004), patients presenting Lewy body pathology developed illness at 65 and 58 years of age and had the disease for 10 and 14 years, respectively. Establishing the frequency of VH in PCA is important for the differential diagnosis of PCA caused by AD or DLB, as VH are a major feature of the DLB diagnostic criteria. The distinction is also important for prognosis and treatment, given that the interventions for DLB and AD differ. The posterior nature of atrophy in PCA has been considered as a possible source of VH. However, posterior atrophy in PCA is pronounced and VH unusual, whereas in DLB there is less posterior atrophy and VH are much more frequent. Therefore, other factors besides posterior atrophy must be sought. Considering anatomic associations, a VBM study of VH in PCA showed that

patients with PCA with VH had more atrophy than those without VH in the primary visual cortex but also in subcortical structures (lentiform nuclei, thalamus, basal forebrain and midbrain). Also, cholinergic and monoaminergic dysfunction in AD and DLB may be contributors to the NPM in these diseases (Geda et al., 2013). It remains unsettled whether the pronounced occipital atrophy observed in PCA contributes to the appearance of VH. So too remains unknown whether there are qualitative differences in the nature of hallucinations experienced by PCA-AD compared with PCA-DLB.

Neuroimaging — Increasingly advanced image analysis techniques have been used to localise and quantify (typically group) differences in patterns of atrophy in patients with PCA, compared either with controls or with patients with typical Alzheimer's disease. Cross-sectional voxel-based morphometry has shown widespread differences in grey matter between patients with PCA and healthy controls, with the most significant reductions found in regions of the occipital and parietal lobes followed by areas in the temporal lobe (Lehman et al., 2011). Direct comparison between individuals with PCA and typical Alzheimer's disease, using both voxel-based morphometry and cortical thickness measures, has shown greater right parietal and less left medial temporal and hippocampal atrophy in patients with PCA. It is noteworthy that in several studies, researchers report asymmetric atrophy patterns in PCA (right greater than left), but these diff erences could be due to selection biases in the diagnosis and recruitment of patients with prominent visual dysfunction. Limited data from diffusion tensor imaging studies also suggest that PCA reduces the integrity of white matter tracts in posterior brain regions (Migliaccio et al., 2011). However, considerable regional overlap in atrophy has also been reported, with regions including the posterior cingulate gyri, precuneus, and inferior parietal lobe being affected in both PCA and typical Alzheimer's disease. Such findings suggest that PCA, when associated with Alzheimer's disease, exists on a spectrum of variation with other phenotypes of Alzheimer's disease (Migliaccio et al., 2009). Fluid

registration of longitudinally acquired structural magnetic resonance images shows the evolution of PCA, with findings of group studies indicating that, by 5 years of symptom duration, atrophy is widespread throughout the cortex, including medial temporal lobe structures. Data from functional imaging studies using single photon emission computed tomography (SPECT) and fluorodeoxyglucose (FDG) PET accord largely with structural changes in parieto-occipital areas. In addition to posterior regions, FDG-PET has indicated specific areas of hypometabolism in the frontal eye fields bilaterally, which can occur secondary to loss of input from occipitoparietal regions and be the cause of oculomotor apraxia in PCA (Kas et al., 2011). In a few studies, researchers have also assessed patterns of amyloid deposition with Pittsburgh compound B (PiB)-PET in patients with PCA. Case studies and small series have shown increased accumulation of amyloid-β, predominantly in the occipital and parietal lobes, relative to individuals with typical Alzheimer's disease. However, in two studies in which PiB uptake was compared in large groups of patients with PCA and typical Alzheimer's disease, no significant difference was reported in amyloid deposition between these groups, with both showing diffuse PiB uptake through out frontal, temporoparietal, and occipital cortex (De Souza et al., 2011).

Diagnostic and research criteria — Two sets of diagnostic criteria for PCA have been proposed (Mendez et al., 2002; Tang-Wai et al., 2004). Suggested core features for a diagnosis of PCA include insidious onset and gradual progression; presentation of visual deficits in the absence of ocular disease; relatively preserved episodic memory, verbal fluency, and personal insight; presence of symptoms including visual agnosia, simultanagnosia, optic ataxia, ocular apraxia, dyspraxia and environmental disorientation; and absence of stroke or tumour. Supportive features include alexia, ideomotor apraxia, agraphia, acalculia, onset before the age of 65 years, and neuroimaging evidence of PCA or hypoperfusion. Although these criteria have proved useful in several clinical and research contexts, they are based on clinical experience at single centres and have

not been validated more widely. Without objective evidence linking clinical phenotype to underlying pathology, there continues to be inconsistency, with the term PCA being used as a descriptive syndromic term and as a diagnostic label. Such inconsistencies present several difficulties in attributing and assessing the validity of a diagnosis of PCA and, particularly, in the design and interpretation of research studies and clinical trials. First, although a syndromic classification could be adequate for some types of research study (eg, brain–behaviour, behavioural intervention), other investigations will need direct consideration of probable underlying pathological features (eg, clinical trials of disease-specific drugs). Second, at present, we have no evidence base on which to judge the eff ectiveness of pharmacological treatments for Alzheimer's disease in individuals with PCA attributable to probable Alzheimer's disease or to decide whether individuals with PCA should be included or excluded from conventional clinical trials of Alzheimer's disease—eg, because of the potential unsuitability of study outcome measures (eg, visual memory tasks) selected for patients with more typical amnestic or global clinical presentations. Third, current criteria provide no guidance about the degree of specifi city needed for a diagnosis of PCA. For example, in the relatively large series reported by Renner and colleagues (Renner et al., 2004), nine of 27 patients presented with PCA as a fairly isolated disorder, whereas in the remaining 18 people it was the prominent feature of a more generalised dementia. Several groups have suggested that PCA, when attributable to probable Alzheimer's disease, lies on a phenotypic continuum with other typical and atypical Alzheimer's phenotypes (eg, amnestic Alzheimer's disease, global cognitive impairment, logopenic or phonological aphasia)(Snowden et al., 2007; Migliaccio et al., 2009), but the boundaries between such phenotypes are defined imprecisely. Fourth, the presentation of visual complaints is a core feature of existing criteria but some patients with neurodegenerative disorders present with predominant impairment of other posterior cortical functions, such as calculation, spelling, and praxis; such individuals could be deemed to fall within the PCA spectrum. Finally, the value

of biomarkers might differ in PCA compared with typical Alzheimer's disease or dementia with Lewy bodies (eg, relative absence of hippocampal atrophy). This issue is especially important in view of the increasing incorporation of such biomarkers in disease-specific diagnostic criteria (Dubois 2010). Future resolution of these issues and development of clinical and research criteria for the defi nition of PCA are likely to be based on a consensus of opinion from many specialist centres, supported by objective evidence of the relation between clinical presentation, neuroimaging and CSF biomarkers, and histopathological data. Establishment of the relative likelihood of different pathologies in large, multicentre datasets would improve the discrimination of potential disease subtypes necessary for trials of disease-modifying agents. One possible approach would be to apply a range of criteria to a multicentre dataset to establish sets of inclusion and exclusion criteria that identify specific disease subgroups (eg, PCA with Alzheimer's disease). By consensus, experts could also investigate frameworks for making criteria useable, in terms of a quantifiable set of diagnostic markers, to help with enrolment into research studies and to improve the comparability of data between institutions.

1.3.3 Corticobasal Syndrome

Corticobasal syndrome (CBS) is a striking and unusual clinical manifestation of various neurodegenerative pathologies, with tauopathies being the most common. The prototype pathology is corticobasal degeneration (CBD), estimated to account for 50% of cases (Boeve, 2007). Other pathologies reported in the literature include Alzheimer's disease (AD), progressive supranuclear palsy (PSP), frontotemporal dementia with parkinsonism linked to chromosome 17, Pick's disease with Pick bodies, dementia with Lewy bodies, neurofilament inclusion body disease, Creutzfeldt-Jakob disease, frontotemporal degeneration due to progranulin gene mutation and motor neuron inclusion body dementia

(Hassan et al., 2011). Unifying the pathologies that produce CBS is a consistent topographic distribution of cortical damage, involving frontal or frontoparietal cortex in an asymmetric fashion (Boeve et al., 1999). The association between AD and CBS is of particular interest as they are distinct neurodegenerative pathologies and share relatively little in common apart from abnormal phosphorylated tau protein deposition. Features that set AD apart from CBD include the specific tau protein isoform deposited, the presence of β-amyloid deposition, the clinical hallmark of dementia of the Alzheimer's type (DAT), and the presence of medial temporal lobe atrophy. To state this latter point further, the brain regions implicated to clinically produce CBS are typically different from those involved in typical AD pathology, hence the conundrum. Ironically, CBD and AD pathology were thought to be pathognomonic for their clinical syndrome, CBS and DAT, respectively. Clinicopathological overlap amongst the tauopathies is now increasingly appreciated, including CBS with AD pathology and dementia with CBD pathology. Factors that may predict underlying AD pathology in cases presenting with CBS will also be examined. Many clinicians have called for further research to look at clinical markers of AD pathology in CBS (Shelley et al., 2009). Trying to accurately predict pathology is of great importance, as therapies are typically specific to the underlying disease process.

Clinical features — This rare clinical syndrome is associated with sporadic disease with typical onset in the sixth to eighth decades. Core clinical features are insidious progressive asymmetric rigidity and apraxia, accompanied by symptoms and signs of cortical (motor, sensory or association cortices) and extrapyramidal dysfunction (Boeve et al., 2007). Cortical signs include cortical sensory loss, alien limb phenomena, myoclonus, apraxia, pyramidal motor signs, agrammatic aphasia, apraxia of speech and visuospatial impairment. Extrapyramidal involvement includes dystonia and levodopa nonresponsive Parkinsonism (rigidity, tremor and bradykinesia). Typical mean survival is 7 years from symptom onset. Asymmetry is emphasized, although symmetric presentations have been described. Thus clinical findings may be explained by

the topographical distribution of cortical damage: cortical sensory loss and apraxia occur with parietal lesions, and occasionally posterior frontal lesions; frontal or parietal lesions can produce alien limb syndrome, mirror movements, pyramidal tact signs or apraxia; and posterior inferior frontal lesions can produce agrammatic aphasia (Joseph et al., 2006b). The lack of a marked response to levodopa is postulated to reflect postsynaptic nigrostriatal dysfunction rather than degeneration of the substantia nigra. However, severe rigidity, dystonia and tremor have been reported in the absence of basal ganglia or substantia nigra damage, and are postulated to reflect damage to the sensorimotor cortex and its extrapyramidal projections (Boeve et al., 1999). The neuropathological substrate of CBS is most commonly a tauopathy, with a subtype of four microtubule-binding repeats (4R-tau) most common, as seen in CBD and PSP pathology. CBS is also associated with TDP-43 pathology, mostly observed in progranulin gene mutation carriers, although sporadic cases are also reported. Small clinicopathological series have shown a significant proportion of CBS cases with AD pathology: a mixed 3R/4R tauopathy (Ling et al., 2010). In one study of 12 CBS cases followed to autopsy, AD pathology represented 50% of CBS and the remaining 50% were CBD (Shelley et al., 2009). Increasing numbers of case reports or small case series comprising two to six patients of CBS-AD have emerged over the past 20 years in the literature, totaling approximately 42 cases (Hassan et al., 2011).

Corticobasal pathology compared with AD pathology— The first cases of CBS described by Rebeiz et al. in 1968 were associated with a unique underlying pathology, now termed corticobasal degeneration (Rebeiz et al., 1968). Current pathologic diagnostic criteria specify tau-positive neuronal and glial lesions in the gray and white cortex and basal ganglia. The abnormal tau protein is hyperphosphorylated and deposited as various inclusions termed astrocytic plaques, thread-like lesions, corticobasal bodies and coiled bodies; swollen or achromatic ballooned neurons are usually present (Dickson et al., 2002). Frontal or parietal cortices and subcortical regions are typically involved, with relative

sparing of the temporal cortex, including the medial temporal cortex. Interestingly, the temporal cortices are the first sites involved in AD, which raises the questions of why and how AD pathology can produce CBS, if topography rather than lesion type is responsible. However, this theory of location of lesion deposition is thought to explain why CBD pathology may produce a variety of clinical phenotypes apart from CBS (e.g., progressive supranuclear palsy syndrome, behavioral variant frontotemporal dementia and apraxia of speech) (Boeve et al., 1999). Abnormal tau deposition occurs in both AD and CBD where tau dysfunction affects axonal transport and microtubule stability in neurons. However, tau isoforms differ between AD and CBD depending on whether exon 10 is spliced in (4R) or spliced out (3R). CBD is a 4R tauopathy, while both 3R and 4R abnormal tau is found in AD. Although both AD and CBD are tauopathies, AD also has coexisting β-amyloid protein deposition; a combination that is unique amongst the dementias. Clinical and pathologic overlap amongst the tauopathies has been explained, in part, by differences in the location of the tau protein deposition.

Demographic factors — Hu et al. noted that CBS-AD cases in their cohort were younger than CBS-CBD cases (Hu et al., 2009). Overall, the age of onset in CBS-AD falls under the time frame of an 'early-onset AD', rather than 'late-onset', which presents at an age of greater than 65 years. Interestingly, it is early-onset AD that tends to show more rapid progression, generalized cortical deficits, cortical atrophy and hypometabolism compared with late-onset patients of a similar stage (Rabinovici et al., 2010).

Clinical factors — Myoclonus is well established as a feature of AD, but has also been associated with CBD. However, Hu et al. noted that it was more common in CBS-AD (four out of five) than CBS-CBD (two out of 11) cases (Hu et al., 2009). Shelley et al. reported two out of six CBS-AD cases with myoclonus, but no CBS-CBD cases (Shelley et al., 2009). The presence of myoclonus may, therefore, be more suggestive of CBS-AD than CBS-CBD. Limb apraxia has been reported to

occur in both pathologies in approximately equal frequencies. Tremor occurred only within the CBD subgroup in the study by Hu et al. Supranuclear gaze palsy was rarely reported in CBSAD, but was more common in CBS-CBD. Parkinsonism may point away from CBS-AD, as higher Unified Parkinson's Disease Rating Scale scores were reported in CBS-CBD compared with CBS-AD (Hu et al., 2009).

Neurocognitive factors — Dementia is recognized in CBS, and may be the most common diagnosis in pathologically confirmed CBD, as it is in AD. The cognitive profile probably varies according to the topographical distribution of pathology. For example, left hemisphere involvement may produce a language disorder, while right hemisphere lesion burden produces visuospatial dysfunction. Memory is usually relatively intact in CBS, consistent with relative sparing of the medial temporal cortex in CBD, but as this is the typical location of AD pathology one would anticipate impairment in these cases. Two studies did not report any difference in memory impairment and attentional deficits between CBS-AD and CBS-CBD (Hassan et al., 2011). However, Shelley et al. noted that initial episodic memory loss appeared to predict CBS-AD (Shelley et al., 2009). Supporting this observation, Borroni et al. (2011) reported early memory impairment in CBS cases with an AD pathology bioprofile (cerebrospinal fluid [CSF] and SPECT imaging consistent with AD), compared with CBS cases with a non-AD profile (Borroni et al., 2011). It has been noted that frontal lobe symptoms (utilization behavior, personality change and frontal release signs) are associated with CBS-CBD. Neuropsychometric evaluation of frontal lobe involvement and dysexecutive function may thus help identify CBS-CBD. Indeed, verbal letter and category fluency testing are abnormal in CBD. Agrammatic aphasia and orobuccal apraxia has also been associated with CBS-CBD, although language can remain preserved. Conversely, visuospatial impairment may indicate CBS-AD; Alladi et al. (2007) reported visuospatial impairment in six out of six cases and Ceccaldi and colleagues in two out of two, although it was found in both CBS-AD and CBS-CBD in the Whitwell et al. Series

(Whitwell et al., 2010). These findings emphasize that frontal disease distribution and less involvement of the medial temporal lobe are correlated with CBS-CBD, while impairment in parietal lobe function is associated with CBS-AD.

Biochemical markers — Biochemical markers for AD that reflect cortical pathology, including neuronal degeneration, β-amyloid plaque deposition and tau hyperphosphorylation, are currently under extensive research. Serum biomarkers have thus far proved disappointing with no consensus, and verification is waiting. CSF biomarkers appear promising. A decline in Aβ42 increase in total tau (t-tau) and phosphorylated tau (p-tau) and ratio of low Aβ42:high tau is characteristic for AD (Irwin et al., 2013). Therefore, CSF biomarkers may be a useful as amyloid-labeled imaging in predicting AD in patients presenting with CBS.

Neuroimaging markers — Much research has correlated anatomical and functional imaging with CBS and DAT, and found specific patterns of atrophy or altered metabolism, respectively. However, the caveat again is that there are very few studies with autopsy-proven diagnosis of CBD or AD, thus these findings are limited in predicting an underlying pathology for CBS. However, one may surmise that perhaps there may be features of AD on antemortem scans in the setting of CBS that may hint at this pathology. Autopsy-proven pathological case series will be required to confirm this hypothesis.

MRI — Typical MRI findings in CBS are asymmetric cortical atrophy, mainly frontoparietal, with the most severe changes contralateral to the more affected clinical side (Koyama et al., 2007). This pattern of atrophy is sensitive to CBS diagnosis, but not specific to any particular underlying pathology. By comparison, the medial temporal lobes, especially the hippocampus and entorhinal cortex, are amongst the earliest site of pathologic involvement in AD, reflected by reduced hippocampal and entorhinal cortex volumes on brain MRI compared with agematched controls. Cortical volume loss in AD is usually extensive and involves frontal, temporal and parietal lobes (Jones et al., 2006).

Thus one could postulate that widespread MRI patterns of atrophy may predict AD pathology. Supporting this, diffuse atrophy was noted in several CBS-AD cases (Hassan et al., 2011). Voxel-based morphology (VBM) uses group analysis to evaluate regional brain atrophy without any a priori assumptions. Whitwell et al. examined CBS cases with various autopsy-proven pathologies, and found the only common site of involvement was the premotor cortex and insula (dominant) and supplementary motor area (dominant and nondominant) (Whitwell et al., 2010). The patterns of atrophy were relatively restricted to inferior and superior posterior frontal regions in CBS-CBD, but were more widespread in CBS-AD, with additional involvement of the temporoparietal lobes. Therefore, a more widespread and posterior pattern of atrophy is associated with CBS-AD. Interestingly, both CBS-CBD and CBS-AD showed relative sparing of the hippocampus, typical for CBD pathology but atypical for AD pathology (Hassan et al., 2011).

The overmentioned asymmetry is also appreciated using DTI to evaluate white matter disease; in fact, Parmera and colleagues (2016) showed that it mainly involves the hemisphere contralateral to the more affected limb, and in particular the midbody of the corpus callosum and perirolandic corona radiata when CBS is compared to bvFTD.

Neuroimaging: other techniques — Resting state functional MRI (fMRI) demonstrates reduced activity in AD in the default mode network, encompassing the posterior cingulate, inferior parietal, inferolateral temporal, ventral anterior cingulate and hippocampus. SPECT imaging studies appear promising: asymmetric hypoperfusion in frontoparietal lobes and basal ganglia is reportedly common in CBS. By comparison, the AD hypoperfusion pattern in autopsy-proven cases involves the parietal and temporal lobes, precuneus and posterior cingulate cortex. Speaking about the Fluorodeoxyglucose-PET (FDG-PET), glucose hypometabolism in the precuneus, posterior cingulate and biparietal regions is observed in AD. This correlates with elevated CSF t-tau and p-tau and

reduced metabolism. By comparison, CBS typically has asymmetric hypoperfusion within the parietofrontal cortex and basal ganglia, although PET findings in pathologically proven CBD are rarely reported. Asymmetric hypometabolism in the contralateral frontoparietal cortex, basal ganglia and cerebellum has been reported. Lastly, Amyloid PET imaging has been shown to be sensitive and specific for amyloid deposition, and has been reliably demonstrated to differentiate AD from FTD, but no comparisons with CBD have yet been reported (Hassan et al., 2011).

Literature summary of CBS-AD compared with CBS-CBD cases — To determine whether any of the mentioned factors may be useful predictors of pathology, a literature summary was compiled by Hassan et colleagues (Hassan et al., 2011) for all cases published up to 2011. Duplicate cases or cases with coexistent pathology with AD were excluded where these could be determined. Cases were included (n = 29) only if there was sufficient detail to include demographic, clinical, imaging and pathologic information to compile a literature summary. These were compared with CBSCBD cases (n = 24) to identify clinical or imaging differences that could increase the antemortem diagnosis of AD. Comparing CBS-AD to CBS-CBD cases, there were several key findings that appeared to be associated with AD pathology: longer disease duration, younger age at onset, hemisensory neglect, memory impairment, visuospatial difficulties, dressing apraxia and myoclonus. Importantly, there was no difference between aphasia, limb apraxia, alien limb phenomenon, fisted hand, parkinsonism, pyramidal motor signs, dystonia or Gerstmann syndrome. This is not surprising given that both subgroups had the same clinical diagnosis of CBS, of which these signs meet inclusion criteria. Perhaps of more interest, there was no difference in change of gait (which is usually normal in typical AD), aphasia (as observed by several small group studies) or personality change or frontal release signs (anticipated for CBD). There were no significant associations with CBS-CBD, although a trend was noted for utilization behavior, rigidity and extraocular dysfunction to be associated with CBS-CBD. These findings are not surprising

given that imaging demonstrates focal frontal lobe atrophy in CBS-CBD, compared with more parietal lobe findings in CBS-AD.

1.3.4 Frontal-variant Alzheimer's Disease

Up to now, this rare AD phenotype has been limited to case reports and small series, and many clinical, neuroimaging and neuropathological characteristics are not well understood. One recent retrospective study assessed the clinical, neuropsychological, morphological and neuropathological features of this clinical syndrome known in the literature as the frontal-variant of Alzheimer's disease (fvAD), or frontal-variant AD (Ossenkoppele et al., 2015a).

The first description of a frontal-variant of Alzheimer's disease was provided by Johnson et al. (Johnson et al., 1999) in three patients with early and predominant executive dysfunction in the face of amyloid plaque and neurofibrillary tangle pathology. Several subsequent studies have reported on a dysexecutive phenotype of Alzheimer's disease (Snowden et al., 2007; Wolk et al., 2010), but only few included autopsy/biomarker-confirmed Alzheimer's disease patients. Other autopsy (Blennerhassett et al., 2014), clinical, and case (Herrero-San Martin et al., 2013) studies have shown that the spectrum of frontal-variant Alzheimer's disease also comprises patients with early personality and behavioural changes such as disinhibition, apathy or compulsiveness. The clinical picture of frontal-variant Alzheimer's disease may mimic that of behavioural variant frontotemporal dementia (FTD), as illustrated by the 10–40% of patients clinically diagnosed with behavioural variant FTD who are found to have Alzheimer's disease pathology on amyloid PET (Rabinovici et al., 2011) or post-mortem evaluation. Although frontal-variant Alzheimer's disease has been incorporated into new diagnostic criteria for Alzheimer's disease dementia (Dubois et al., 2014), little is known about the initial symptoms, risk factors, genetic predispositions, behavioural and neuropsychological profiles and co-pathologies

that characterize this phenotype. There is a need for better understanding of neurodegenerative diseases that cross boundaries of distinct clinical entities, as this may improve clinicians' ability to discern the histopathological cause of dementia. Ossenkoppele and colleagues (Ossenkoppele et al., 2015a) compared autopsy/biomarker-defined Alzheimer's disease patients selected based on 'behavioural' or 'dysexecutive' predominant presentations against carefully matched and autopsy/biomarker-confirmed typical Alzheimer's disease and behavioural variant FTD patients, along with a group of healthy controls. As a group, patients with Alzheimer's disease selected based on behavioural-predominant presentations more often presented initially with cognitive than behavioural symptoms, both memory and executive functions were more impaired than in behavioural variant FTD, and prevalence of APOE e4 was high. Patients with Alzheimer's disease selected based on dysexecutive features presented as a primarily cognitive phenotype with minimal behavioural abnormalities and intermediate APOE e4 prevalence. Both behavioural and dysexecutive Alzheimer's disease patients were distinguished by a prevalent temporoparietal-predominant atrophy. The two groups together are comprised in the frontal-variant AD group, although it could be useful to describe them separately when the one of the two aspects is clearly predominant.

Clinical features and neuropsychological profiles — In line with Forman et al. (2006), patients with fvAD presented twice as often with cognitive as opposed to behavioural symptoms. About 80% of patients were around the threshold required to meet clinical criteria for possible behavioural variant FTD (meeting 2–4 of 6 criteria, with 3/6 criteria required for the diagnosis of 'possible behavioural variant FTD'; Rascovsky et al., 2011), while 52% met formal criteria, illustrating the diagnostic dilemmas these patients can produce. On the other hand, patients with frontal-variant Alzheimer's disease had the most profound neuropsychological deficits, showing equivalent memory performance to patients with typical Alzheimer's disease and worse executive functioning than

behavioural variant FTD and typical Alzheimer's disease patients. Altogether, these findings suggest that a combination of early primary cognitive deficits, objectively-confirmed memory deficits and an intermediate behavioural profile can help to differentiate behavioural Alzheimer's disease from behavioural variant FTD clinically. In line with our hypothesis, dysexecutive Alzheimer's disease presented as a primarily cognitive phenotype with minimal behavioural abnormalities. Breakdown of the first cognitive symptoms revealed that patients with dysexecutive Alzheimer's disease and/or their caregivers rarely complain about dysexecutive features (only 10%), suggesting that their symptoms are often misclassified as 'memory-related'.

Potential risk factors — The proportion of patients with frontal-variant Alzheimer's disease carrying an APOE e4-allele (59.5%) was within the range typically observed in patients with Alzheimer's disease. APOE e4 is known to predispose for medial temporal lobe vulnerability and memory dysfunction (Wolk et al., 2010) and so could partially account for these features. The prevalence of APOE e4-carriers in patients with dysexecutive Alzheimer's disease (40%) was intermediate to that of typical Alzheimer's disease and controls, which is in accordance with other studies in nonamnestic variants of Alzheimer's disease (Wolk et al., 2010). Future research should assess for potential other genetic risk factors contributing to fvAD. In agreement with previous reports (Devi et al., 2004), approximately half of the behavioural Alzheimer's disease and dysexecutive Alzheimer's disease groups had a positive family history (first or second degree) of dementia or a psychiatric disorder. Medical histories of behavioural Alzheimer's disease and dysexecutive Alzheimer's disease patients showed roughly equivalent presence of most conditions, e.g. hypertension (30–35%), diabetes mellitus (10%) and sleeping disorder (11–17%), compared to epidemiological studies (Nwankwo et al., 2013). The proportion of depression (18–24% received treatment) and traumatic brain injury (15–19% experienced at least one moderate or severe event) seemed

overrepresented in behavioural Alzheimer's disease and dysexecutive Alzheimer's disease patients compared to the general population (Corrigan et al., 2010).

Clinico-anatomical dissociation — In behavioural Alzheimer's disease and dysexecutive Alzheimer's disease patients, the frontal lobe, traditionally considered to be the regulatory core of behaviour and executive functioning, was relatively spared compared to the temporoparietal regions in voxel-based morphometry group-level analyses. Although slightly more affected than in typical Alzheimer's disease, frontal atrophy was less prominent than hypothesized a priori based on the behavioural and dysexecutive phenotypes. There are several explanations for this clinico-anatomical dissociation. First, liberal criteria were used to define behavioural Alzheimer's disease group by Ossenkoppele et al. (2015a). Due to lack of consensus clinical criteria, behavioural Alzheimer's disease has often been operationalized as patients meeting behavioural variant FTD criteria in the face of primary Alzheimer's disease pathology at autopsy (Forman et al., 2006). To capture more broadly the clinical spectrum of these patients, the large sample study of Ossenkoppele and colleagues (2015a) did not only include patients who met formal criteria for behavioural variant FTD, but also included patients who were clinically labelled as having 'frontal Alzheimer's disease' or having a differential diagnosis consisting of both behavioural variant FTD and behavioural Alzheimer's disease. When only looking at patients with behavioural Alzheimer's disease who were initally diagnosed with behavioural variant FTD, frontal atrophy was more prominent than that in the total behavioural Alzheimer's disease group, but temporoparietal atrophy remained predominant. While previous case studies demonstrate that profound frontal involvement can be observed in patients with behavioural Alzheimer's disease, these single-subject effects may have been washed in group-level voxel-based morphometry analyses. The W-score frequency maps in the Ossenkoppele and colleagues' study were sensitive to

individual atrophy patterns, and indeed visual inspection of these maps indicated more frontal involvement compared to the voxelbased morphometry results. Second, vascular damage in frontal white matter may result in fronto-parietal disconnection and has been associated with both neuropsychiatric symptoms and executive dysfunction in Alzheimer's disease. Similarly, lesions in basal ganglia that affect fronto-subcortical circuitries have been shown to exert behavioural or dysexecutive symptoms (Pa et al., 2009). Third, it is conceivable that structural MRI did not capture the full extent of neurodegeneration as a recent study did show increased frontal hypometabolism in patients with Alzheimer's disease with the highest score on a behavioural questionnaire (Woodward et al., 2014). This suggests that 18F-fluorodeoxyglucose (FDG) PET might be able to detect neuronal injury in an earlier stage. Finally, patients with behavioural Alzheimer's disease and those with dysexecutive Alzheimer's disease might have reduced frontal reserve related to neurodevelopmental factors, life events (e.g. traumatic brain injury), or differences in premorbid personality traits or genes that regulate behaviour. This would make them more vulnerable to frontal dysfunction when general brain homeostasis is disturbed and could potentially trigger a frontal profile when pathogenic processes occur. Future studies applying functional MRI, 18F-FDG PET, quantification of white matter integrity, subcortical volumetrics or premorbid personality questionnaires are essential to further unravel the neurobiology underlying frontal-variant Alzheimer's disease.

Neuroimaging distinction between fvAD and behavioural variant FTD — Clinicians often struggle to differentiate Alzheimer's disease from behavioural variant FTD (Rabinovici et al., 2011), and diagnostic decision-making will likely be even more complex in patients with a frontal presentation of Alzheimer's disease. A key finding is that structural MRI clearly distinguish the two groups, as behavioural variant FTD patients showed a characteristic atrophy pattern in anterior brain regions, while the frontal-variant Alzheimer's disease group

showed a classical Alzheimer's disease pattern involving wide regions of the temporoparietal cortex. Direct statistical comparison between the groups survived P5 0.05 FWE correction, and even within a subset (n = 13) of patients with autopsy/biomarker-defined Alzheimer's disease with an initial clinical diagnosis of behavioural variant FTD the temporoparietal cortex was the predominant locus of brain atrophy (Ossenkoppele et al., 2015b). This suggests that posterior versus anterior brain atrophy on structural MRI provides helpful information when clinicians are uncertain whether Alzheimer's disease or frontotemporal lobar degeneration (FTLD) pathology is driving a frontal presentation.

Some information about the involvement of the WM in AD patients with a clinical frontal variant are showed in a study of Sjobeck and colleagues (2010), who found that reduced performance on cognitive testing of executive function of patients with AD pathology correlated significantly with an increasing degree of frontal white matter changes detected by DTI.

Neuropathological findings — In the subset of patients with frontal Alzheimer's disease who underwent autopsy (n = 24), dual Alzheimer's disease and FTLD pathology as co-primary cause for dementia was restricted to two patients with mixed progressive supranuclear palsy and Alzheimer's disease. Another patient harboured unclassifiable limbic/paralimbic TARDBP (also known as TDP) inclusions, which was considered a contributing, rather than the causative, pathology by the neuropathologist. FTLD-tau and FTLDTDP pathology were thus relatively rare (5.10% of all patients), and occurred at a lower rate compared to previous studies demonstrating non-Alzheimer's disease tauopathy in 10–40% and TDP inclusions in 19–57% of more typical Alzheimer's disease patients (Forman et al., 2006; Josephs et al., 2014). Several other copathologies were frequently present, but in general these were less extensive compared to the classical plaque and tangle pathology and were thought to have contributed little to the patient's clinical deficits. The proportion of Lewy body disease (42%),

cerebrovascular disease (25%) and argyrophilic grain disease (44%) in our patients with frontal Alzheimer's disease falls within the range of previous reports on sporadic Alzheimer's disease, while cerebral amyloid angiopathy (64%) may be somewhat less frequent compared to 90% found in earlier neuropathological studies in Alzheimer's disease (Attems, 2005). Due to the young average age of patients with frontal Alzheimer's disease, comparisons against post-mortem studies in typical Alzheimer's disease should be interpreted with caution as it is known that the onset of a diversity of pathologies accelerates with ageing. Thus argyrophilic thorny astrocyte clusters were found in three patients (Munoz et al., 2007). These 4-repeat tau-positive inclusions may be of interest for future studies as they preferentially localize in frontotemporal and parietal grey– white matter junctions, and may be a common neuropathological feature in atypical manifestations of Alzheimer's disease (Munoz et al., 2007). Future studies will also need to further assess the distribution of amyloid plaques and neurofibrillary tangles in patients with frontal Alzheimer's disease (Blennerhassett et al., 2014).

Frontal-variant Alzheimer's disease: a continuum or distinct clinical entities? — Driven by previous studies and clinical experience, two distinct sets of inclusion criteria for behavioural-predominant and dysexecutive-predominant Alzheimer's disease patients were created to cover the spectrum of 'frontal Alzheimer's disease'. Although several potential mechanisms were identified that may differ between behavioural and dysexecutive-predominant presentations of Alzheimer's disease (i.e. APOE e4 status and cognitive/behavioural profiles), the presence of a single (behaviour) rather than a double dissociation (behaviour and executive dysfunction), suggests at least a certain degree of overlap between the two phenotypes. Whether these patients represent a single phenotype on a continuum including behavioural features and executive dysfunction, or two separate clinical entities is subject to future studies. Ossenkoppele and colleagues (2015a) concluded that: (i) the majority of patients

selected based on behavioural-predominant presentations also had memory deficits proportionate to or greater than executive impairment; (ii) there were also patients selected based on dysexecutive-predominant presentations showing no significant behavioural changes; and (iii) applying the inclusion criteria resulted in modest overlap between the groups (9/75, 12%).

Clinical relevance — Clinical, imaging and neuropathological features of patients with frontal Alzheimer's disease may serve as a roadmap to identify these patients in a clinical setting. This is important for studying the effects of disease-modifying agents and for appropriate symptomatic treatment (e.g. patients with frontal-variant Alzheimer's disease may show clinical benefit from acetylcholinesterase inhibitors). The key diagnostic features to distinguish behavioural Alzheimer's disease from behavioural variant FTD are the magnitude of memory impairment and brain atrophy affecting predominantly regions in the temporoparietal cortex. Additional clues are provided by a cognitive onset of the disease, presence of an APOE e4 allele and a behavioural profile that is generally less severe than that observed in patients with behavioural variant FTD. Conversely, patients with a dysexecutive presentation without prominent behavioural changes are more likely to have underlying Alzheimer's disease than FTLD pathology (Ossenkoppele et al., 2015a).

Chapter 2

AIMS

In the present study, we started with a frequency-based model of disease progression based on T1-weighted MRI data, validated with comparison to pathological and neuropsychological data. This MRI-based phasing analysis infers the anatomical origin of disease from the frequency of atrophy in each region within a patient cohort; areas with progressively lower frequency of atrophy are interpreted as reflecting later stages of disease. Investigating the anatomical progression of disease in non-amnestic Alzheimer's disease (naAD) phenotypes additionally allowed us to assess commonalities and differences in regional atrophy across these naAD variants. We predicted that naAD phenotypes would have unique areas of peak atrophy early in the course of disease, corresponding to previously reported loci of atrophy for each naAD variant and suggesting phenotypic differences in the anatomical origin and progression of atrophy. Additionally, we expected that naAD variants would continue to display relatively less MTL atrophy and thus differ from amnestic AD (aAD) throughout the course of disease.

Then we decided to use longitudinal MRI models to possibly confirm the results from the cross-sectional phasing analysis and to investigate whether aAD and naAD differ in longitudinal rate and anatomic distribution of grey matter (GM) atrophy over time. We reasoned that differences in the longitudinal rate and distribution of degeneration could explain differences in clinical progression across aAD and naAD variants. In order to demonstrate those hypotheses, we used two different approaches: 1) a hypothesis-driven analysis based on the sites of onset showed by the earlier cross-sectional work, where we investigated differences in GM volume at the time of initial MRI as well as volume change over time in regions-of-interest (ROIs) associated with lvPPA, PCA, fvAD, and aAD; 2) an accessory voxelwise analysis of cortical thickness to identify group differences not captured by these ROIs. We sought to identify group differences in atrophy distribution and progression independent of age, which has been previously reported to differ between typical and atypical forms of Alzheimer's disease (Murray et al., 2011). Based on the high neocortical disease burden and

domain-specific cognitive deficits that we previously observed in naAD, we predicted that naAD patients would exhibit faster rates of atrophy in phenotype-specific neocortical ROIs relative to aAD. Additionally, we tested the hypothesis that naAD patients would exhibit slower atrophy than aAD patients in the hippocampus and surrounding MTL areas, as a possible explanation for the relative memory sparing associated with these structures in naAD.

Finally, we compared patterns of atrophy progression over time to measures of inter-regional structural connectivity based on a large population of healthy controls; we anticipated that connectivity would predict longitudinal atrophy, consistent with the transmission hypothesis.

Chapter 3

METHODS

3.1 Cross-sectional study

3.1.1 Participant characteristics

Participants comprised individuals recruited through both the Penn Frontotemporal Degeneration Center (FTDC) and the Penn Memory Center who were clinically diagnosed by experienced neurologists from April 2001 to June 2016. Research protocols were approved by the Institutional Review Board of the University of Pennsylvania, and all patients or caregivers acting on their behalf gave informed written consent, in accordance with the principles of the Declaration of Helsinki. Diagnoses were confirmed in consensus meetings by clinicians with expertise in dementia. General selection criteria included native English speaking ability; age of 45+ years; no evidence of major cerebrovascular disease, history of stroke or head trauma; and no comorbid psychiatric, neurodegenerative, or developmental disorders. Additional criteria included insidious onset, gradually progressive cognitive symptoms, and (for naAD patients) relatively preserved episodic memory. Patient MRIs were reviewed for cerebrovascular disease, hydrocephalus, or white matter lesions; however, GM atrophy was not considered in diagnosis in order to avoid circularity with imaging analyses. AD pathology was confirmed through autopsy (n=22) or cerebrospinal fluid (CSF) total tau/beta-amyloid 1–42 ratio greater than 0.34 (n=107); this cutoff discriminates AD pathology from normal cognition (Shaw et al., 2009) and frontotemporal lobar degeneration (FTLD) (Irwin et al., 2012) with high sensitivity and specificity. CSF protein quantification was performed using the Luminex platform or by enzyme-linked immunosorbent assay (ELISA); ELISA measurements were harmonized with Luminex values using published methods (Irwin et al., 2012). Criteria for aAD followed McKhann et al. (2011) and included primary memory impairment plus deficits in one or more additional cognitive domains. Patients were classified as aAD if they followed an amnestic course across all observations; 6 patients initially diagnosed with amnestic mild

	Control	aAD	lvPPA	PCA	CBS	fvAD	Significative differences
N (MRIs)	115 (238)	40 (68)	41 (90)	27 (51)	17 (31)	23 (39)	
Sex (% male)	42	43	40	41	41	52	
Education (years)	15.9	16.8	16.2	16.0	14.5	15.9	
Age at MRI (years)	62.8	67.9	63.2	59.2	60.1	64.6	
Disease duration (years)	-	4.2	4.0	3.3	4.4	4.6	
MMSE (0–30)	-	20.1	20.9	21.1	16.0	21.4	
PVLT trials 1-5		17.05 (6.64)	20.76 (11.15)	24.63 (8.15)	23.91 (13.60)	19.71 (9.05)	
PVLT delayed recall		0.74 (1.19)	3.76 (3.16)	3.00 (2.68)	4.10 (3.75)	3.71 (2.82)	
PVLT Recognition		0.59 (0.13)	0.77 (0.20)	0.65 (0.22)	0.79 (0.15)	0.79 (0.15)	
Forward Digit Span		5.04 (1.43)	4.22 (1.50)	5.72 (1.26)	4.68 (1.62)	4.88 (2.15)	
Reverse Digit Span		2.75 (1.48)	2.89 (1.14)	3.01 (1.06)	2.05 (1.40)	2.81 (1.59)	
F Letter Fluency		9.36 (6.12)	7.82 (4.50)	11.49 (5.39)	5.15 (4.06)	5.50 (3.98)	PCA > aAD ($t(91)=2.33$, $p<0.022$)
Animal Fluency		7.91 (4.70)	9.33 (5.79)	13.12 (5.96)	8.65 (5.44)	7.95 (3.73)	PCA > aAD ($t(95)=2.66$, $p<0.009$)
Pyramid & Palm Trees		23.85 (2.03)	23.07 (2.68)	23.57 (1.40)	22.73 (1.90)	22.36 (4.70)	
Rey Copy		13.13 (11.61)	27.94 (8.45)	11.78 (11.27)	15.93 (14.50)	20.55 (10.12)	fvAD > aAD ($t(84)=3.27$, $p<0.002$)

Table 1: Participant characteristics at the time of first scan and descriptive statistics and significative differences among groups on neuropsychological analysis. All continuous variables are reported as means (SD).

cognitive impairment (aMCI) subsequently progressed to AD. Conversely, all scans for a patient with an initial non-amnestic presentation were analyzed as the same naAD phenotype, even if that patient subsequently developed memory deficits. Criteria for lvPPA were based on Gorno-Tempini et al. (2011): 24 of 41 cases met full criteria, while 17 of 41 met relaxed criteria allowing the presence of additional semantic or grammatical impairments or the preservation of sentence

repetition abilities (Giannini et al., 2017). PCA diagnosis required visuospatial disturbances (e.g., deficits in object and spatial perception, visual neglect, or oculomotor apraxia) and preservation of other cognitive abilities (Crutch et al., 2012, 2017; Tang-Wai et al., 2004). CBS was diagnosed on the basis of asymmetric extrapyramidal symptoms, corticosensory loss, ideomotor apraxia, and deficits in spatial cognition (as well as other cognitive domains). Finally, fvAD cases were diagnosed on the basis of deficits in executive function or social behavior. Demographic characteristics and Mini-Mental Status Exam (MMSE) total scores are shown in Table 1. The Philadelphia Brief Assessment of Cognition (PBAC; Avants et al., 2014a; Libon et al., 2011b) was used to support patient diagnoses. Demographic differences were assessed using analyses of variance (ANOVAs) with subsequent Tukey's tests for pairwise comparisons (for continuous variables) and $\chi 2$ tests (for dichotomous data). The threshold for statistical significance was $p<0.05$ (two-tailed) for all tests; post-hoc tests were Bonferroni-adjusted for multiple comparisons. Differences in age, disease duration, and Mini-Mental Status Exam (MMSE) score at time of baseline MRI scan were marginally significant [$F(4,124)=2.3$, $p<0.07$; $F(4,124)=2.0$, $p<0.1$; and $F(4,110)=2.4$, $p<0.06$, respectively]; no pairwise differences on these variables were statistically significant (all $p<0.1$, corrected for multiple comparisons). Education did not differ between groups [$F(4, 124)=1.1$, $p<0.4$], nor did sex [$\chi 2(4)=0.8$, $p>0.95$]. The aAD cohort's mean age of 64.9 years facilitates comparison with naAD patients, who tend to have a younger disease onset, but it may limit generalization of aAD results to late-onset AD patients. Patients were characterized on cognitive assessments within 6 months of MRI dates. Global cognition was evaluated by two multidomain assessment scales: the MMSE (Folstein et al., 1975) and the PBAC. Additionally, we analyzed multiple domain-specific cognitive tasks, including the Philadelphia Verbal Learning Test (PVLT; Libon et al., 2011a), from which trials 1–5 total recall, delayed free recall, and recognition discrimination were analyzed; animal category fluency (Weintraub et al., 2009); F-letter fluency (Spreen and Strauss, 1998); forward and reverse digit span (Wechsler et al., 1987);

the Rey Figure (Osterrieth, 1944; Rey, 1944) copy score; and Pyramids and Palm Trees (Howard and Patterson, 1992).

3.1.2 Neuroimaging acquisition and processing

We collected 279 T1-weighted anatomical MRI scans from cognitively normal seniors (controls) and 375 patient scans on the same 3.0-Tesla Siemens TIM Trio scanner. Two raters blinded to each other assigned quality scores using a 5-point scale; cases in which these ratings differed by more than 1 were resolved by consensus. An average score of 3/5 was required for inclusion; this quality check excluded 117 scans, primarily due to patient head motion and poor tissue contrast from older MRI protocols. A single rater similarly evaluated control scans, excluding 41 images. Patients could contribute multiple observations separated by at least 3 months; to prevent overrepresentation of any individual, no patient contributed more than three timepoints or 5% of the scans for a given phenotype, whichever was more inclusive. This criterion resulted in the exclusion of 18 scans. The final sample comprised 238 scans from 115 controls and 240 scans from 129 patients (Table 1).

All T1-weighted images were were acquired axially with 0.98 mm x 0.98 mm x 1 mm voxels, a 256 x 192 matrix, a repetition time of 1620 ms, an inversion time of 950 ms, and a flip angle of 15; they were then processed using the ANTsCorticalThickness function implemented in Advanced Normalization Tools (ANTS; Avants et al., 2014b; Tustison et al., 2014), which implements a symmetric diffeomorphic algorithm (Avants et al., 2011; Klein et al., 2009) with N4 bias-field correction (Sled et al., 1998; Tustison et al., 2010). Images were segmented into 6 classes (cortical GM, subcortical GM, deep white matter, CSF, brainstem, and cerebellum) using template-based priors. We selected 116 regions of interest (ROIs) from the Mindboggle label set (Klein et al., 2012), which were aligned to each T1-weighted image and intersected with GM probability maps to obtain GM

volume estimates for each ROI. Volume was computed from voxels in each ROI with a GM probability greater than 50 percent. GM volumes were normalized by intracranial volume and converted to z-scores based on GM volume in control images. To control for changes over time in scanner hardware and acquisition methods, control groups were created for 3 acquisition periods: 2003–2008, 2008–2012 and 2012–2016. Patients and controls were pair-matched in each subgroup based on age at MRI, education, sex, race, and ethnicity. ROI volumes were statistically adjusted for age at MRI. We then performed outlier checks (i.e., z-scores with an absolute value > 3.0) to identify extreme values due to segmentation error or other artifacts. One scan with outlier values in more than 29 ROIs (representing 25% of the data for that scan) was excluded on this basis.

3.1.3 MRI phasing algorithm

We used a frequency-based phasing algorithm (Figure 1) to model disease progression in each cohort, paralleling the approach of histopathology staging studies. Chronology of atrophy was inferred from the proportion of individuals exhibiting atrophy in each ROI. Atrophy was defined categorically based on a z-score threshold (see below). The ROI with the highest frequency of atrophy was found for each phenotype, and ROIs with atrophy between 90% (inclusive) and 100% of this value were designated Phase 1 regions, representing areas of earliest atrophy. Similarly, Phases 2, 3, and 4 comprised ROIs atrophic in 80–90%, 70–80%, and 60–70% of this highest atrophy rate (inclusive of the lower boundary for each phase). Higher ROI phases thus represent late or inconsistent atrophy across participants. Regions that did not appear in Phases 1–4 represent a hypothetical "Phase 5", i.e., regions that are expected to atrophy in more advanced stages of disease. ROI phase values were subsequently compared to regional measures of pathology (Sections 2.5 and 2.6). Each MRI scan was then compared to the cumulative atrophy patterns predicted in phases 1-4 for the corresponding

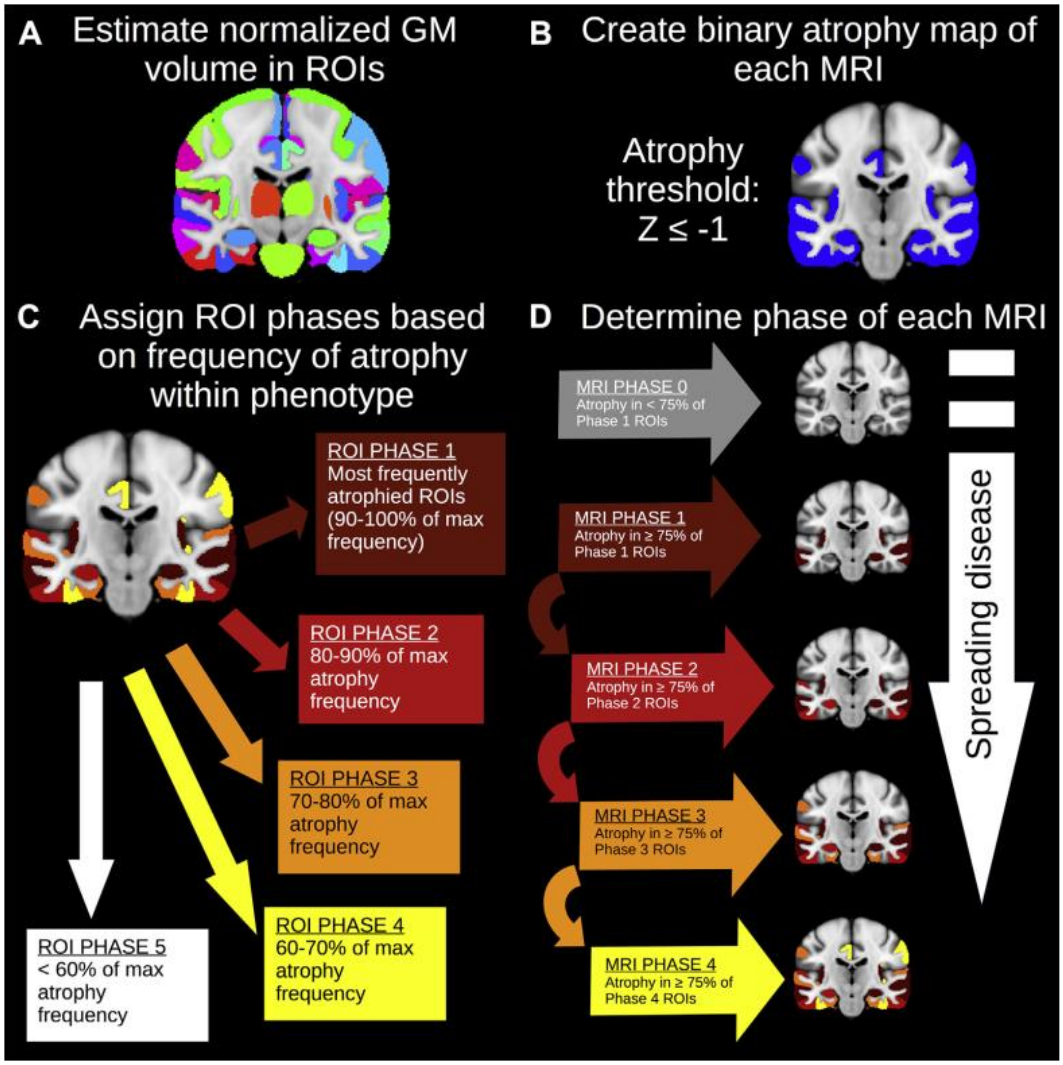

Fig. 1. Frequency-based MRI phase assignment algorithm. Within each patient group, ROIs were ranked by frequency of atrophy. Phase 1 comprised ROIs with an atrophy frequency of 90%e100% of the maximum frequency; phase 2 represented ROIs atrophied in 80%e90% of the maximum; phase 3 included ROIs atrophied in 70%e80% of the maximum; and phase 4 included ROIs atrophied in 60%e70% of the maximum. ROIs with less-frequent atrophy constituted a hypothetical phase 5, that is, they were assumed to be atrophic only in late disease stages. Each scan was subsequently assigned the highest phase value for which it exhibited atrophy in at least 75% of the corresponding ROIs. Scans that did not meet criteria for phase 1 are classified as "phase 0" and assumed to reflect very mild disease progression. Abbreviations: MRI, magnetic resonance imaging; ROI, region of interest.

phenotype. A scan was assigned the highest phase value for which it exhibited atrophy in at least 75% of the ROIs associated with that phase (as well as all preceding phases). This scan-specific phase value (hereafter referred to as "MRI phase" to distinguish from region-specific ROI phase values) was interpreted as a global measure of disease progression for that individual at the time of the scan; higher MRI phases thus indicated more severe global atrophy (Fig. 1D). If a scan did not meet criteria for MRI phase 1, it was classified as a "phase 0" image. The focus of our study was disease progression in naAD; thus, the aAD group was used to determine appropriate parameters for the phasing analysis. The chief parameter tested in this analysis was the z-score threshold used to classify regions as atrophic, which indicates GM volume in units of standard deviation relative to controls, adjusting for intracranial volume and age at time of scan. Threshold values of -2.0, -1.5, -1.0, -0.5, and 0 were assessed; we additionally varied the interval used to delineate one phase from another over values of 5, 10, and 15 percent. We determined the combination of parameters that maximized the association (measured by Spearman's correlation) between ROI phases in the aAD model and Braak staging of AD pathology. Each ROI was assigned a Braak stage based on the earliest appearance of tau neurofibrillary tangle (NFT) pathology in that region, as described by Braak and colleagues (Braak et al., 1990, 1991, 1995, 2006). Because Braak stages 1–2 are generally thought to correspond to an asymptomatic state, and all patients in the current sample were symptomatic, Stages 1–2 regions were collapsed with Stage 3. The z-score threshold (-1.0) and frequency interval (10%) that produced the highest correlation (ρ=0.35, $p<0.001$) were applied to the phasing analysis of naAD phenotypes (Figure 2).

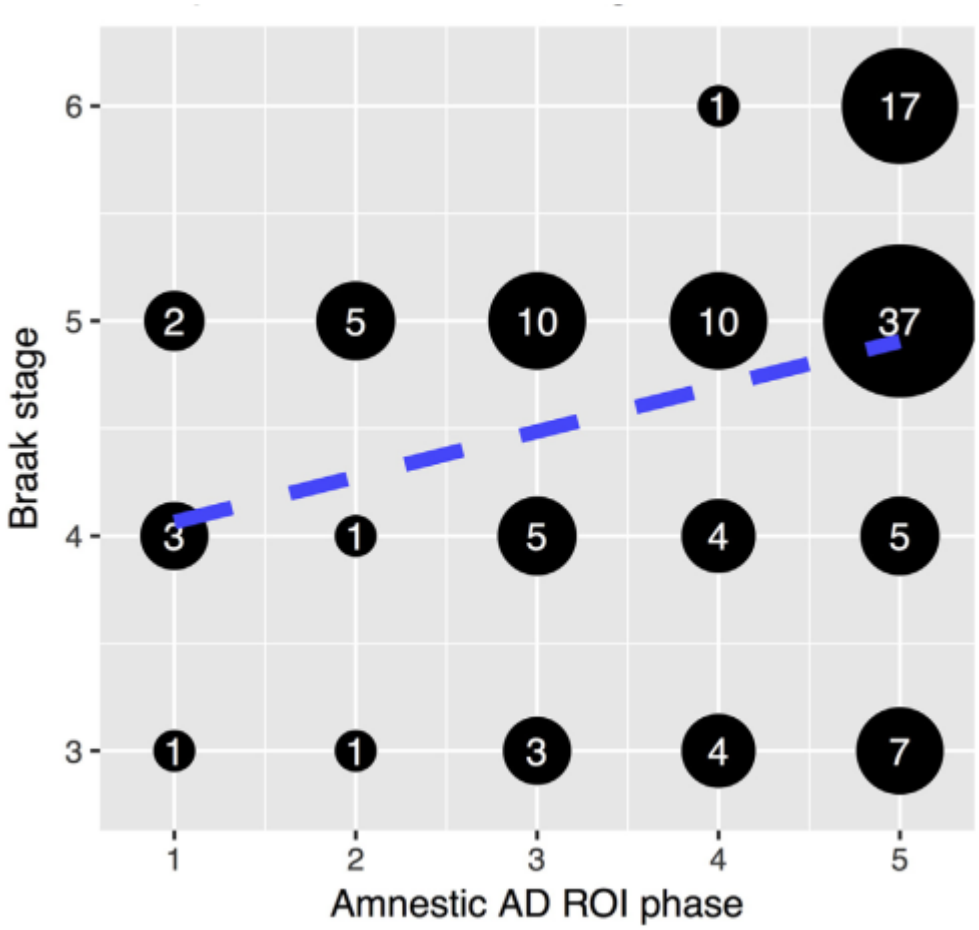

Fig. 2. Scatterplot of ROI phases for the optimal aAD model versus the stage in which tau neurofibrillary tangle pathology first appears, according to the Braak model. Numbers within each black circle indicate the number of data points overplotted in that circle. The blue line is the best-fit regression line. The optimal aAD model used a z-score threshold of 1 to determine atrophy and a frequency interval of 10% to distinguish ROI phases. ROI phase was correlated with Braak stage (9 ¼ 0.35, $p < 0.001$). Abbreviations: aAD, amnestic Alzheimer's disease; ROI, region of interest. (For interpretation of the references to color in this figure legend, the reader is referred to the Web version of this article.)

3.1.4 Associations with neuropathological measures

The MRI phasing algorithm was evaluated by assessing associations between ROI phase and postmortem histopathologic ratings from the Integrated Neurodegenerative Disease Database (Toledo et al., 2014). These ordinal ratings assessed phosphorylated tau (evaluated using anti-PHF1 antibody), β-amyloid

plaques (stained with thioflavin-s), neuronal loss severity, and gliosis (both visually assessed) (Irwin et al., 2016; Montine et al., 2012). Amnestic AD patients were excluded from this analysis to avoid potential bias introduced by the parameter-fitting analysis described in the previous section. Histopathology was performed by expert neuropathologists (EBL and JQT) from the Center for Neurodegenerative Disease Research; data were available for 6 lvPPA, 3 PCA, 4 CBS, and 4 fvAD patients. All measures were represented by scores from 0 (absence of pathology) to 3 (most severe grade) with 6–9 distinct levels, sampled from 11 different regions from a single, randomly-selected hemisphere. The 11 rated regions were the amygdala, hippocampus (average of dentate gyrus and CA1/subiculum ratings), enthorinal area, middle frontal gyrus, angular gyrus, superior/middle temporal gyri, cingulate gyrus, occipital cortex, caudate/putamen, globus pallidus, and thalamus. We used linear mixed effects models (Laird and Ware, 1982) to test associations between these scores and ROI phases for corresponding regions in the same hemisphere. A random intercept term was included in the mixed-effects model to account for correlations among the pathology outcome measures from multiple regions. Additionally, we used general estimating equations (GEEs; Zeger et al., 1988) with a logit link function and exchangeable correlation structure to test the hypothesis that higher ROI phase (indicating later regional onset of atrophy) was associated with lower pathology scores. In this analysis, each pathology variable was binarized such that scores of 2 or higher represented a null outcome, while scores less than 2 represented a positive outcome. This coding scheme was used in order to yield an intuitively interpretable odds ratio (OR) from GEE models. The GEE method accounts for correlations among the binary pathology outcome measures from multiple regions. ORs were computed by exponentiating the ROI phase coefficient

from each GEE model; 95% confidence intervals (CIs) were computed by exponentiating the coefficient +/- 1.96 times its standard error. Finally, we compared the strength of association with ROI phase for each pair of pathology

variables using GEEs that additionally included a factor of pathology measure (e.g., tau 6vs. amyloid) as well as its interaction with ROI phase. Due to the scarcity of autopsy data, all associations with pathology measures were analyzed by collapsing over phenotypes; each patient's histopathology data were compared to ROI phases from the model for the appropriate phenotype. In both linear mixed effects models and GEEs, disease duration at death was included as a covariate. For mixed effects and GEE models, the threshold for statistical significance was $p<0.0125$, corresponding to a threshold of $p<0.05$ with Bonferroni correction for tests of the 4 pathology measures.

3.1.5 Associations with clinical measures

Linear mixed-effects models were used to assess associations of MRI phase with age, disease duration, and neuropsychological performance. Fixed effects included MRI phase, phenotype, and (for cognitive measurements only) patients' baseline values for each outcome, while a random effect of patient was used to model the dependency between repeated measurements collected for each participant across time.

3.1.6 Model-based discrimination of clinical phenotypes

To assess the similarity of atrophy patterns across naAD phenotypes, we first computed each scan's similarity to model-predicted atrophy patterns for all phenotypes. Each scan was converted to a binary atrophy map based on the z-score threshold described above; similarity was then computed using the Sørensen-Dice coefficient (Yushkevich et al., 2010) between this map and model-predicted atrophy patterns for both the same and contrasting phenotypes for the MRI phase associated with that scan. The resulting values reflect the degree to

which a patient's atrophy pattern matches the prediction of the MRI-based phase model for a particular phenotype. We used logistic regression to distinguish scans associated with every pair of phenotypes (a total of 10 models) based on similarity to the atrophy patterns predicted by the two models. We assessed discrimination in terms of sensitivity and specificity. The analyses presented in Figure 6 included patients from all MRI phases. In each model, the phenotype represented by more scans formed the reference group of the regression model (i.e., the "control" outcome), while the phenotype with the smaller sample formed a positive outcome (i.e., "cases"). Clinically similar phenotypes were expected to exhibit more similar patterns of atrophy, resulting in poorer discrimination; clinically dissimilar phenotypes were expected to be well differentiated by patterns and thus have good discriminability. Sample sizes did not permit testing in an independent validation cohort. Furthermore, methods such as leave-one-out or k-fold cross-validation were not well suited to our frequency-based algorithm, as each iteration of cross-validation would generate a new phase model for each phenotype, with substantial variation in the number of classificatory features (i.e., the number of ROIs newly atrophied in each phase). We thus present discrimination results for the study cohort, with the caveat that discrimination performance in independent datasets must be assessed in future research.

3.2 Longitudinal study

3.2.1 Participant characteristics

The longitudinal study used a case-control design starting from the sample of the cross-sectional study: 54 of the 74 patients who composed the final sample were also part of the overmentioned analysis. The final sample thus included 181 T1-weighted MRI scans from 74 patients (25 with lvPPA, 20 PCA, 12 with fvAD, and

	Control	aAD	lvPPA	PCA	fvAD	P
N (MRIs)	37 (85)	17 (40)	25 (66)	20 (48)	12 (27)	
Male	16 (43.2%)	6 (35.3%)	9 (36.0%)	7 (35.0%)	7 (58.3%)	0.672
Education	16.0 [16.0, 18.0]	16.0 [14.0, 18.0]	16.0 [14.0, 19.0]	16.0 [12.0, 16.0]	16.0 [13.5, 18.0]	0.421
Age at MRI (years)	61.9 [57.9, 65.6]	59.4 [53.5, 70.3]	58.5 [56.9, 64.5]	58.0 [55.1, 61.4]	63.9 [59.7, 69.5]	0.137
Inter-scan interval (years)	1.2 [0.9, 1.7]	1.2 [0.9, 1.5]	1.1 [0.9, 1.3]	1.0 [0.9, 1.2]	1.0 [0.7, 1.1]	0.162
Disease duration (years)	—	3.0 [1.9, 4.0]	2.7 [1.7, 3.9]	2.2 [1.3, 4.0]	2.2 [1.8, 5.2]	0.747
MMSE (0–30)	29.0 [28.0, 30.0] (20)	23.0 [20.0, 25.0] (17)	25.0 [23.0, 28.0] (25)	24.5 [18.8, 25.2] (20)	23.0 [17.0, 26.0] (12)	<0.001
Recognition memory (discrimination, 0–1)	1.0 [0.9, 1.0] (7)	0.6 [0.5, 0.7] (10)	0.8 [0.8, 1.0] (25)	0.7 [0.6, 0.9] (19)	0.6 [0.6, 0.8] (12)	<0.001
Speech (0–4)	4.0 [4.0, 4.0] (3)	2.5 [2.5, 3.0] (9)	2.5 [2.0, 3.0] (19)	3.0 [3.0, 4.0] (15)	3.5 [2.2, 4.0] (11)	0.004
Letter fluency (# words/60 s)	19.0 [17.5, 20.5] (7)	9.0 [5.0, 13.0] (13)	8.5 [5.2, 10.8] (22)	10.0 [6.5, 15.5] (19)	6.5 [3.0, 11.0] (12)	0.001
Forward digit span (length correct)	7.0 [7.0, 8.0] (11)	5.0 [3.0, 6.0] (9)	5.0 [4.0, 5.0] (25)	6.0 [5.0, 7.0] (20)	5.0 [4.0, 6.0] (12)	0.005
Rey figure copy (0–12)	12.0 [12.0, 12.0] (3)	11.0 [4.0, 12.0] (9)	12.0 [11.0, 12.0] (19)	2.5 [0.0, 8.8] (12)	9.5 [4.5, 11.0] (10)	0.001
Judgment of line orientation (0–6)	6.0 [6.0, 6.0] (3)	3.0 [0.8, 5.0] (8)	5.0 [4.0, 6.0] (19)	2.0 [0.0, 4.0] (13)	4.0 [3.0, 5.0] (9)	0.004
Social behavior (0–18)	17.0 [17.0, 17.0] (3)	17.5 [16.8, 18.0] (8)	18.0 [17.0, 18.0] (19)	17.0 [16.0, 18.0] (15)	13.0 [11.1, 16.5] (11)	0.004
Oral trail-making test (0–6)	6.0 [5.5, 6.0] (3)	0.0 [0.0, 3.0] (5)	2.0 [0.2, 3.0] (10)	0.5 [0.0, 2.8] (10)	2.0 [0.2, 3.8] (6)	0.051
Reverse digit span (length correct)	6.0 [4.5, 6.0] (11)	3.0 [3.0, 3.0] (9)	3.0 [3.0, 4.0] (25)	3.0 [2.0, 3.0] (19)	3.0 [2.0, 3.2] (12)	<0.001

Table 2: Participant characteristics at time of first scan. Median values and interquartile ranges (square brackets) are given for all continuous variables. Education, disease duration, and age at MRI are expressed in years. For each cognitive score, numbers in parentheses indicate the number of observations per group. P-values reflect the results of a chi-squared test for sex and Kruskal-Wallis tests for all other variables.

17 with aAD) and 85 scans from 37 demographically-matched controls. Not all of the patients could be included as they had to have at least two timepoints; we did't have enough data to include CBS patients, so we decided to drop this variant for the longitudinal analysis. In order to keep a sufficient statical power

we extended the sample with 20 new subjects, recruited through the Penn Frontotemporal Degeneration Center (FTDC) and the Penn Memory Center (PMC). A majority of participants (48/74 patients and 29/37 controls) had only 2 available scans; the remaining participants contributed 3–4 scans each. We included scans acquired with a minimum inter-scan interval of 6 months up to 3.5 years from the initial MRI; beyond this window, there were insufficient observations for a valid analysis. Seven patients had primary neuropathologic diagnoses and 67 had CSF biomarkers (total tau/ ratio greater than 0.34) indicative of Alzheimer's disease pathology as for the cross-sectional study. APOE genotyping was performed on 66 of 74 patients. One patient (white male, aAD, age 51 at onset) with an APOE ε3/ε4 genotype was found to have a mutation in the PSEN1 gene; supplementary analyses indicated that excluding this patient did not have substantive effects on the outcome of key analyses. All patients were clinically diagnosed by experienced neurologists, and diagnoses were confirmed by consensus after patients' initial visit by clinicians with expertise in dementia. NaAD patients had relatively preserved abilities in all cognitive domains except their domain of primary impairment at initial presentation. Due to the challenges of clinically differentiating behavioral/dysexecutive syndromes due to AD vs. FTLD, we performed additional screening on the fvAD group, considering clinical criteria for behavioral-variant frontotemporal dementia per Rascovsky et al.'s (2011), autopsy data without any other comorbidity (2/12 patients), or reviewing CSF data for the others, thus considering also the CSF amyloid values alone (<192 pg/mL; Shaw et al., 2009); among these, sex also had 18F-florbetaben amyloid PET or 18F-flortaucipir Tau PET scans consistent with AD pathology.

Shapiro-Wilks tests indicated non-normal distributions for education and disease duration, age, and MMSE score at initial MRI (all $p<0.001$). Kruskal-Wallis tests of group differences were non-significant, with the exception of MMSE [$(4)=38.5$, $p<0.001$], reflecting patients' cognitive deficits relative to controls. Mann-Whitney tests confirmed that all patient groups exhibited significantly lower MMSE scores

than controls (all U>=428, p<0.001); all other pairwise comparisons were non-significant. To further corroborate naAD patients' domain-specific cognitive impairment, we analyzed neuropsychological performance on assessments independent of those used in clinical diagnosis, including performance on specific items of the Philadelphia Brief Assessment of Cognition (PBAC) (Libon et al., 2011b). Language was assessed in terms of speech features (with lower scores indicating speech and language impairment), forward digit span as a measure of repetition (Giannini et al., 2017), and letter fluency, which is sensitive to deficits in executive-mediated lexical retrieval (Rascovsky et al., 2007; Ramanan et al., 2017). Visuospatial function was assessed by patients' ability to copy a modified version of the Rey complex figure as well as the judgment of line orientation. Social behavior was assessed on an 18-point scale evaluating social comportment, apathy, disinhibition, agitation, empathy, and ritualistic behaviors. Executive function was evaluated through an oral version of the trail-making test as well as backward digit span. Finally, episodic memory was assessed by recognition on the Philadelphia Verbal Learning Test (PVLT) (Libon et al., 2011a) or the PBAC verbal memory test, as available. All neuropsychological assessments were acquired within 1 year of the initial MRI scan (PVLT: mean=0.19 years, SD=0.25; letter fluency: mean=0.14 years, SD=0.25; PBAC: mean=0.21 years, SD=0.27; digit span: mean=0.11 years, SD=0.21). Results were consistent with each phenotype's primary impairment in all domains except for executive function (Table 2).

3.2.2 Neuroimaging methods

T1-weighted MR images were acquired and processed using the same method and parameters of the cross-sectional study until the tissue segmentation phase (included). The processed images were then used to estimate cortical thickness, an altermative method to quantify GM atrophy, instead of GM probability as for the cross-sectional analysis; ANTs cortical thickness measurements have been

extensively validated relative to surface-based methods such as FreeSurfer (Tustison et al., 2014; Klein et al., 2017). We used a joint label fusion approach (Wang et al., 2013) to align the Mindboggle-101 labels (based on the Desikan-Killainy-Tourville label scheme) (Klein and Tourville, 2012) with each image using pseudo-geodesic registration (Tustison and Avants, 2013) and calculated the volume of GM voxels within each label, normalized by intracranial volume and converted to a z-score relative to controls' initial scans. To perform voxelwise group analyses, we warped cortical thickness images to the template using the previously-computed spatial transforms; these images were then spatially smoothed with a 2-sigma Gaussian kernel and downsampled to 2 mm isotropic voxels.

3.2.3 Statistical Analyses

In a hypothesis-driven analysis, we analyzed GM volumes in phenotype-specific ROIs motivated by the cross-sectional analysis for what concerned the naAD variants, while we hypothesized that the aAD group would demonstrate selective atrophy in the MTL, more extensively than what observed in the earlier analysis, so we decided to include bilateral hippocampi, parahippocampal gyri, and entorhinal cortex. Atrophy at the time of initial MRI was analyzed using multiple linear regression models with a factor of group and covariates for age, sex, and MMSE score at the time of initial MRI; controls formed the reference group in these models. Longitudinal atrophy was assessed using linear mixed effects (LME) models with fixed factors of group, time since first scan, and the interaction of group x time. As in the baseline model, covariates included age, sex, and MMSE score at initial MRI. A subject-specific random intercept was included to account for intra-individual correlations in imaging measures. Post-hoc comparisons were performed for the effect of group at initial MRI as well as

the group x time interaction in longitudinal models; values of $p<0.05$, FDR-corrected, were considered significant.

We used LME models to relate GM volume change to neuropsychological performance within 1 year of each imaging session. Due to the limited number of observations, only linear associations between atrophy and time were assessed. The mean interval between test and MRI was 0.30 years (SD=0.30) for recognition memory; 0.22 years (SD=0.29) for letter fluency; 0.18 years (SD=0.29) for digit span; and 0.25 years (SD=0.33) for all other longitudinal neuropsychological measures. Separate LME models were computed for each measure and change in associated ROIs. Thus, recognition performance was related to GM volume in each of the 6 MTL ROIs; language measures were compared to volume change in left middle and superior temporal gyrus; visuospatial measures were related to change in the right superior parietal lobule, precuneus, and angular, supramarginal, and middle temporal gyri; and behavioral and executive measures were related to left anterior insula and middle frontal gyrus as well as right middle temporal gyrus. Neuropsychological performance formed the outcome in each model; predictors treated as fixed effects included regional GM volume at initial MRI and subsequent volume change, as well as covariates of sex and education. Additionally, a subject-specific random intercept was included in the LME model. Due to limited neuropsychological data, controls were omitted from these models. The association with regional volume change in each model was assessed at a significance level of $p<0.05$, FDR-corrected.

Additionally, we performed an accessory voxelwise analysis to investigate differences in cortical thickness that were not assessed by a priori ROIs. ROI-based and voxelwise analyses both present distinct advantages and weaknesses. Voxelwise analysis is not constrained by the borders of anatomically-defined ROIs, and it allows more precise anatomical localization of effects. However, ROI volume is regarded as a more reliable measure of GM atrophy than cortical thickness (Schwarz et al., 2016). Moreover, voxelwise parametric tests depend on patients' displaying neurodegeneration at the same precise point within a brain

area. Thus, ROI-based volumetric analysis may be more sensitive to atrophy if the precise focus of atrophy within a region differs across individuals. Voxelwise analysis did not include hippocampus, where cortical thickness is not well estimated (Han et al., 2006; Gronenschild et al., 2012; Schwarz et al., 2016), but did include entorhinal cortex and parahippocampal gyri. As in ROI-based analysis, we used multiple regression to assess group differences at initial MRI and an LME model to investigate longitudinal atrophy. These voxelwise models used the same regression formulae as ROI-based models, and the LME was implemented in the 3dLME (Chen et al., 2013) function from the Analysis of Functional NeuroImaging (AFNI) software suite. Multiple comparisons correction was performed by first thresholding voxelwise results at $p<0.001$ (uncorrected), then applying a cluster extent threshold corresponding to a cluster-wise alpha value of 0.05. To calculate cluster extent thresholds, we first estimated spatial auto-correlation from the model residuals using AFNI's 3dFWHMx. We then used the 3dClustSim function, which is based on a Monte Carlo approach (Forman et al., 1995; Cox et al., 2017), to determine the cluster size corresponding to a false-positive rate of 0.05 at a voxelwise threshold of $p<0.001$ (uncorrected). These simulations indicated a cluster threshold of 73 voxels (i.e., 584) for the baseline MRI model and a threshold of 75 voxels (600) for the longitudinal LME model. For both the baseline effect of group and the group x time interaction, we performed post-hoc contrasts between all groups, which were corrected to cluster-wise $p<0.05$ using the same method.

3.4 Structural connectivity

To investigate associations between atrophy progression and brain connectivity, we related longitudinal atrophy to population-average structural connectivity measures computed by Yeh et al. (2018). The decision to use population-average connectivity measures rather than estimating connectivity from patients was

based on both practical and conceptual considerations. First, constraining participant selection by the availability of white-matter imaging data would have further reduced sample sizes. Second, white-matter degeneration in patients' brains might adversely affect fiber tractography, leading to false negatives in estimating region-to-region brain connectivity.

Yeh and colleagues reported a whole-brain connectivity matrix (available at http://brain.labsolver.org/) based on diffusion MRI data from 842 healthy participants in the Human Connectome Project; connectivity values represent average anisotropy values for white-matter fiber tracts connecting 65 regions in a modified version of the Automated Anatomical Labeling (AAL) brain parcellation (Tzourio-Mazoyer et al., 2002). Because label boundaries for major cortical structures vary between the AAL and Mindboggle parcellations, we warped the modified AAL atlas into the native acquisition space for each of the T1-weighted scans in the current study and re-computed GM volumes based on this parcellation.

Using the igraph package for R (https://igraph.org/r/), we created an unweighted, undirected graph of structural connectivity from Yeh et al.'s (2018) connectivity matrix, omitting the cerebellum and brainstem to yield a total of 62 nodes (i.e., brain areas). The degree of each node was computed as the number of non-zero white-matter connections with other regions. Self-connections were excluded; thus, the maximum possible degree of a node was 61. As with Mindboggle labels, volumes were normalized by each participants' intracranial volume and converted to a z-score relative to the region-wise mean and standard deviation of the control sample. We calculated annualized change in GM volume over time for each region by subtracting these z-score volume measures from the first and last available scans for each participant and dividing by the time interval. We then computed a linear mixed effects model with annualized change as the outcome and fixed effects of group, node degree, and the group x degree interaction, covarying for the baseline volume of each region, patients' age at initial MRI, and sex. The average volume of each region (i.e., raw volume divided

by intracranial volume) among control participants was also included as a covariate to ensure that variation in node degree did not simply reflect differences in region size. A random intercept was estimated for each participant, and a significance threshold of $p<0.05$ was used.

Chapter 4

RESULTS

4.1 Cross-sectional study

4.1.1 Atrophy originates in and progresses throughout the neocortex in naAD

We observed a unique distribution of atrophy for each phenotype. As in autopsy studies of pathology, which assume that areas commonly affected across the brains of both mild and more advanced disease patients are chronologically the first to develop such pathology, phase 1 ROIs are interpreted as the anatomical origin of atrophy (Fig. 3). Over phases 1-4, the aAD group showed severe involvement of MTLs and lateral temporal lobes with slight right lateralization. Phase 1 ROIs for the aAD group included the right hippocampus and STG as well as bilateral MTG, left anterior insula, and left supramarginal gyrus (SMG). In subsequent phases, this atrophy appeared to spread to the left hippocampus and bilateral MTL; left lateral temporal, parietal, and ventral prefrontal lobes; right temporal and dorsal prefrontal lobes; and bilateral medial parietal regions. In comparison, naAD groups exhibited unique profiles of progression that differed from aAD. The lvPPA cohort exhibited strong asymmetry, with frequent atrophy in phase 1 focused on the left MTG and STG. The lvPPA model indicated progression to ipsilateral parietal and frontal lobes and the contralateral temporal lobe. The PCA model indicated an asymmetric onset in phase 1 in the right ANG, superior parietal lobule, precuneus, SMG, and MTG; subsequent progression was notable throughout left parietal and bilateral temporal, occipital, and (to a lesser extent) frontal lobes. The CBS group exhibited a left-dominant atrophy onset, with phase 1 involving the left ANG, SMG, MTG, precuneus, and planum temporale as well as bilateral superior parietal lobule; disease progression heavily involved the remaining neocortex, from lateral occipitoparietal regions to temporal and frontal cortices.

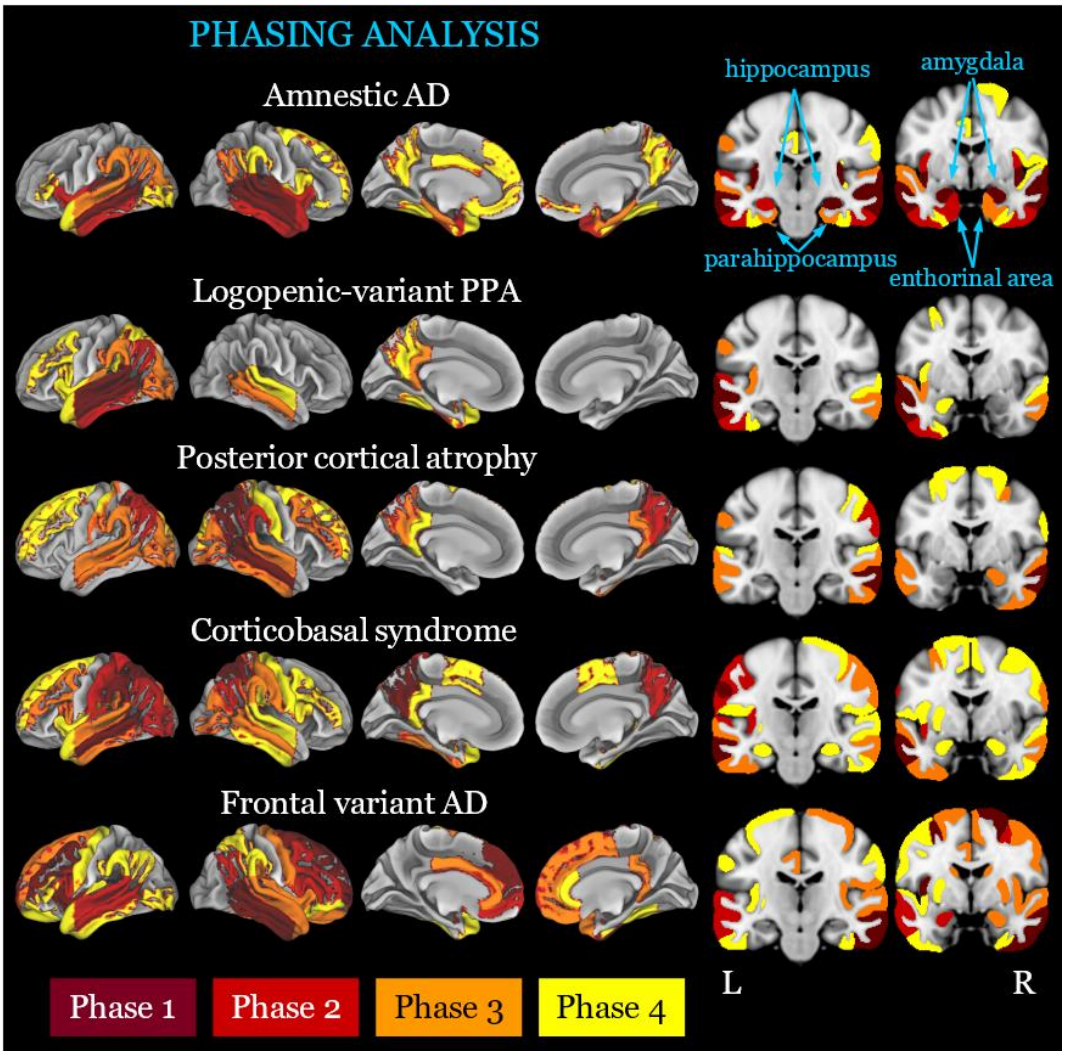

Fig. 3. Phenotype-specific disease progression models. Phases 1–4 are indicated by maroon, red, orange, and yellow colors, respectively. Left: projections on lateral and medial cortical surfaces; right: coronal slices at the level of the hippocampus and parahippocampus (left) as well as the amygdala and entorhinal cortex (right).

Finally, phase 1 ROIs in the fvAD model included the left MFG, left anterior insula, and right MTG. This model indicated a subsequent spread of atrophy to bilateral prefrontal, temporal, and inferior parietal cortices. Notably, aAD was the only phenotype that showed early involvement of the hippocampus and MTL, which were relatively spared in the other phenotypes. Indeed, only the CBS and PCA groups exhibited hippocampal atrophy, which occurred in phases 3-4. Atrophy patterns increasingly overlapped across phenotypes as disease progressed (Fig. 7), as indicated by a main effect of phase on model-based

atrophy predictions [$t(38) = -7.6$, $p < 0.001$]. Furthermore, ROIs with lower phase values were more severely atrophied: across phenotypes, mean adjusted volume for phase 1 ROIs was -2.7 (1.3); for phase 2, -2.1 (1.4); for phase 3, -1.8 (1.4); for phase 4, -1.5 (1.4); and for phase 5, -0.5 (1.3). These means reflected a significant linear relationship between ROI phases and adjusted ROI volumes [$\beta = -0.32$, $t(27{,}710) = -58.8$, $p < 0.001$]. In addition, restricting the data set to include only the first available scan for each patient yielded highly similar ROI phase assignments (Table 3).

Group	-2	-1	0	1	2
aAD	0.00	0.06	0.85	0.09	0.00
lvPPA	0.00	0.07	0.93	0.00	0.00
PCA	0.02	0.18	0.78	0.03	0.00
CBS	0.03	0.19	0.76	0.03	0.00
fvAD	0.00	0.10	0.80	0.09	0.01

Table 3. Distribution of differences in ROI phase (all scans available versus only first scan per patient). Values represent the proportion of the 116 Mindboggle labels exhibiting a given difference for each group

4.1.2 ROI phase is associated with multiple histopathologic measures

In each phenotype, phase 1 ROIs were few in number, consistent with a relatively focal disease origin; in contrast, the phase 5 ROI category represented the largest category for each phenotype. Among early-phase brain areas, which begin to atrophy early in the disease course, nearly all exhibited severe pathology in postmortem examination. Conversely, late-phase brain areas, which were presumed to be atrophied only late in the disease course, had a wider distribution of pathology scores, including a higher proportion of regions with minimal pathology. In linear mixed-effects models, all 4 neuropathological measurements were thus inversely associated with ROI phases in naAD

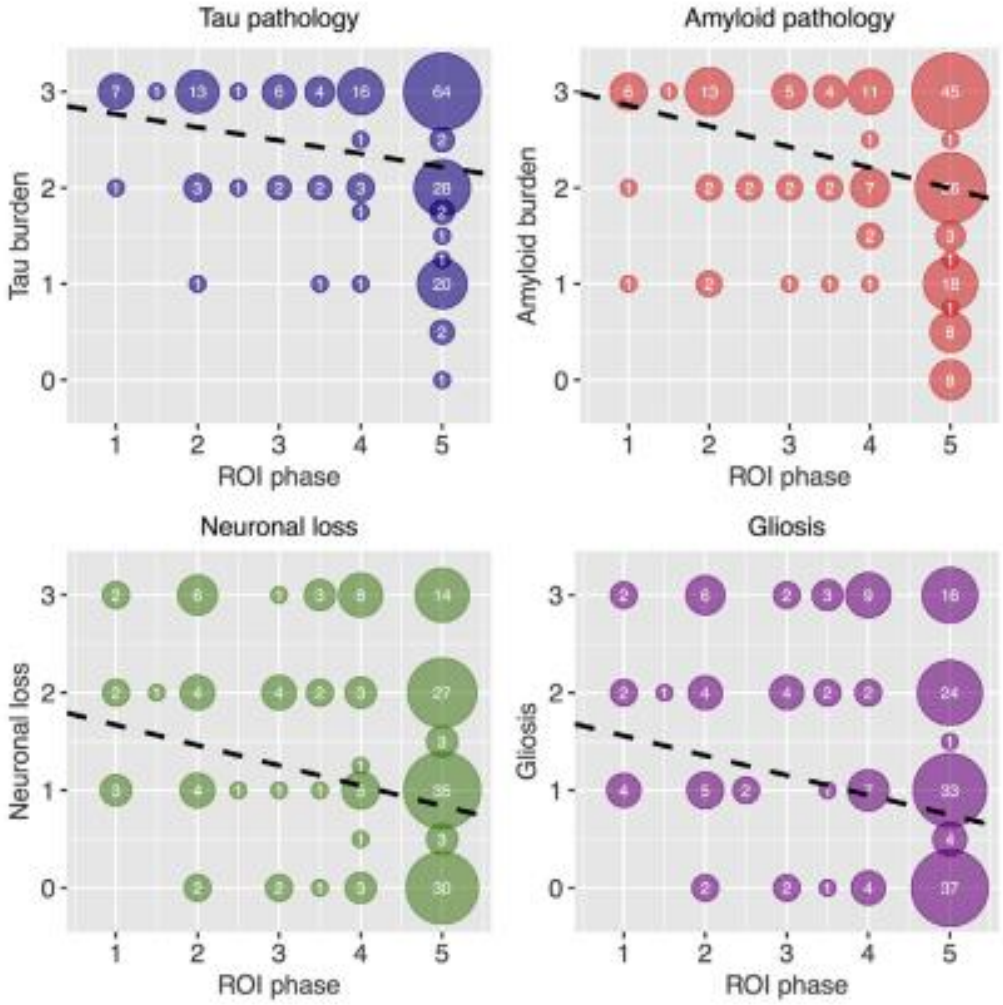

Fig. 4. Associations between ROI phase and regional micropathology ratings. Top left: tau neurofibrillary tangle burden; top right: b-amyloid burden; bottom left: neuronal loss; and bottom right: gliosis burden. Each data point represents one of 11 brain areas in one of 17 naAD patients. Numbers within each circle indicate the number of observations overplotted in that circle. The dashed black line in each plot is plotted from the slope and intercept terms of the corresponding linear mixed-effects model. Abbreviations: naAD, nonamnestic Alzheimer's disease; ROI, region of interest.

phenotypes (Fig.4): tau burden [b β = -0.14, t(168) = -3.2, p < 0.005], β-amyloid plaque burden [β = -0.22, t(168) = -4.2, p < 0.001], neuronal loss severity [β = -0.21, t(155) = -3.7, p < 0.001], and gliosis [β = -0.20, t(162) = -3.8, p < 0.001]. Similarly, analysis of binarized pathology outcomes indicated that higher ROI phase was associated with lower scores for all measures. The greatest effect based on OR

magnitude was observed for tau pathology (OR = 2.2, 95% CI ¼ 1.1, 4.1), followed by amyloid pathology (OR = 1.7, 95% CI = 1.1, 2.5), neuronal loss (OR = 1.4, 95% CI = 1.1, 1.8), and gliosis (OR = 1.4, 95% CI = 1.1, 1.7). In direct comparisons, however, associations with an ROI phase did not significantly differ for any of the pathology variables analyzed (i.e., no interactions of ROI phase and variable type, all $z < 1.3$, $p > 0.17$).

4.1.3 Clinical profile is associated with MRI phases

Across the entire cohort, the MRI phase was associated with disease duration [Fig. 5A; $\beta = 0.71$, $t(109)$ ¼ 9.4, $p<0.001$], indicating that a 1-phase increment was associated with approximately 8.5 months of disease duration. In addition, MRI phase was associated with 2 multidomain cognitive measures (Fig. 5B and C): MMSE [$\beta = -0.92$, $t(74) = -4.2$, $p<0.001$] and PBAC [$\beta = -1.1$, $t(17) = -2.7$, $p<0.05$]. Fig. 5D-I illustrates associations with MRI phases for domainspecific neuropsychological assessments: associations included measures of verbal learning and recall, lexicosemantic retrieval, executive control, short-term and working memory, and visuospatial cognition (see regression coefficients in figure). The MRI phase was not associated with recognition [$\beta = -0.01$, $t(37) = -1.2$, $p<0.3$], letter fluency [$\beta = -0.3$, $t(51) = -2.0$, $p<0.06$], or the Pyramids and Palm Trees task (word stimuli, even trials only; [$\beta = -3$, $t(21) = -2.0$, $p<0.06$]).

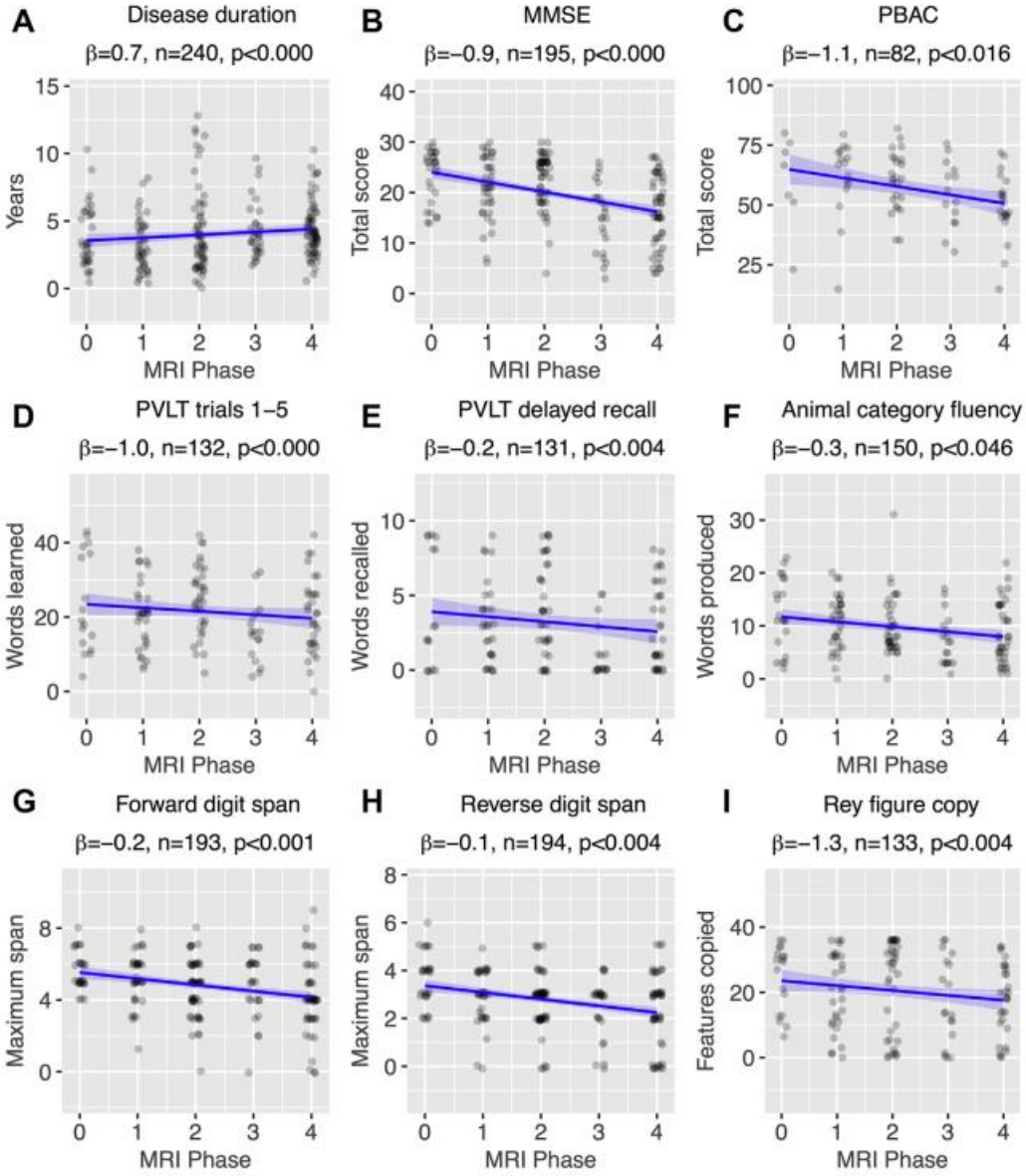

Fig. 5. Associations between MRI phase and (A) disease duration or (B-I) neuropsychological performance. Each data point represents a single observation associated with a single scan. All phenotypes are plotted together; the x-axis indicates the MRI phase associated with each scan, as a measure of disease progression. Each plot title includes the regression coefficient for the association with MRI phase, the number of observations in each analysis, and the p-value for the MRI phase regression coefficient. Abbreviations: MMSE, MinieMental Status Examination; MRI, magnetic resonance imaging; PBAC, Philadelphia Brief Assessment of Cognition; PVLT, Philadelphia Verbal Learning Test.

4.1.4 Logistic regression based on MRI phase models discriminates clinical phenotypes

Logistic regression models accurately distinguished AD phenotypes based on similarity to atrophy patterns predicted by phase models (Fig. 6). Moreover, sensitivity and specificity varied with the clinical similarity of AD phenotypes. Perfect separation was observed for comparison of fvAD scans (which most frequently exhibited prefrontal and temporal atrophy) to both PCA and CBS scans (which exhibited frequent parietal and posterior temporal atrophy). The contrast of PCA and CBS yielded the poorest performance of all 10 models, reflecting similar atrophy in these 2 phenotypes.

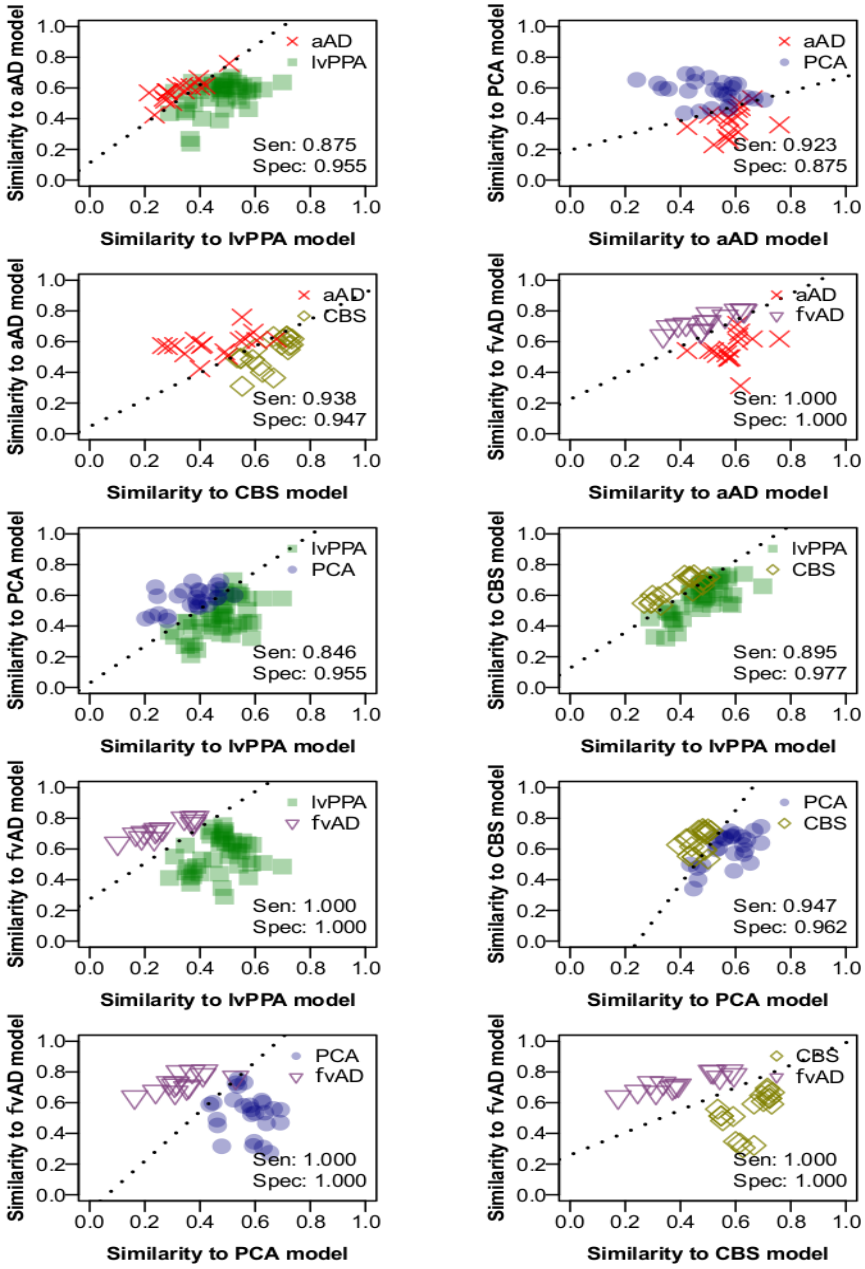

Fig. 6. Phenotype discriminability based on disease progression models. Each panel represents a logistic regression model trained to discriminate between 2 AD phenotypes. Each point represents a single scan from a patient with one of the 2 clinical phenotypes. The x- and y-axes represent spatial overlap (expressed by Sorensen-Dice coefficients) between the binary atrophy map for a single scan and the modelpredicted atrophy map for the appropriate phenotype and MRI phase. Abbreviations: aAD, amnestic Alzheimer's disease; fvAD, behavioral/dysexecutive Alzheimer's disease; CBS, corticobasal syndrome; lvPPA, logopenic-variant primary progressive aphasia; MMSE, MinieMental Status Examination; MRI, magnetic resonance imaging; PCA, posterior cortical atrophy; Sen, sensitivity, indicating proportion of scans correctly identified for the phenotype on the y-axis; Spec, specificity, indicating scans correctly identified for the phenotype on the x-axis.

Atrophy patterns in aAD and naAD became more similar with higher MRI phases (Fig. 7), reflecting the convergence of phenotypes in advanced disease. In fact, to quantify overlap between disease progression patterns for different phenotypes, and to assess the utility of MRI phase models for distinguishing different phenotypes, we calculated dissimilarity measures (1 – the Sørensen-Dice coefficient) between cumulative binary atrophy maps for every pair of phenotypes in each phase (Fig. 7, black lines). This analysis confirmed that the disease progression models in Figure 3 were most distinct in early phases (1–2) and became more similar as disease progressed. In addition to model overlap, we assessed the overlap of binary atrophy maps for individual scans (Fig. 7, green lines) by comparing every MRI Phase 1 scan for a given phenotype to every MRI Phase 1 scan of a second phenotype; every Phase 2 scan of the first phenotype to every Phase 2 scan of the second phenotype; and so forth. Overlap of individual scans was lower than overlap between atrophy models, possibly due to atrophy in ROIs not included in the models.

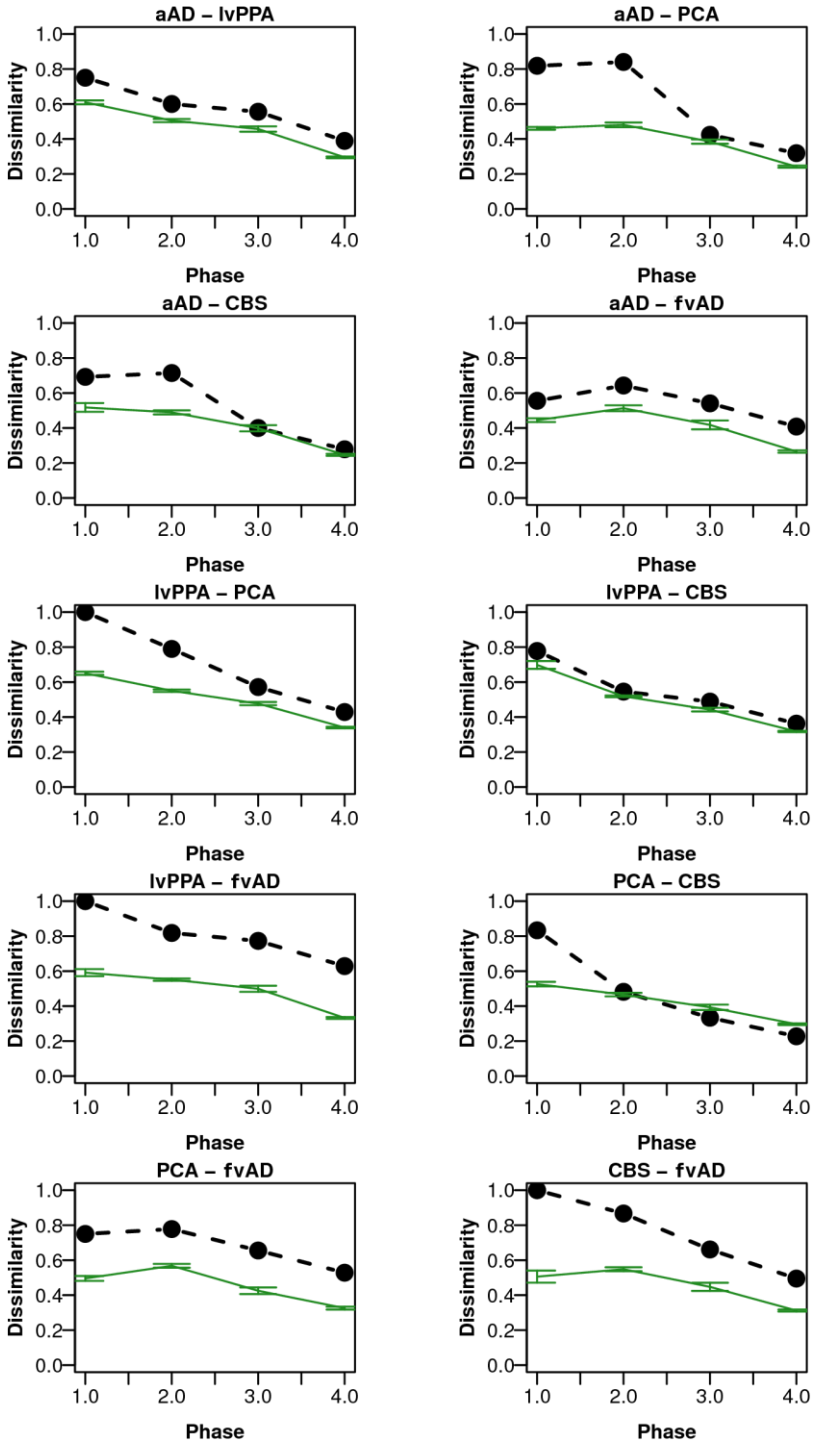

Figure 7. Pairwise dissimilarity of AD phenotypes at each MRI phase. The y-axis of each plots represents 1 minus the Sorensen–Dice coefficient for comparisons of binary atrophy maps, such that 0 indicates two identical maps, while 1 indicates completely dissimilar maps. Black lines: dissimilarity for two disease progression models, where each phase represents cumulative atrophy from the current and all previous phases. Green lines: mean dissimilarity for all pairwise comparisons of scans in one group with all those in a second group, stratified by MRI phase. Error bars indicate the standard error of the mean.

4.2 Longitudinal study

4.2.1. Hypothesis-driven analysis of ROI volumes

Areas of earlier atrophy in each phenotype

We first assessed both regional volume at initial MRI and longitudinal volume change in each group relative to matched controls in ROIs associated a priori with each phenotype. The purpose of this hypothesis-driven analysis was two-fold: first, to dissociate effects of earlier vs. later degeneration that are confounded by cross-sectional studies; and second, to test hypotheses regarding differential rates of atrophy between phenotypes. This analysis identified multiple regions displaying initial atrophy in each phenotype (Table 4), which reflect atrophy prior to patients' initial scans. While a subset of these regions continued to degenerate over the follow-up period (Table 4, green cells), others exhibited no further change (blue cells). Additionally, we detected a number of regions that were not atrophied relative to controls at the initial scan but demonstrated progression over the follow-up period (red cells); these areas are interpreted as areas of later disease spread in each phenotype. In cross-sectional analysis of participants' initial MRI scans, all ROIs exhibited a main effect of group, independent of age and MMSE.

Patterns of atrophy at initial MRI corroborated prior cross-sectional studies of naAD, supporting the accuracy of clinical diagnoses. LvPPA patients exhibited strong lateralization of disease, with early atrophy relative to controls and other patient groups in left superior and middle temporal gyri (Table 4, Figure 8). Additionally, they had significant atrophy relative to controls in left anterior insula, hippocampus, and middle frontal gyrus as well right middle temporal gyrus. PCA patients, in turn, had significant atrophy at first MRI in right

A priori association	Region	$F_{First\ MRI}(4,103)$	aAD	lvPPA	PCA	fvAD	$F_{Group\ x\ Time}(4,150)$	aAD	lvPPA	PCA	fvAD
aAD	L entorhinal	7.2***	-3.4	-1.5	-1.5	-0.1	6.7***	-2.2	-3.7	-3.3	-3.9
	R entorhinal	5.5***	-2.6	0.7	-1.9	-0.1	7.4***	-4.1	-2.9	-4.1	-3.0
	L hippocampus	8.4***	-4.6	-3.2	-2.1	-1.6	5.4***	-4.1	-2.9	-2.9	-0.3
	R hippocampus	7.4***	-4.3	-1.7	-3.1	-1.8	4.7**	-3.5	-2.3	-3.4	-1.2
	L parahippocampal	2.8**	-1.7	-2.1	0.1	0.8	5.6***	-3.5	-4.0	-2.6	-2.1
	R parahippocampal	1.6*	-2.2	-0.5	-1.3	-0.3	5.9***	-3.7	-2.5	-4.0	-0.5
lvPPA	L middle temporal	30.5***	-3.0	-7.3	-3.2	-3.0	34.7***	-9.6	-9.2	-6.4	-5.3
	L superior temporal	21.5***	-2.6	-6.8	-2.3	-1.8	17.3***	-4.4	-8.1	-3.7	-2.8
PCA	R angular	14.7***	-2.8	-1.3	-3.9	-3.0	2.4	-1.4	-2.6	-2.5	-1.0
	R precuneus	9.8***	-0.7	-0.5	-4.4	-1.3	13.7***	-6.5	-4.8	-4.5	-0.9
	R superior parietal lobule	16.7***	0.6	0.0	-5.5	-1.7	4.2**	-3.6	-2.7	-2.1	-0.1
	R supramarginal	6.4***	0.2	0.4	-2.6	-0.6	11.2***	-6.5	-3.1	-2.6	-0.5
fvAD	L anterior insula	10.3***	-2.1	-2.6	0.6	-3.4	3.5*	-2.0	-1.6	-0.4	-3.3
	L middle frontal	15.3***	-2.6	-3.8	-2.4	-4.4	8.2***	-3.9	-4.9	-3.8	-2.1
PCA, fvAD	R middle temporal	23.6***	-2.8	-2.7	-5.6	-4.2	44.8***	-11.3	-9.3	-7.5	-6.4
Reference ROI	L precentral	3.4***	0.8	-1.3	-1.4	1.2	3.7**	-3.1	-3.1	-2.1	-1.3
	R precentral	5.4***	0.2	-0.7	-2.9	-0.7	5.0**	-3.3	-3.3	-3.3	-0.6

Table 4: Differences in grey matter volume at initial MRI and longitudinal atrophy in hypothesis-driven analysis of regional brain volumes, relative to matched controls. Hypotheses included selective atrophy of neocortical areas associated with early disease in naAD10 and of the MTL (hippocampus, entorhinal cortex, and parahippocampal gyrus) in aAD patients. The left and right precentral gyri are included to demonstrate the regional specificity of atrophy. F-statistics indicate the main effect of group at initial MRI scan and the group x time interaction across all scans. Additional columns report z-statistics for pairwise contrasts of each patient group vs. controls. Blue cells indicate significant differences in volume only at initial MRI; red cells indicate significant differences in longitudinal atrophy rates; and green cells indicate differences in both initial volume and longitudinal atrophy, based on a threshold of p<0.05, FDR-corrected. n.s.=non-significant; *p<0.05; **p<0.01; ***p<0.001

hippocampus, angular gyrus, precuneus, and superior parietal lobule as well as bilateral middle temporal gyri. FvAD patients had significant atrophy in left anterior insula and middle frontal gyrus; right angular gyrus; and bilateral middle temporal gyri. The precentral gyrus, which comprises primary motor areas, exhibited early atrophy only in the PCA group and was restricted to the right hemisphere, consistent with these patients' global atrophy pattern; the relative sparing of these structures is consistent with patients' preserved motor function and demonstrates the regional specificity of atrophy patterns. The aAD patients exhibited initial atrophy relative to controls in bilateral hippocampi and entorhinal cortex, left middle frontal gyrus, bilateral temporal cortex, and right angular gyrus. These temporoparietal areas have been previously characterized as nodes of the

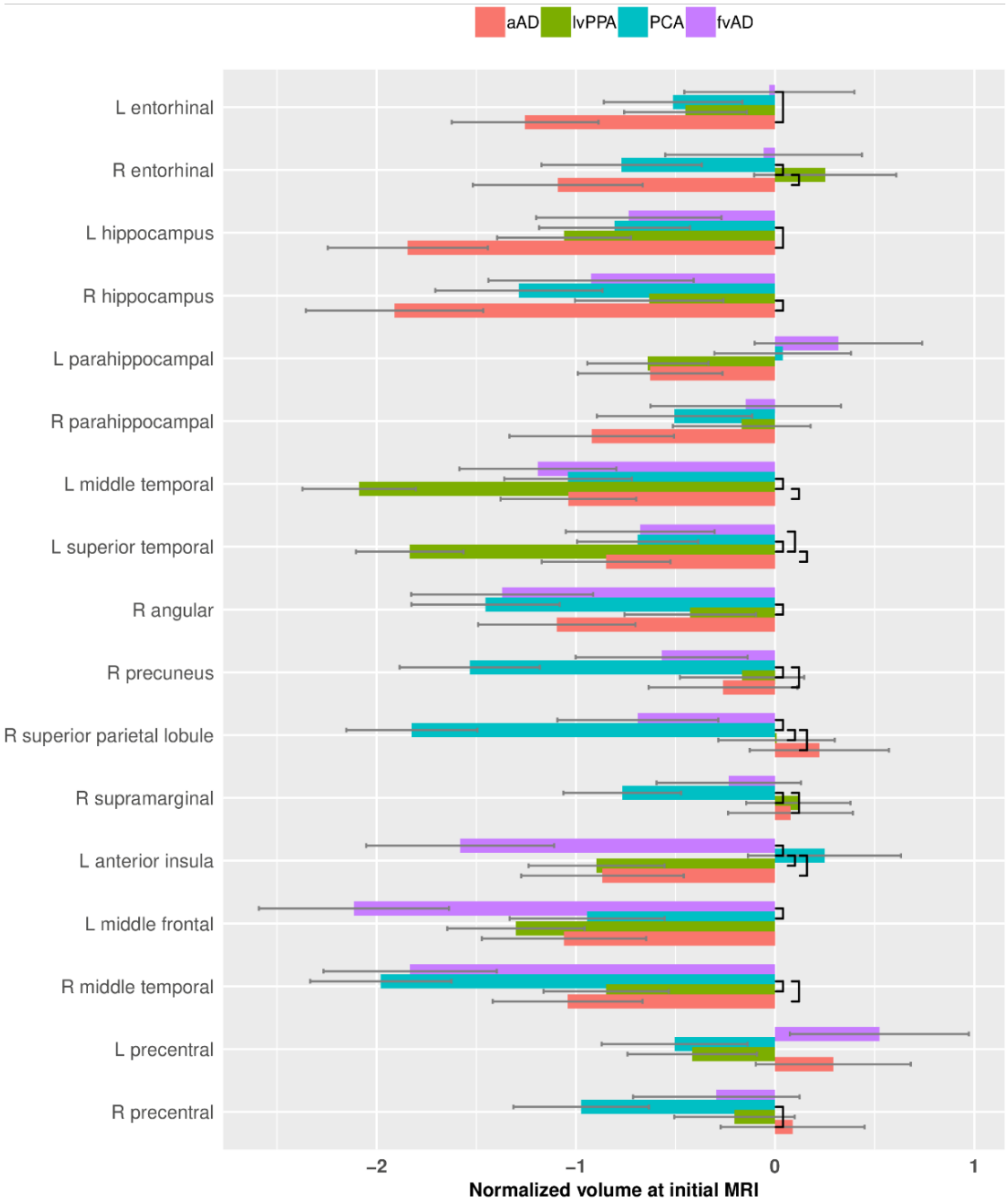

Figure 8: Patient group differences at time of initial MRI in normalized volumes for a priori regions of interest. Plotted values are the regression coefficients representing the difference in regional grey matter volume between each patient group and the healthy control reference group, expressed in z-score units. Error bars represent the standard error of each regression coefficient. More negative values on the x-axis indicate greater atrophy. Black brackets indicate significant pairwise group differences ($p<0.05$ after FDR correction).

posterior default mode network in which different AD phenotypes demonstrate convergence of atrophy patterns (Ossenkoppele et al., 2015a). Additionally, aAD patients demonstrated more severe atrophy than naAD groups in bilateral hippocampi and entorhinal cortex (Figure 8). Non-amnestic patients exhibited characteristic sparing of MTL structures, with initial atrophy limited to left hippocampus in lvPPA and right hippocampus in PCA. In longitudinal models, areas of significant early atrophy tended to demonstrate further progression over the follow-up period relative to controls (Table 4, green cells). However, a subset of brain areas had a non-significant slope of change over time (Table 4, blue cells), suggesting a slowing of atrophy. These areas included left entorhinal and right angular gyrus in aAD; left anterior insula in lvPPA; right superior parietal lobule in PCA; and left middle frontal gyrus in fvAD.

Longitudinal analysis identifies areas of later change in each phenotype

Additionally, multiple brain areas in each phenotype demonstrated significant change over time despite an absence of atrophy at initial MRI (Table 4, Figures 8 and 9); these areas appear to represent disease spread in later stages. In the neocortex, lvPPA patients exhibited longitudinal atrophy in right temporoparietal areas, while PCA patients exhibited new left-hemisphere atrophy in superior temporal and middle frontal gyrus. FvAD patients exhibited new atrophy in left superior temporal gyrus, marking lateral temporal cortex as one of the most consistent areas of longitudinal change across patient groups. In the MTL, aAD, lvPPA, and PCA patients all exhibited later atrophy in bilateral parahippocampal gyri; and all three naAD groups demonstrated later atrophy in bilateral entorhinal cortex. Additionally, PCA patients exhibited later-stage atrophy in right hippocampus. Finally, in precentral gyrus reference regions, all patient groups except fvAD exhibited longitudinal change relative to controls, consistent with their more advanced disease status; however, in the PCA group

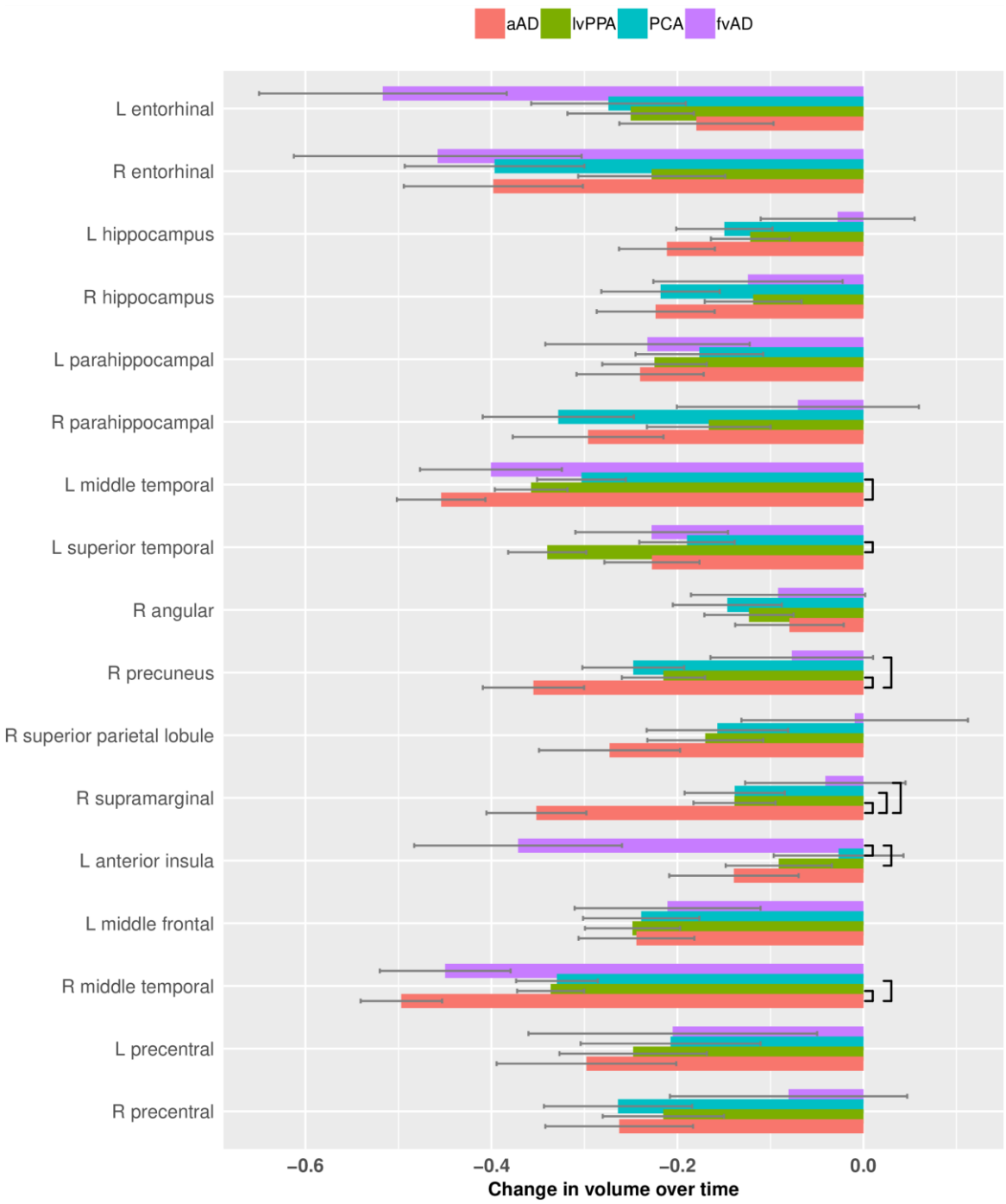

Figure 9: Patient group differences in the effect of time for a priori regions of interest. The plot displays regression coefficients for annualized change in regional grey matter volume in each group, expressed in z-score units relative to the healthy control reference group. Error bars represent the standard error of each regression coefficient. More negative values on the x-axis indicate more rapid atrophy over time. Black brackets indicate significant pairwise group differences ($p<0.05$ after false discovery rate correction).

this change remained restricted to the right hemisphere.

Group differences in regional rates of change

The longitudinal design allowed us to test the hypothesis that each naAD phenotype would exhibit faster atrophy in its associated neocortical ROIs than other patient groups, consistent with phenotype-specific disease patterns (Fig. 9). Additionally, we predicted that naAD patients would exhibit more gradual rates of change in MTL structures than aAD patients, providing a dynamic correlate of MTL sparing in naAD. These hypotheses were tested through pairwise contrasts of group x time interaction terms from linear mixed effects models of GM volume change. Consistent with hypotheses, lvPPA patients had more rapid atrophy than PCA patients in left superior temporal gyrus ($z=2.8$, $p<0.02$) as well as marginally more rapid change than aAD patients ($z=2.1$, $p<0.09$). Similarly, the fvAD group exhibited significantly greater atrophy rates in left anterior insula than lvPPA ($z=2.5$, $p<0.04$) and PCA patients ($z=2.9$, $p<0.02$). Contrary to hypotheses, PCA patients did not exhibit faster neurodegeneration during the follow-up period than other phenotypes. Because PCA is associated with heterogeneous disease distributions including ventral occipito-temporal variants (Crutch *et al.*, 2017), we performed supplementary analyses of longitudinal atrophy in lateral occipital cortex, which we represented through bilateral inferior occipital gyri. While PCA patients exhibited significantly lower GM volumes than controls in both left and right inferior occipital gyri, there were no significant differences in either mean volumes or rates of longitudinal change with other patient groups (data not shown).

In addition, aAD patients had more rapid atrophy in right middle temporal gyrus than lvPPA ($z=3.5$, $p<0.01$) and PCA patients ($z=3.2$, $p<0.01$); in left middle temporal gyrus relative to lvPPA ($z=2.7$, $p<0.03$); in right precuneus relative to lvPPA ($z=2.5$, $p<0.04$) and fvAD ($z=3.0$, $p<0.02$); and in right supramarginal gyrus relative to all three naAD groups (all $z>3.3$, $p<0.01$). We had predicted that naAD patients would exhibit more gradual atrophy than aAD patients in MTL

structures. However, all patient groups demonstrated significant atrophy relative to controls in one or more MTL structures (Table 4), and we found no significant differences between patient groups in atrophy rates for bilateral hippocampi, entorhinal cortex, or parahippocampal gyri. To address limitations in statistical power, we performed a supplementary analysis on MTL ROIs in which all naAD phenotypes were combined into a single group; while both the naAD and aAD groups had significantly faster atrophy than controls in all 6 MTL regions, we again observed no difference in atrophy rates between naAD and aAD (Table 5).

Region	Comparison	Z	P
Right Hippocampus	**aAD-Control**	**-3.52**	**0.001**
	naAD-Control	**-3.27**	**0.002**
	naAD-aAD	1.21	0.275
Left Hippocampus	**aAD-Control**	**-4.10**	**0.000**
	naAD-Control	**-3.28**	**0.002**
	naAD-aAD	1.81	0.095
Right Ent entorhinal area	**aAD-Control**	**-4.10**	**0.000**
	naAD-Control	**-4.30**	**0.000**
	naAD-aAD	1.04	0.336
Left Ent entorhinal area	**aAD-Control**	**-2.16**	**0.045**
	naAD-Control	**-4.75**	**0.000**
	naAD-aAD	-1.31	0.238
Right PHG parahippocampal gyrus	**aAD-Control**	**-3.62**	**0.001**
	naAD-Control	**-3.52**	**0.001**
	naAD-aAD	1.13	0.306
Left PHG parahippocampal gyrus	**aAD-Control**	**-3.51**	**0.001**
	naAD-Control	**-4.33**	**0.000**
	naAD-aAD	0.40	0.701

Table 5: Post-hoc contrasts of longitudinal change in medial temporal lobe regions after combining lvPPA, PCA, and fvAD patients into a single non-amnestic AD (naAD) group.

4.2 Accessory voxelwise analysis

Accessory voxelwise analysis was performed to identify areas of early atrophy and later spread that were not captured by a priori ROIs. As in ROI analysis (Table 4), areas were categorized by whether they exhibited significant atrophy at patients' first MRI and whether they exhibited significant longitudinal change during the follow-up period relative to controls. As mentioned above, the hippocampi were excluded from voxelwise analysis due to the difficulty of reliably segmenting and estimating cortical thickness for this structure (Han et al., 2006; Gronenschild et al., 2012; Schwarz et al., 2016).

Voxelwise cortical thickness differences at initial MRI

Whole-brain atrophy patterns at initial MRI corroborated ROI-based analyses and indicated areas of earlier neurodegeneration that fell outside of a priori ROIs. At initial MRI, the lvPPA group exhibited lower cortical thickness vs. controls in left middle and superior temporal gyri, our hypothesized disease focus for lvPPA, corroborating ROI volume analysis (Figure 10A). In addition to these regions, lvPPA patients exihibited early atrophy in multiple left-hemisphere temporal, parietal, and frontal areas including central and parietal opercula; planum temporale; planum polare; and inferior temporal, fusiform, supramarginal, angular, inferior occipital, and middle occipital gyri (Fig. 10). In prefrontal cortex, lvPPA patients had cortical thinning in left anterior insula and frontal operculum as well as bilateral middle and superior frontal gyri. Moreover, nearly all of these areas continued to exhibit longitudinal change during the follow-up period (Figure 10, green areas). Voxelwise analysis of the PCA group not only demonstrated expected atrophy in right parietal, occipital, and posterior temporal areas, but also in their left-hemisphere homologues (Figure 10B). Additionally, PCA patients' baseline atrophy extended into right precentral, middle frontal, and superior frontal gyri. Among these areas, the

bilateral precuneus/posterior cingulate gyrus and middle temporal gyrus continued to demonstrate change during the follow-up period. Overall, baseline results thus indicated that despite some right lateralization of disease, PCA patients in the current sample had bilateral cortical involvement consistent with recent consensus criteria for PCA

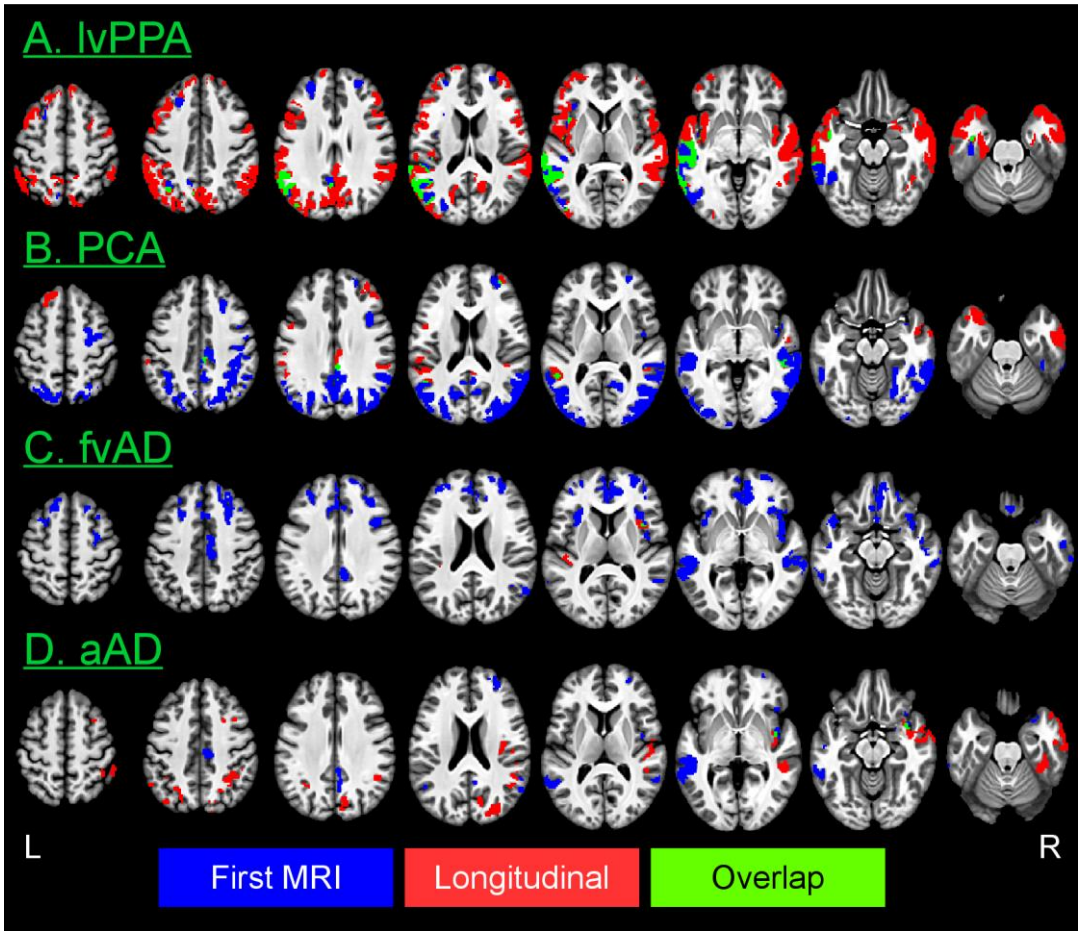

Figure 10: Voxelwise differences in cortical thickness relative to matched controls. Image overlays are binarized t-statistic maps for simple contrasts of controls minus each patient group. Blue: simple effect of group (patients<controls) from cross-sectional analysis of participants' initial MRI scans; red: group x time interaction from longitudinal LME models, indicating where patients have more rapid cortical thinning than controls; green: overlap between group and group x time effects. All results were calculated from linear mixed effects (LME) models and thresholded at voxelwise $p<0.001$ with a minimum cluster volume of 600, corresponding to a corrected cluster-wise threshold of $p<0.05$.

(Crutch et al., 2017). As in ROI-based analysis, fvAD patients exhibited initial atrophy relative to controls in left anterior insula and middle frontal gyrus, right angular gyrus, and bilateral middle temporal gyri. However, areas of early atrophy extended far beyond these regions to include right insula and middle frontal gyrus as well as bilateral medial and ventral prefrontal cortex, inferior and superior frontal gyri, temporal poles, and opercular cortex (Figure 10C). The fvAD group also had initial atrophy relative to controls in the anterior and dorsal portion of right entorhinal cortex, a finding that was not captured by ROI-based analysis. In apparent contrast to the findings of Ossenkoppele and colleagues (Ossenkoppele et al., 2015b), posterior atrophy was limited, most notably including the right precuneus. Among areas of initial atrophy in fvAD, only right anterior insula and bilateral central opercula displayed significant cortical thinning over the follow-up period. The aAD group exhibited expected atrophy in right entorhinal cortex as well as bilateral middle and superior temporal gyri, partially replicating ROI-based findings (Figure 10D). Outside *a priori* ROIs, aAD patients also exhibited early atrophy in bilateral parietal areas including the precunei and middle cingulate, posterior cingulate, angular, and supramarginal gyri; right insula; and right frontal lobe areas including anterior orbital, middle frontal, superior frontal, and medial precentral gyri. Of these areas, only the right insula demonstrated continued atrophy throughout the follow-up period. Figure 11 presents contrasts between patient groups of initial cortical thickness. Consistent with expectations from our cross-sectional analysis and previous studies from other authors, these results indicate left lateralized atrophy in lvPPA (Figure 11A); parietal and occipitotemporal disease in PCA that exhibits some right-hemisphere bias (Figures 11B, D, and F), and greater frontal lobe involvement in fvAD than in other phenotypes (Figures 11C, E, and F). Collectively, these results replicate initial volume differences from ROI-based analysis and highlight additional phenotype-specific areas of atrophy reported in prior studies of lvPPA (Rogalski *et al.*, 2016), PCA (Lehmann *et al.*, 2012), and fvAD (Whitwell *et al.*, 2011).

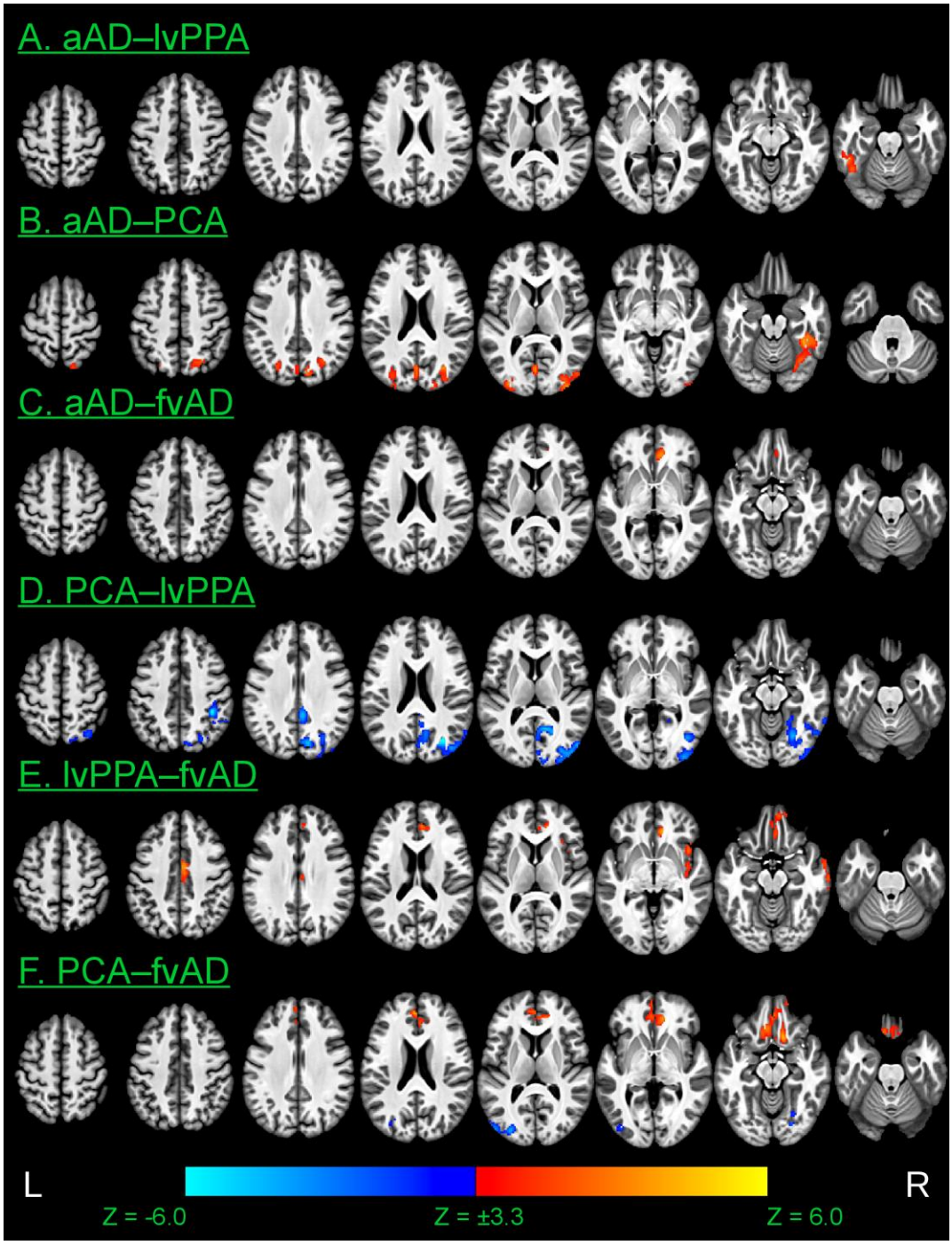

Figure 11: Voxelwise differences between patient groups in cortical thickness at time of initial MRI scan. Results are thresholded at voxelwise $p<0.001$ with a minimum cluster volume of 584, corresponding to a corrected cluster-wise threshold of $p<0.05$. Warm colors indicate thinner cortical grey matter in the second group than the first; cool colors indicate thinner cortical grey matter in the first group than the second.

Voxelwise analysis of longitudinal disease spread

Longitudinal whole-brain analysis also allowed us to identify brain areas that were not significantly atrophied at baseline but demonstrated progressive atrophy over the follow-up period. As in ROI-based analysis, we interpret these effects to indicate the spread of disease to brain areas that were relatively spared in early disease stages. The lvPPA group showed extensive new atrophy in right temporoparietal areas and throughout bilateral prefrontal, medial parietal, and anterior temporal cortex (Figure 10A, red regions), suggesting spread of disease to these areas following patients' initial scans. In PCA, progressive atrophy was observed in several areas unaffected at initial MRI, including the temporal poles, bilateral superior frontal gyri, and bilateral perisylvian cortex (Figure 10B). In contrast to lvPPA and PCA patients, areas of newer atrophy progression were sparse among fvAD patients, limited to portions of right anterior insula as well as left opercular and perisylvian cortex (Figure 10C). Because the small sample size of this group might have limited statistical sensitivity, we also present voxelwise contrasts vs. controls at a liberal statistical threshold of $p<0.01$, without cluster-wise correction for multiple comparisons (Figure 12). While these results must be interpreted with caution due to the potential for false positive results, they suggest more extensive disease spread to left posterior insula, left dorsolateral prefrontal cortex, and bilateral anterior prefrontal areas. Finally, aAD patients showed new longitudinal change during the follow-up period in bilateral parietal cortex as well as right posterior temporal, anterior temporal, opercular, and prefrontal areas (Figure 10D).

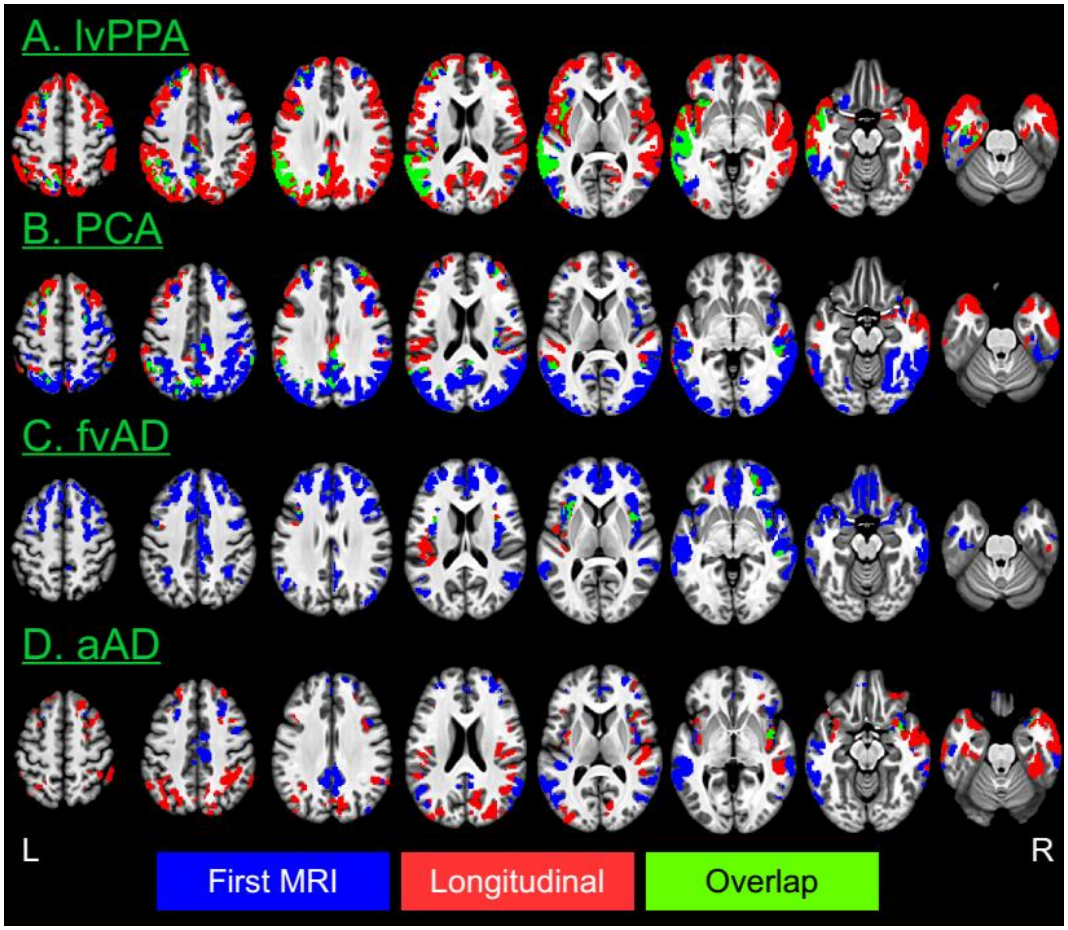

Figure 12: Voxelwise differences in cortical thickness relative to matched controls at a threshold of $p<0.01$, uncorrected for multiple comparisons. Results are for the same contrasts as shown in Figure 10. Image overlays are binarized t-statistic maps for simple contrasts of controls minus each patient group. Blue: simple effect of group (patients<controls) from cross-sectional analysis of participants' initial MRI scans; red: group x time interaction from longitudinal LME models, indicating where patients have more rapid cortical thinning than controls; green: overlap between group and group x time effects. All results are displayed with a minimum cluster volume of 600 μl.

Voxelwise differences in regional rates of change

As in ROI-based analysis, we assessed group differences in the regional pace of cortical thinning over time. Consistent with ROI-based analysis (Figure 2), lvPPA patients had significantly more rapid atrophy than aAD patients in left anterior and posterior superior/middle temporal gyri (Figure 13A). Additionally, aAD patients exhibited faster atrophy progression than fvAD patients in right middle

occipital gyrus and superior parietal lobule (Figure 13B), consistent with parietal differences observed between these groups in ROI-based analysis. Similarly, lvPPA patients exhibited more rapid atrophy than fvAD patients in left precuneus and bilateral middle occipital gyri (Figure 13C). These results corroborate ROI-based findings that suggest neocortical rates of atrophy may vary by region according to patient phenotype.

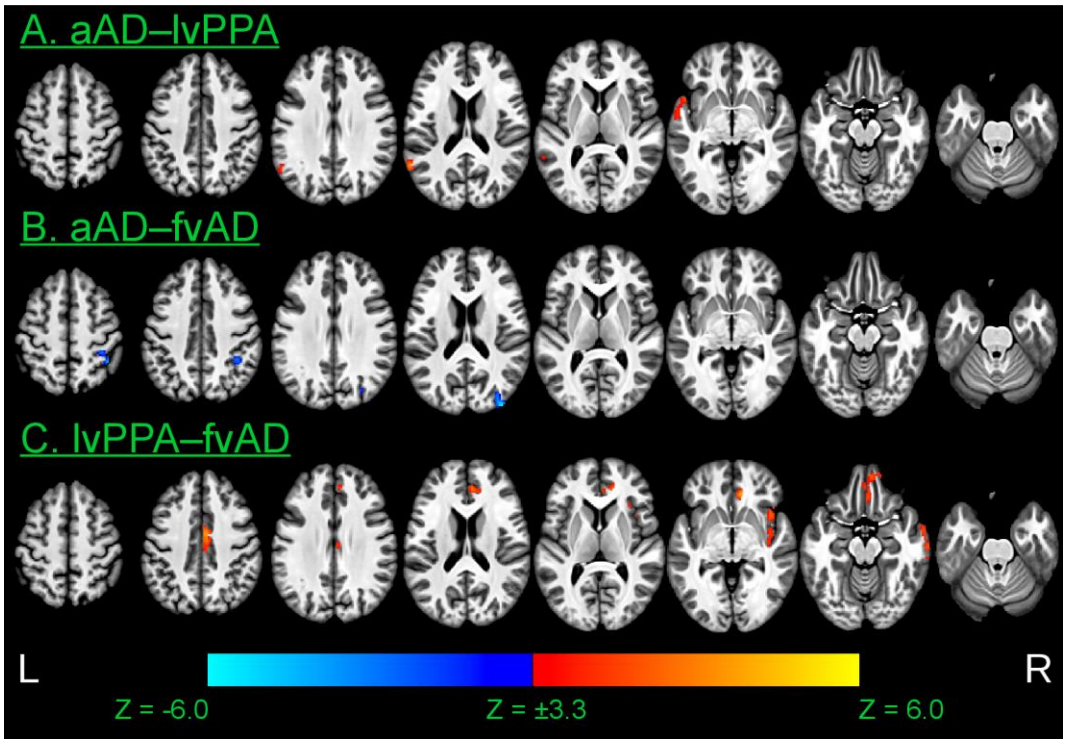

Figure 13: Voxelwise differences between patient groups in rates of cortical thinning over time. Image overlays are t-statistic maps for the interaction of each group with time, calculated from linear mixed effects (LME) models and thresholded at voxelwise $p<0.001$ with a minimum cluster volume of 600, corresponding to a corrected cluster-wise threshold of $p<0.05$. Warm colors indicate that cortical thinning over time is more rapid in the second group than the first; cool colors indicate that cortical thinning is more rapid in the first group than the second. No differences in rates of cortical thinning were observed between aAD and PCA patients or between lvPPA and PCA patients.

Degree of structural connectivity predicts longitudinal atrophy

Nodes in the AAL region graph had a median degree of 20 (interquartile range=17–27). Nodes in the top quartile corresponded to several *a priori* ROIs, including bilateral superior parietal lobules; bilateral inferior, middle, and superior temporal gyri; and right angular gyrus. Degree values for left and right hippocampus labels (which encompassed proximal MTL structures) were 18 and 17, respectively; left insula, 23; left middle frontal gyrus, 22; right supramarginal gyrus, 21; right precuneus, 23; and left and right precentral gyri, 22 and 19, respectively. Node degree was positively associated with regions' average volume among controls (Pearson's $R=0.42$, $p<0.001$); to account for this potential confound, average control volume for each region was included as a covariate. Linear mixed effects modeling showed that higher node degree predicted greater annualized GM volume loss in each patient group (Figure 14), as evidenced by group x degree interaction terms: for lvPPA, $\beta=-0.0090$, $t(6265)=-5.7$, $p<0.001$; for PCA, $\beta=-0.0074$, $t(6265)=-4.0$, $p<0.001$; for fvAD, $\beta=-0.0056$, $t(6265)=-2.5$, $p<0.02$; and for aAD, $\beta=-0.0097$, $t(6265)=-5.3$, $p<0.001$. The main effect of degree was marginally significant [$\beta=-0.0019$, $t(6265)=1.9$, $p>0.07$], reflecting the lack of substantial GM volume loss in the control group (Figure 14). Among covariates, volume at participants' first MRI was significantly associated with annualized change [$\beta=-0.016$, $t(6265)=-4.2$, $p<0.001$], as was average control volume [$\beta=-17.9$, $t(6265)=-11.1$, $p<0.001$]. Simple effects of group were non-significant, as were age and sex (all $p>0.17$); pairwise post-hoc contrasts of group and group x degree interaction terms were also non-significant (all $z<1.7$, $p>0.1$). Importantly, these associations were based on GM volumes estimated for AAL labels and are thus unaffected by differences in the AAL and Mindboggle parcellation schemes.

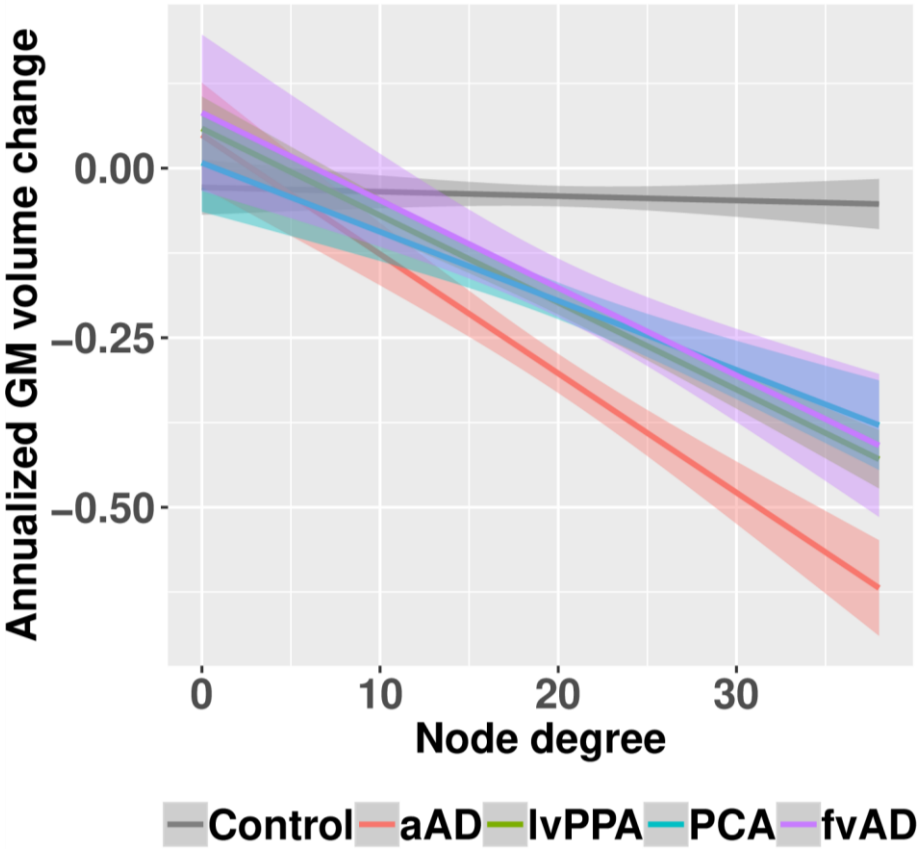

Figure 14: Node degree predicts annualized grey matter volume decline among study participants in regions defined by the Automated Anatomical Labeling (AAL) atlas. Node degree is based on structural connectivity measures computed by Yeh et al. (2018) and reflects the number of white matter connections that each AAL region has with other regions. Shaded areas show the pointwise 95% confidence interval for each regression line.

Effects of global cognition and age

Initial MMSE score (which was included as a measure of global cognitive impairment) was positively associated with GM volume in the majority of ROIs [all $t(103)>=2.3$, $p<0.03$], with the exception of bilateral hippocampi and parahippocampal gyri [all $t(103)<1.0$, $p>0.3$]. In contrast, age at initial MRI was inversely associated with volume in all 6 MTL regions investigated, including left and right hippocampus [$t(103)=-2.5$, $p<0.02$ and $t(103)=-3.2$, $p<0.02$, respectively, after FDR correction], left and right parahippocampal gyri [$t(103)=-3.7$, $p<0.001$ and $t(103)=-4.9$, $p<0.001$], and left and right entorhinal cortex [$t(103)=-3.2$, $p<0.002$ and $t(103)=-3.8$, $p<0.001$]. In addition, age effects were observed in bilateral

precentral gyri [both t(103)<-2.9, p<0.01], suggesting age-related atrophy in motor cortex. No other ROIs displayed an effect of age. To determine whether this age effect differed by group, we performed secondary analyses on MTL volumes at the time of first scan using multiple regression models with predictors of group, age, and their interaction, covarying for MMSE score and the interval between MMSE and MRI. After FDR correction, no MTL regions showed a significant group x age interaction [all F(4,99)<2.3, p>0.2], suggesting that the association of increased age with MTL atrophy was similar across groups. Age and MMSE effects for the accessory voxelwise analysis are shown in Figure 15. Consistent with ROI-based results, voxelwise associations with baseline MMSE score were distributed throughout all lobes of the brain (Figure 15, bottom). Voxelwise analysis further showed robust age effects in the MTL as well as the precentral gyri, anterior temporal lobes, and ventral prefrontal cortex. Conversely, age was positively associated with cortical thickness in the precuneus, which exhibits greater atrophy in earlier-onset than later-onset Alzheimer's disease (Möller *et al.*, 2013). No significant effects of sex were observed in either ROI-based or voxelwise analysis.

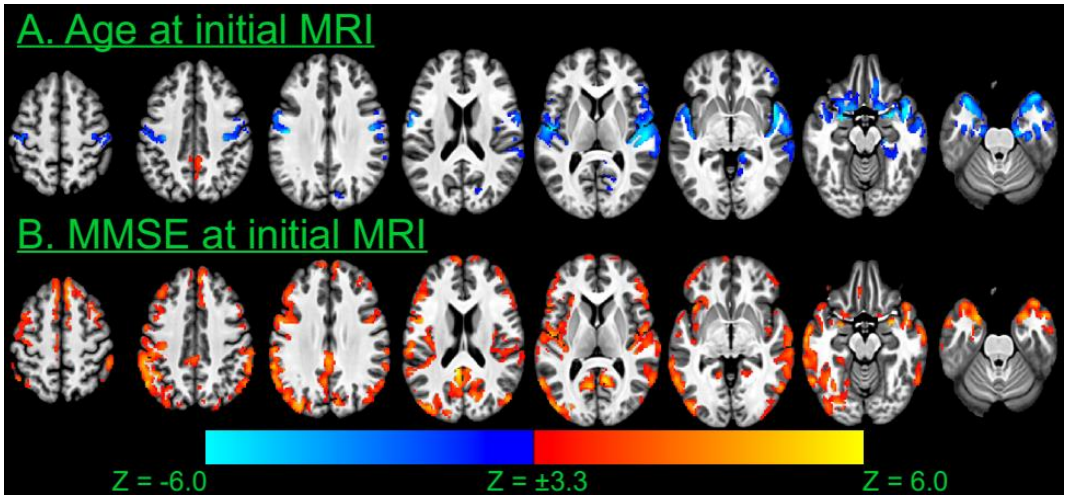

Figure 15. Voxelwise associations of cortical thickness with age and MMSE score at initial MRI. Image overlays are t-statistic maps from linear mixed effects (LME) models, thresholded at voxelwise p<0.001 with a minimum cluster volume of 600 μl, corresponding to a corrected cluster-wise threshold of p<0.05. Warm colors indicate that

cortical thickness over time is positively associated with each variable; cool colors indicate inverse associations

Effects of APOE genotype

We additionally assessed the distribution of APOE genotypes among aAD and naAD patients. Genotyping data were unavailable for one lvPPA, one PCA, one fvAD, and two aAD patients. One aAD, three PCA, and three fvAD patients each carried one copy of the ε2 allele, which is associated with lower risk for Alzheimer's disease (Corder *et al.*, 1994). The proportions of lvPPA, PCA, fvAD, and aAD patients carrying 1–2 copies of the APOE ε4 allele were 29.2%, 36.8%, 63.6%, and 73.3%, respectively. The frequency of individuals carrying zero, one, or two copies of the ε4 allele significantly differed across patient groups [χ^2 (6)=14.9, p<0.02]. In post-hoc comparisons, these frequencies differed between the lvPPA and PCA groups [χ2 (1)=8.3, p<0.02] and between the PCA and fvAD groups [χ2 (1)=6.1, p<0.05]. Because APOE genotypes were unavailable for control participants, we recomputed LMEs for *a priori* ROIs using lvPPA (the largest group) as the reference group and number of ε4 alleles as a covariate. No ROIs exhibited an association with number of ε4 alleles independent of group (all p>0.2).

Longitudinal associations between neuropsychological performance and grey matter volume

Associations between longitudinal neuropsychological performance and concurrent GM volume loss were evaluated in patients that had two or more assessments, each within one year of a structural MRI scan. This longitudinal analysis contrasts with previous studies that have inferred associations by correlating brain imaging data from a single timepoint with cognitive change. For recognition memory, this yielded 121 observations from 51 patients, including 21 lvPPA, 13 PCA, eight aAD, and nine fvAD patients. For letter fluency, 129 observations were available from 20 lvPPA, 14 PCA, 12 aAD, and

nine fvAD patients. For forward and reverse digit span, 117 observations were available from 21 lvPPA, 13 PCA, eight aAD, and eight fvAD patients. A total of 90 PBAC observations, from which all other test measures were obtained, were available for 17 lvPPA, 11 PCA, seven aAD, and seven fvAD patients. In all cognitive domains except for social behavior, longitudinal cognition was directly associated with GM volume change in one or more associated brain areas, independent of volume at the time of initial MRI (Table 6). In the memory domain, volume loss in bilateral hippocampi and left entorhinal predicted declines in recognition discrimination. In the language domain, volume loss in left middle and superior temporal gyri was associated with decreases in letter fluency and forward digit span. In the visuospatial domain, Rey figure copy performance over time was associated with volume loss in right angular, middle temporal, and supramarginal gyrus as well as right precuneus. Judgment of line orientations was likewise associated with right precuneus volume change. No significant associations were found for social behavior; however, left middle frontal gyrus, left anterior insula, and right middle temporal gyrus predicted reverse digit span, a measure of working memory and executive function (Kramer *et al.*, 2003).

Task	Region	T	P
Recognition memory	**L entorhinal**	**t(69)=2.7**	**0.02**
	L hippocampus	**t(69)=4.8**	**0.0003**
	L parahippocampal	t(69)=2.0	0.08
	R entorhinal	t(69)=1.9	0.2
	R hippocampus	**t(69)=3.3**	**0.006**
	R parahippocampal	t(69)=1.3	0.3
Speech	L middle temporal	t(46)=1.0	0.5
	L superior temporal	t(46)=1.2	0.4
Letter fluency	**L middle temporal**	**t(73)=3.7**	**0.003**
	L superior temporal	**t(73)=3.2**	**0.007**
Forward digit span	**L middle temporal**	**t(66)=4.3**	**0.0007**
	L superior temporal	**t(66)=5.1**	**0.0002**
Rey copy	**R angular**	**t(40)=3.5**	**0.005**
	R middle temporal	t(40)=3.5	0.005
	R precuneus	**t(40)=3.6**	**0.005**
	R superior parietal lobule	t(40)=2.3	0.06
	R supramarginal	**t(40)=3.4**	**0.006**
Judgment of line orientation	R angular	t(37)=1.6	0.2
	R middle temporal	t(37)=2.1	0.07
	R precuneus	**t(37)=2.6**	**0.03**
	R superior parietal lobule	t(37)=2.1	0.07
	R supramarginal	t(37)=2.1	0.08
Social behavior	L anterior insula	t(44)=1.2	0.4
	L middle frontal	t(44)=-0.4	0.8
	R middle temporal	t(44)=0.4	0.8
Oral Trails	L anterior insula	t(18)=-0.3	0.8
	L middle frontal	t(18)=1.0	0.5
	R middle temporal	t(18)=1.0	0.4
Reverse digit span	**L anterior insula**	**t(65)=2.5**	**0.04**
	L middle frontal	**t(65)=2.9**	**0.02**
	R middle temporal	**t(65)=3.0**	**0.02**

Table 6. Associations between neuropsychological performance and grey matter volume change in task-specific ROIs. P-values are corrected for multiple comparisons using the false discovery rate method; values<0.05 are considered statistically significant and shown in bold.

Chapter 5

DISCUSSION

5.1 A multimodal study of atrophy onset and progression over time in naAD phenotypes

The cross-sectional analysis initially performed represented a completely novel approach to study atrophy onset and progression in several Alzheimer's disease phenotypes, with particular regard to naAD; atrophy onset and spread in aAD is in fact well known since the study of Braak and Braak (1991), but considering it was necessary to interpretate naAD variants results. Pathological staging studies like the overmentioned from Braak and Braak, which have inferred disease progression over time based on post-mortem pathology, actually inspired our approach for the phasing analysis. This model had strong validations, through the association of ROI phases with neuropathological data, and of MRI phases with clinical data, so we considered it a solid basis for further investigations. In particular, we decided to perform a longitudinal analysis through the direct observation of within-patient effects of earlier versus later disease progression comparing different naAD phenotypes (as well as aAD), which also represents a novelty. Few studies to date have in fact addressed the longitudinal spread of disease in naAD; previous longitudinal imaging studies of non-amnestic Alzheimer's disease have focused on single variants such as lvPPA (Rogalski et al., 2011; Rohrer et al., 2013) and PCA (Lehmann et al., 2012). We differentiated earlier and later disease stages through a two-part approach. Region of interest-based analysis was designed starting from the most likely sites of disease onset for each naAD phenotype highlighted through the cross-sectional study, although we had to exclude CBS syndrome for insufficient longitudinal data, while for the aAD variant we decided to consider the whole MTL as likely area of onset. A second, accessory analysis of whole-brain cortical thickness values allowed us to examine disease spread outside this cluster of a priori ROIs. In each phenotype, we observed a combination of local spread surrounding areas of early atrophy and distal spread to brain areas that were not significantly atrophied at the beginning of the follow-up period. Both patterns of initial atrophy and subsequent progression differed between phenotypes. Further, we

found that longitudinal rates of neurodegeneration differed across patient groups in phenotype-specific neocortical disease foci, a result which could at least partially account for each phenotype's characteristic disease distribution. In contrast, we observed no evidence of phenotype-dependent differences in atrophy rates within the MTL, although MTL atrophy appeared to begin later in non-amnestic than in amnestic Alzheimer's disease. Finally, we found that structural connectivity, assessed by node degree, was a significant predictor of grey matter volume loss over time in both amnestic and nonamnestic Alzheimer's disease; this result supports brain connectivity as a general factor mediating atrophy progression in Alzheimer's disease

5.2 Possible sites of early pathology in naAD

The cross-sectional analysis allowed us to narrow the field of brain areas where disease is likely to originate in each non-amnestic Alzheimer's disease variant. In each naAD phenotype, phase 1 regions encompassed unique and canonical areas of degeneration associated with clinical features that distinguish these syndromes, as reported in autopsy studies of patients with each phenotype: left temporal and inferior parietal areas for lvPPA (Gefen et al., 2012; Giannini et al., 2017); right temporoparietal and bilateral occipital regions for PCA (Crutch et al., 2017; Tang Wai et al., 2004); bilateral posterior parietal and left temporal areas for CBS (McMillan et al., 2016); and prefrontal and temporal cortices for fvAD (Blennerhassett et al., 2014; Ossenkoppele et al., 2015b); the significance association between ROI-phases and neuropathological data in naAD was a strong validation of our model, thus we decided to further analyze these regions through cross-sectional contrasts of patients' first MRI scans (with the exception of CBS, as already mentioned). In the cross-sectional analysis we regarded aAD as a reference group to set proper parameters, thus we didn't investigate for associations between its ROI phases and neuropathological data; for this reason

we considered that the whole MTL could likely represent a site of eatly atrophy, with an a-priori approach similar to naAD variants. We consider significant baseline atrophy an expected and necessary marker for identifying potential sites of disease onset, although early atrophy alone is not sufficient to determine these onset sites. A priori ROIs for each naAD phenotype highlighted by the cross-sectional analysis and the MTL in aAD demonstrated significant initial atrophy compared to healthy controls, consistent with hypotheses. However, the lvPPA and PCA groups also exhibited lateralized hippocampal atrophy versus controls at initial MRI; although this atrophy was mild relative to the amnestic Alzheimer's disease group (Fig. 8), we cannot rule out early, lateralized hippocampal disease in these phenotypes. Longitudinal imaging of patients from earlier disease stages (i.e. MCI or even preclinical phases), when atrophy will presumably be more focal than in the current sample, is thus necessary to conclusively determine whether focal neocortical disease precedes, follows, or arises concurrently with MTL disease in these phenotypes. Nevertheless, the current study narrows the field of brain areas where disease is likely to originate in each non-amnestic Alzheimer's disease phenotype, providing a valuable prior constraint on future hypothesis testing. Overall, we propose that the current results are more consistent with the prevailing hypothesis that non-amnestic Alzheimer's disease patients have disease originating in the neocortex, as inferred by cross-sectional or single-group longitudinal imaging studies (Rogalski et al., 2011; Lehmann et al., 2012; Rohrer et al., 2013; Ossenkoppele et al., 2015a; Xia et al., 2017) as well as autopsy studies of hippocampal-sparing Alzheimer's disease (Giannakopoulos et al., 1994; Murray et al., 2011; Ferreira et al., 2017). Phenotypic variability in initial atrophy patterns (Table 4), including sparing of primary motor cortex at the time of initial MRI, supports the regional specificity of atrophy in non-amnestic Alzheimer's disease patients. Interestingly, some areas of initial atrophy continued to change over time, while others did not. From the data at our disposal, we cannot say with certainty what differentiates these regions. One statistical explanation is simply that variability prevented

reliable detection of longitudinal atrophy in some regions and phenotypes. An alternative, biological explanation is that areas that failed to exhibit further change over the follow-up period (Table 4 and Fig. 10) had already undergone massive atrophy by the time of patients' first MRI, reaching a plateau determined by the limited amount of remaining grey matter tissue (Sabuncu et al., 2011; Schuff et al., 2012). The right superior parietal lobule in PCA and left middle frontal gyrus in frontal-variant Alzheimer's disease may exemplify such slowing: in region of interest-based analysis, both regions were severely atrophied at initial MRI and did not significantly progress over time in their respective phenotypes. Further research is needed to determine why the pace of atrophy changes in some areas of early degeneration but not others.

5.3 Comparison of topographical distribution and progression of neocortical atrophy among AD variants

Areas that exhibited longitudinal atrophy in the absence of initial cross-sectional differences provide a window onto disease spread in each phenotype. In region of interest-based analysis, the lvPPA group showed strong left lateralization of atrophy at baseline, both in our cross-sectional and longitudinal analyses, which is also consistent with prior studies (Rogalski et al., 2016). This pattern included left lateral temporal cortex, an area specifically associated with language deficits in lvPPA (GornoTempini et al., 2011). ROI-based longitudinal analysis also indicated early atrophy in left prefrontal cortex, anterior insula, and hippocampus; and right lateral temporal areas. Voxelwise analysis indicated atrophy in left precuneus and right prefrontal cortex as well. Over the follow-up period, we observed new progressive atrophy in brain areas both adjacent to and distal from these areas of initial atrophy. Proximal disease spread was observed throughout the left temporal and parietal lobes as well as bilateral frontal lobes. This proximal atrophy may indicate diffusive spread of pathology through the

extracellular medium or along short-distance axonal connections between neighbouring cells in cortex (Guo and Lee, 2014). However, we also observed progression through parts of bilateral frontal lobes and right temporoparietal cortex distal from foci of initial atrophy (Fig. 10); diffusive spread from adjacent disease areas appears insufficient to account for this progression. Two possible explanations may account for new, distal atrophy progression. First, pathology may have arisen independently in these areas. Second, pathogenic proteins may have been transmitted to these areas via long-distance white matter projections, according to the transmission hypothesis of neurodegenerative disease (Guo and Lee, 2014). It is particularly interesting to consider these two possibilities with respect to cross-sectional reports of right temporal atrophy in lvPPA, which—if observed—tends to be much milder than left temporal atrophy. In such cases, it is tempting to infer that right temporal atrophy results from the spread of disease from left to right hemispheres via callosal projections. However, this apparent 'progression' may result from a subset of patients having bilateral disease. The current study cannot rule out this possibility, as region of interest-based analysis indicated right temporal atrophy that predated lvPPA patients' first MRI (Table 4). Earlier recruitment and longitudinal imaging of patients with language disturbances is thus necessary to conclusively demonstrate interhemispheric disease spread in lvPPA.

The PCA group also exhibited a combination of proximal and distal disease spread. Initial atrophy was observed in bilateral precunei and temporoparietal regions (Fig. 10) as well as right hippocampus (Table 4). These parietal areas, in particular, are important to visuospatial processing (Astafiev et al., 2003; Greenberg et al., 2010; Gmeindl et al., 2016) and are consistent with early disease patterns observed in prior studies of PCA (Tang-Wai et al., 2004; Lehmann et al., 2012). In voxelwise analysis, patients with PCA had newer atrophy extending from areas of early disease into inferior parietal, posterior temporal, and insular/ opercular cortex; they also exhibited spread proximal to areas of prefrontal atrophy observed at baseline. In addition, however, the PCA group exhibited

atrophy progression in the anterior temporal lobes distal from any cluster of existing atrophy (Fig. 10). This finding suggests testable hypotheses regarding the diffusion of disease-causing agents along fibre pathways that terminate in anterior temporal cortex. These pathways include projections from MTL areas as well as more distal connections via the inferior longitudinal fasciculus to striate and prestriate cortex, which may in turn connect with parietal cortex (Nieuwenhuys et al., 2008).

In the frontal-variant Alzheimer's disease group, region of interest-based and voxelwise analysis collectively indicated grey matter volume loss at initial MRI in bilateral prefrontal, temporal, and anterior insular cortex as well as right middle cingulate and angular gyri. The involvement of the insula is particularly interesting given this group's behavioural dysfunction, as anterior insula is crucially implicated in primates' emotion (Phan et al., 2002) as well as in empathy and social life (Singer, 2006). The anterior insula is also implicated in behavioural-variant frontotemporal dementia (bvFTD) (Seeley, 2010), and Ossenkoppele et al. (2015c) found that insula was one of the few regions of atrophy specific to behavioural-variant Alzheimer's disease patients who were initially misdiagnosed as bvFTD. While our findings suggest early involvement of frontal, temporal, and limbic regions, previous studies of frontal- (or behavioural/dysexecutive) variant Alzheimer's disease have shown either predominantly frontal (Blennerhassett et al., 2014) or predominantly temporal (Ossenkoppele et al., 2015a) disease. In region of interest-based analysis, the frontal-variant Alzheimer's disease group demonstrated new atrophy progression only in left perisylvian cortex; voxelwise analysis indicated additional disease progression in bilateral insular/opercular cortex. These findings are located proximally to atrophy clusters observed at first MRI and thus may reflect local, diffusive spread of disease. Although more distal atrophy progression was not observed, we emphasize that null results in this group should be interpreted with extreme caution due to the small sample size; while the reported foci may represent the areas of most robust atrophy in the current

sample, true disease progression may be missed due to type II statistical error and may be more anatomically widespread than reported here.

In the amnestic Alzheimer's disease group, region of interest-based analysis showed new neocortical atrophy in bilateral precentral gyri as well as right temporoparietal cortex (Table 4). Voxelwise analysis similarly indicated neocortical atrophy progression throughout the right temporal lobe as well as in bilateral parietal cortex and right prefrontal cortex. The slight lateralization of disease progression (right hemisphere > left) may be incidental to the current sample, and we do not propose that it is characteristic of amnestic Alzheimer's disease generally. However, the results are broadly consistent with spreading neocortical disease in later Braak stages (Braak and Braak, 1991). Clusters of newer atrophy in right temporal cortex may indicate local, diffusive spread from right angular gyrus, which was atrophied at initial MRI in the amnestic Alzheimer's disease group. However, other areas of new progression observed in the voxelwise analysis (Fig. 10) are distal from sites of early atrophy and may result from either white-matter-mediated disease spread or de novo accumulation of pathology. Notably, structural connectivity data from healthy adults indicates that the superior parietal lobule is connected to the hippocampus and angular gyrus, both of which exhibited baseline atrophy in the amnestic Alzheimer's disease group; newer areas of superior parietal atrophy in amnestic Alzheimer's disease may thus result from disease transmission along white-matter pathways connecting these areas.

5.4 Differences in MTL atrophy between aAD and naAD

We observed in the cross-sectional analysis that the hippocampus was relatively preserved in naAD, especially for earlier phases (1-2), where no naAD group showed significant atrophy; hippocampal atrophy was instead observed in later

phases in the PCA (phase 4) and CBS (phases 3-4) groups. For what concerns atrophy within the parahippocampal gyrus, it did not appear among phases 1-4 in any of the naAD phenotypes.

When analyzing the MTL in the longitudinal study, patients with naAD demonstrated similar findings. In ROI-based analysis, atrophy at initial scan was limited to left hippocampus in lvPPA and right hippocampus in PCA, with no involvement of remaining MTL among all the naAD groups; these patterns of lateralization were consistent with the general hemispheric bias observed in both phenotypes. In turn, patients with aAD demonstrated significant atrophy in bilateral entorhinal cortex and hippocampi at baseline, as expected from Braak staging (Braak and Braak, 1991). Bilateral parahippocampal gyri were not atrophied, but they demonstrated significant change over the follow-up period; this pattern of results is consistent with progression from approximate Braak stages IV–V (Whitwell et al., 2008) among our amnestic Alzheimer's disease sample. Based on well-characterized patterns of disease spread in amnestic Alzheimer's disease, these MTL foci may be the source of disease spread to the neocortex. The hippocampus has well-characterized white matter connections to posterior cortical areas via the posterior cingulate (Nieuwenhuys et al., 2008; Teipel et al., 2010); these pathways thus represent tracts of interest for investigating the spread of pathogenic proteins to the neocortex.

Over the follow-up period, patients with non-amnestic Alzheimer's disease demonstrated significant atrophy progression in the MTL (Table 4); in the frontal-variant Alzheimer's disease group, these changes were limited to bilateral entorhinal cortex, although null findings in other MTL structures may reflect the small size of this group. MTL progression in patients with non-amnestic Alzheimer's disease suggests that sparing of the hippocampus and surrounding MTL is a graded rather than an absolute phenomenon, and that patients with non-amnestic Alzheimer's disease may become increasingly susceptible to hippocampal degeneration at older ages and in more advanced disease. Indeed, age was a strong predictor of MTL atrophy, as evidenced by both region of

interest-based results (see above, 'Effects of global cognition and age') and voxelwise results (Fig. 15). We note that while patients with non-amnestic Alzheimer's disease tend to be younger than typical amnestic Alzheimer's disease patients, the current study controlled for this potential confound both by demographic balancing of groups and by covarying for age in statistical models. Thus, baseline differences between amnestic and non-amnestic Alzheimer's disease patients in grey matter volume within the MTL (Fig. 8) were not attributable to age differences between these patient groups. Seminal studies of hippocampal sparing in Alzheimer's disease (Giannakopoulos et al., 1994; Murray et al., 2011; Whitwell et al., 2012) grouped patients based on post-mortem pathology findings; these studies may not have included patients who initially presented with non-amnestic syndromes but developed hippocampal pathology in later disease.

5.5 Comparison of rates of atrophy progression among AD variants

The design of the current study not only allowed us to investigate differences between phenotypic groups in the topographical distribution of atrophy but also differences in the rate of atrophy progression within each region. We reasoned that each phenotype might exhibit more rapid degeneration within its associated disease foci, reflecting phenotype-specific susceptibility to disease (Bergeron et al., 2016; Mattsson et al., 2016) in that area. Among neocortical areas associated with non-amnestic Alzheimer's disease phenotypes, we found evidence to support this reasoning. Patients with lvPPA demonstrated more rapid atrophy in the left temporal cortex than the PCA group (ROI-based analysis, Fig. 9) and the amnestic Alzheimer's disease group (voxelwise analysis, Fig. 13). Patients with frontal-variant Alzheimer's disease, in turn, had more rapid atrophy in left anterior insula than both PCA and lvPPA patients in region of interest-based

analysis (Fig. 9); and voxelwise analysis indicated additional prefrontal, temporal, and insular differences between frontal-variant Alzheimer's disease and lvPPA (Fig. 13C). Contrary to our initial hypotheses, we saw no difference in MTL atrophy rates between amnestic and non-amnestic Alzheimer's disease patients, even when all three naAD variants were combined to enhance statistical power. Considered together with amnestic Alzheimer's disease patients' significant MTL atrophy at initial MRI, this result suggests that relative MTL sparing in non-amnestic Alzheimer's disease may result from a delayed onset of degeneration in these structures, but that once neurodegeneration has begun, it proceeds at a similar rate as in amnestic Alzheimer's disease. However, we caution that these findings warrant replication in longitudinal studies involving larger sample sizes.

5.6 Associations between longitudinal atrophy and brain connectivity

To investigate the possible role of brain connectivity in mediating disease spread, we related patients' atrophy patterns to population-average structural connectivity, as estimated from Human Connectome Project white-matter imaging data (Yeh et al., 2018). Several a priori regions of interest in the current study corresponded to hubs in Yeh et al.'s structural connectivity matrix, as evidenced by their high node degree. These findings replicate established functional connectivity results that have related the neuroanatomy of Alzheimer's disease to brain network hubs including bilateral middle temporal, inferior parietal, and superior parietal cortex (Buckner et al., 2009; Crossley et al., 2014). Moreover, we found that node degree was a significant predictor of regional grey matter volume loss over time in each of the patient groups. We caution that this result is correlative in nature and does not demonstrate long-distance disease spread along white-matter pathways. Indeed, network

influences on neurodegeneration need not to be limited to physical transport of pathogenic proteins along white-matter tracts; rather, they may reflect effects such as diaschisis (Che´telat, 2018), with disease in one area leading to metabolic and functional disruptions in its network neighbors. Computational analysis of atrophy patterns using network models such as those of Raj and colleagues (2012, 2015), Iturria-Medina et al. (2014), and Hu et al. (2016) offers a more rigorous approach for testing hypotheses regarding disease spread in brain networks. Nevertheless, associations between atrophy and node degree provide supporting evidence for the hypothesis that atrophy progression is mediated by structural connectivity. Importantly, the structural connectivity analysis reported here does not address potential hypotheses regarding connectivity differences in non-amnestic and amnestic Alzheimer's disease. Indeed, initial research on this question suggests that the connectivity of specific brain networks may differ between typical and atypical presentations of Alzheimer's disease (Lehmann et al., 2015; Whitwell et al., 2015). Because the current study relied on population-averaged structural connectivity values, it was limited to showing a general relationship between degree of connectivity and magnitude of longitudinal change; future analysis of patients' specific connectivity patterns remains a high priority.

5.7 Convergence of atrophy in advanced disease

Discrimination analyses in the cross-sectional analysis allowed us to effectively distinguish naAD phenotypes from aAD and from each other. Clinically dissimilar phenotypes, such as fvAD and PCA or lvPPA and PCA, could be effectively distinguished from one another on the basis of atrophy alone, even in advanced disease. We caution that these discrimination analyses were implemented primarily to quantify the similarity of atrophy patterns across phenotypes. Owing to sample size limitations, results could not be validated in

an independent cohort, although such validation is a primary goal for future research. Discrimination for independently acquired scans (e.g., those collected on different scanners or with different MRI protocols) is likely to be lower than that observed in the present study. Even without an independent validation, we found a paticularly interesting result from this analysis when comparing the cumulative binary atrophy maps between earlier (1-2) and later phases (3-4); in fact, the disease progression models in Figure 3 were most distinct in the former rather than the latter (see also Fig. 7), showing that the topographical progression of atrophy became more similar as disease progressed. The same conclusion is evident when considering individual scans instead of models (Fig. 7).

These results were confirmed by the longitudinal study, where a common temporoparietal pattern of atrophy is shown over time among typical and atypical patients with Alzheimer's disease. The spread of disease along white-matter pathways may help explain the reported convergence of atrophy patterns across Alzheimer's disease phenotypes. For example, Ossenkoppele et al. (2015b) proposed that the common temporoparietal atrophy observed among lvPPA, PCA, early-onset Alzheimer's disease, and late-onset Alzheimer's disease patients could result from convergent disease in nodes of the posterior default mode network. In support of the convergence hypothesis, we note that amnestic and non-amnestic Alzheimer's disease variants alike had common early atrophy and subsequent progression in bilateral temporal cortex (Table 4).

In the cross-sectional study, however, we found that simple logistic regression models could effectively discriminate non-amnestic and Alzheimer's disease phenotypes from one another based on atrophy patterns, although those results were not confirmed within an independent validation cohort. Moreover, post-mortem studies of Alzheimer's disease variants show that regional differences in pathology burden persist among Alzheimer's disease variants even until the end of life. One proposal for resolving these apparently conflicting results is the proposal of Warren et al. (2012) that different clinical presentations of Alzheimer's disease involve a common temporal, parietal, and frontal network,

but that genetic variation or other factors cause the nodes of these networks to be differentially engaged across syndromes.

5.7 Conclusions and limitations

Strengths of the current study include novel approaches for cross-sectional and longitudinal comparison of anatomical changes in multiple clinically-defined non-amnestic Alzheimer's disease phenotypes using both a priori region of interest-based and wholebrain voxelwise analyses. The longitudinal study design allowed us to differentiate areas of earlier and later atrophy and to compare these patterns of disease progression across phenotypes. Moreover, we sought to ensure the comparability of the heterogeneous patient groups included here by controlling for demographic and clinical characteristics both during sample selection and in statistical analysis. The relevance of a priori regions of interest is supported by analyses showing that longitudinal anatomical change is associated with concurrent domain-specific cognitive decline.

However, one major limitation was the inability to evaluate non-linear atrophy progression in Alzheimer's disease, within both cross-sectional and longitudinal analyses: prior evidence suggests that an initial acceleration due to spreading cumulative damage is followed by a deceleration due to the reduction of intact tissue (Sabuncu et al., 2011; Schuff et al., 2012). Such non-linearities complicate study design and interpretation in ways that may not be fully addressed by equating patient groups for chronological age and estimated disease duration: for example, in the current study, it is possible that areas of early atrophy in each phenotype (i.e. those exhibiting atrophy at initial MRI) have entered the deceleration phase, while for other phenotypes the same regions may have been imaged during the acceleration phase. Investigating longitudinal change in earlier-stage patients may allow us to observe a more complete trajectory of neurodegeneration, thus future studies should possibly include patients with MCI; moreover, including a minimum of three to four imaging time points may

allow us to discriminate between linear, quadratic, and sigmoid models of neurodegeneration. Another possible limitation in our findings is statistical power, which is likely to have affected voxelwise analysis more severely than region of interestbased analysis due to the much stricter multiple-comparisons correction of the former. Power limitations may thus have resulted in underestimation of disease spread in the relatively small frontal-variant and amnestic Alzheimer's disease groups; we thus emphasize the importance of further longitudinal study, particularly of patients for whom post-mortem pathological diagnoses are available to rule out the possibility of co-morbid FTLD or other pathologies. Relatedly, the PBAC behavioural scale did not demonstrate expected worsening of behavioural symptoms over time in the frontal-variant Alzheimer's disease group; while it is possible that this null result stems from successful treatment of behavioural symptoms through psychiatric medications, future research should strive to include more sensitive measures of behavioural dysfunction. An additional limitation is that patients in the current sample were not selected based on availability of white-matter imaging data, preventing us from performing a structured white matter analysis to support interpretations of disease spread along white matter pathways. This is now an important goal for our future researches, possibly including instruments such as diffusor tensor imaging (DTI) and deterministic tractography. The current study was also not designed to investigate associations with the APOE genotype or other genetic risk modifiers for Alzheimer's disease. We found that APOE ε4 allele counts added little predictive power to our imaging models after accounting for group effects; however, continued study of the APOE genotype and other genetic risk modifiers in non-amnestic Alzheimer's disease remains an important research aim. Finally, future studies should include patients with CBS due to underlying Alzheimer's disease pathology, as we did only relatively to the cross-sectional study; insufficient timepoints per patient prevented us from including this uncommon non-amnestic Alzheimer's disease phenotype in the longitudinal study.

Investigating the neuropathological and clinical heterogeneity of Alzheimer's disease is crucial to understand the mechanisms of its progression. The current study not only corroborated probable areas of early disease for naAD variants, but also showed that each phenotype has a different pattern of atrophy progression across the cortex. Moreover, we report novel evidence that the longitudinal rate of neocortical atrophy varies by region and phenotype in non-amnestic Alzheimer's disease, reflecting phenotype-specific cognitive decline. In contrast, the rate of MTL atrophy in non-amnestic Alzheimer's disease was similar to that found in amnestic Alzheimer's disease, suggesting that early sparing of these structures results from a later onset of MTL atrophy in non-amnestic Alzheimer's disease. Finally, we observed associations between longitudinal atrophy and structural brain connectivity, providing indirect support for models of interregional disease spread in association with white-matter fibre pathways in non-amnestic Alzheimer's disease

.

REFERENCES

Alexopoulos GS, Kiosses DN, Choi SJ, et al. Frontal white matter microstructure and treatment response of late-life depression: a preliminary study. Am J Psychiatry 2002;159:1929–32.

Alladi S, Xuereb J, Bak T, Nestor P, Knibb J, Patterson K, Hodges JR. Focal cortical presentations of Alzheimer's disease. Brain. 2007 Oct;130(Pt 10):2636-45. PubMed PMID: 17898010.

Astafiev SV, Shulman GL, Stanley CM, Snyder AZ, Van Essen DC, Corbetta M. Functional Organization of human intraparietal and frontal cortex for attending, looking, and pointing. J Neurosci 2003; 23: 4689–99.

Attems J. Sporadic cerebral amyloid angiopathy: pathology, clinical implications, and possible pathomechanisms. Acta Neuropathol 2005; 110: 345–59

Avants BB, Libon DJ, Rascovsky K, et al. Sparse canonical correlation analysis relates network-level atrophy to multivariate cognitive measures in a neurodegenerative population. *Neuroimage*. 2014a;84:698–711. doi:10.1016/j.neuroimage.2013.09.048

Avants BB, Tustison NJ, Stauffer M, Song G, Wu B, Gee JC. The Insight ToolKit image registration framework. Front Neuroinform. 2014 Apr 28;8:44. doi: 10.3389/fninf.2014.00044. eCollection 2014b. PubMed PMID: 24817849; PubMed Central PMCID: PMC4009425.

Ayers D, Scerri C. Non-coding RNA influences in dementia. Noncoding RNA Res. 2018 Sep 29;3(4):188-194. doi: 10.1016/j.ncrna.2018.09.002.

Bentley P, Driver J, Dolan RJ. Modulation of fusiform cortex activity by cholinesterase inhibition predicts effects on subsequent memory. Brain. 2009;132:2356–2371.

Bergeron D, Bensaı¨dane R, Laforce R. Untangling Alzheimer's disease clinicoanatomical heterogeneity through selective network vulnerability - an effort to understand a complex disease. Curr Alzheimer Res 2016; 13: 589–96

Bernick C, Cummings J, Raman R, et al. Age and rate of cognitive decline in Alzheimer disease: implications for clinical trials. Arch Neurol 2012; 69:901.

Blennerhassett R, Lillo P, Halliday GM, Hodges JR, Kril JJ. Distribution of pathology in frontal variant Alzheimer's disease. J Alzheimers Dis.2014;39(1):63-70. doi: 10.3233/JAD-131241. PubMed PMID: 24121962.

Blennow K, Zetterberg H. Biomarkers for Alzheimer's disease: current status and prospects for the future. J Intern Med. 2018 Dec;284(6):643-663. doi: 10.1111/joim.12816. Epub 2018 Aug 19.

Bobinski M, et al. The histological validation of post mortem magnetic resonance imaging-determined hippocampal volume in Alzheimer's disease. Neuroscience 2000;95:721–725.

Boccardi V, Comanducci C, Baroni M, Mecocci P. Of Energy and Entropy: The Ineluctable Impact of Aging in Old Age Dementia. Int J Mol Sci. 2017 Dec 9;18(12).

Boeve BF, Lang AE, Litvan I. Corticobasal degeneration and its relationship to progressive supranuclear palsy and frontotemporal dementia. Ann Neurol. 2003; 54(Suppl 5):S15–S19. [PubMed: 12833363]

Boeve BF. Links between frontotemporal lobar degeneration, corticobasal degeneration, progressive supranuclear palsy, and amyotrophic lateral sclerosis. Alzheimer Dis Assoc Disord. 2007; 21(4):S31–S38.

Boeve BF, Maraganore DM, Parisi JE, et al. Pathologic heterogeneity in clinically diagnosed corticobasal degeneration. Neurology. 1999; 53(4):795–800. [PubMed: 10489043]

Borroni B, Premi E, Agosti C, et al. CSF Alzheimer's disease-like pattern in corticobasal syndrome: evidence for a distinct disorder. J Neurol Neurosurg Psychiatry. 2011; 82(8):834–838.

Bouwman FH, et al. CSF biomarkers and medial temporal lobe atrophy predict dementia in mild cognitive impairment. Neurobiol Aging 2007;28:1070–1074

Braak H, Alafuzoff I, Arzberger T, Kretzschmar H, Del Tredici K. Staging of Alzheimer disease-associated neurofibrillary pathology using paraffin sections and immunocytochemistry. Acta Neuropathol. 2006 Oct;112(4):389-404. Epub 2006 Aug 12. PubMed PMID: 16906426; PubMed Central PMCID: PMC3906709.

Braak H, Braak E. Neurofibrillary changes confined to the entorhinal region and an abundance of cortical amyloid in cases of presenile and senile dementia. Acta Neuropathol. 1990;80(5):479-86. PubMed PMID: 2251904.

Braak H, and Braak E. Neuropathological stageing of Alzheimer-related changes. Acta Neuropathol. 1991;82(4):239-59. Review.

Braak H and Braak E. Staging of Alzheimer's disease-related neurofibrillary changes. Neurobiol Aging. 1995 May-Jun;16(3):271-8; discussion 278-84. Review.

Braak H, Braak E. Frequency of stages of Alzheimer-related lesions in different age categories. Neurobiol Aging 1997; 18:351.

Buckner RL, Sepulcre J, Talukdar T, Krienen FM, Liu H, Hedden T, et al. Cortical hubs revealed by intrinsic functional connectivity: mapping, assessment of stability, and relation to Alzheimer's disease. J Neurosci 2009; 29: 1860–73.

Byun MS, Kim SE, Park J, Yi D, Choe YM, Sohn BK, et al. Heterogeneity of regional brain atrophy patterns associated with distinct progression rates in Alzheimer's disease. PLoS One 2015; 10: e0142756

Castellano JM, Kim J, Stewart FR, et al. Human apoE isoforms differentially regulate brain amyloid-β peptide clearance. Sci Transl Med 2011; 3:89ra57.

Chen G, Saad ZS, Britton JC, Pine DS, Cox RW. Linear mixed-effects modeling approach to FMRI group analysis. NeuroImage 2013; 73:176–90.

Che´telat G. Multimodal neuroimaging in Alzheimer's disease: early diagnosis, physiopathological mechanisms, and impact of lifestyle. J Alzheimer's Dis 2018; 64: S199–211.

Corrigan JD, Selassie AW, Orman JA. The epidemiology of traumatic brain injury. J Head Trauma Rehabil 2010; 25: 72–80.

Cox RW, Chen G, Glen DR, Reynolds RC, Taylor PA. FMRI clustering in AFNI: false-positive rates redux. Brain Connect 2017; 7: 152–71

Crossley NA, Mechelli A, Scott J, Carletti F, Fox PT, McGuire P, et al. The hubs of the human connectome are generally implicated in the anatomy of brain disorders. Brain 2014; 137: 2382–95

Crutch SJ, Lehmann M, Schott JM, Rabinovici GD, Rossor MN, Fox NC. Posterior cortical atrophy. Lancet Neurol. 2012 Feb;11(2):170-8. doi: 10.1016/S1474-4422(11)70289-7. Review. PubMed PMID: 22265212; PubMed Central PMCID: PMC3740271.

Crutch SJ, Schott JM, Rabinovici GD, Murray M, Snowden JS, van der Flier WM, Dickerson BC, Vandenberghe R, Ahmed S, Bak TH, Boeve BF, Butler C, Cappa SF, Ceccaldi M, de Souza LC, Dubois B, Felician O, Galasko D, Graff-Radford J, Graff-Radford NR, Hof PR, Krolak-Salmon P, Lehmann M, Magnin E, Mendez MF, Nestor PJ, Onyike CU, Pelak VS, Pijnenburg Y, Primativo S, Rossor MN, Ryan NS, Scheltens P, Shakespeare TJ, Suárez González A, Tang-Wai DF, Yong KXX, Carrillo M, Fox NC; Alzheimer's Association ISTAART Atypical Alzheimer's Disease and Associated Syndromes Professional Interest Area. Consensus classification of posterior cortical atrophy. Alzheimers Dement. 2017 Aug;13(8):870-884. doi: 10.1016/j.jalz.2017.01.014. Epub 2017 Mar 2. PubMed PMID: 28259709; PubMed Central PMCID: PMC5788455.

De Souza LC, Corlier F, Habert MO, et al. Similar amyloid-β burden in posterior cortical atrophy and Alzheimer's disease. Brain 2011; 134: 2036–43

Devi G, Williamson J, Massoud F, Anderson K, Stern Y, Devanand DP, et al. A comparison of family history of psychiatric disorders among patients with early- and late-onset Alzheimer's disease. J Neuropsychiatry Clin Neurosci 2004; 16: 57–62.

Dickerson BC, McGinnis SM, Xia C, Price BH, Atri A, Murray ME, Mendez MF, Wolk DA. Approach to atypical Alzheimer's disease and case studies of the major subtypes. CNS Spectr. 2017 Dec;22(6):439-449. doi: 10.1017/S109285291600047X. Epub 2017 Feb 15.

Dickson DW, Bergeron C, Chin SS, et al. Office of Rare Diseases neuropathologic criteria for corticobasal degeneration. J Neuropathol Exp Neurol. 2002; 61(11):935–946. [PubMed:

12430710]

Duara R., Loewenstein DA, Shen Q, Barker W, Greig M T, Varon D, Dickson DW. Regional patterns of atrophy on MRI in Alzheimer's disease: Neuropsychological features and progression rates in the ADNI cohort. Advances in Alzheimer's Disease 2013; 02(04), 135--147. https://doi.org/10.4236/aad.2013.24019

Dubois B, Feldman HH, Jacova C, Hampel H, Molinuevo JL, Blennow K, et al. Advancing research diagnostic criteria for Alzheimer's disease: the IWG-2 criteria. Lancet Neurol 2014; 13:614–29.

Dubois B. Markers of prodromal Alzheimer's disease in the clinic. Alzheimers Dement 2010; 6 (4 suppl): S86–87 (abstr F2-01-01). DOI:10.1016/j.jalz.2010.05.261

Ferreira D, Verhagen C, Herna´ndez-Cabrera JA, Cavallin L, Guo C-J, Ekman U, et al. Distinct subtypes of Alzheimer's disease based on patterns of brain atrophy: longitudinal trajectories and clinical applications. Sci Rep 2017; 7: 46263

Folstein MF, Folstein SE, McHugh PR. "Mini-mental state". A practical method for grading the cognitive state of patients for the clinician. J Psychiatr Res.1975 Nov;12(3):189-98. PubMed PMID: 1202204.

Forman SD, Cohen JD, Fitzgerald M, Eddy WF, Mintun MA, Noll DC. Improved assessment of significant activation in functional magnetic resonance imaging (fMRI): use of a cluster-size threshold. Magnet Resonan Med 1995; 33: 636–47

Forman MS, Farmer J, Johnson JK, Clark CM, Arnold SE, Coslett HB, et al. Frontotemporal dementia: clinicopathological correlations. Ann Neurol 2006; 59: 952–62

Frisoni GB, Fox NC, Jack CR Jr, Scheltens P, Thompson PM. The clinical use of structural MRI in Alzheimer disease. Nat Rev Neurol. 2010 Feb;6(2):67-77. doi: 10.1038/nrneurol.2009.215.

Galantucci S, Tartaglia MC, Wilson SM, et al. White matter damage in primary progressive aphasias: a diffusion tensor tractography study. Brain. 2011;134(Pt 10):3011–3029. doi:10.1093/brain/awr099

Galton CJ, Patterson K, Xuereb JH, Hodges JR. Atypical and typical presentations of Alzheimer's disease: A clinical neuropsychological, neuroimaging and pathological study of 13 cases. Brain 2000; 123: 484–98.

Gandy S, DeKosky ST. Toward the treatment and prevention of Alzheimer's disease: rational strategies and recent progress. Annu Rev Med 2013; 64:367.

Geda YE, Schneider LS, Gitlin LN, et al. Neuropsychiatric symptoms in Alzheimer's disease: past progress and anticipation of the future. Alzheimers Dement 2013;9(5):602–8.

Gefen T, Gasho K, Rademaker A, Lalehzari M, Weintraub S, Rogalski E, Wieneke C, Bigio E, Geula C, Mesulam MM. Clinically concordant variations of Alzheimer pathology in

aphasic versus amnestic dementia. Brain. 2012 May;135(Pt 5):1554-65. doi: 10.1093/brain/aws076. Epub 2012 Apr 19. PubMed PMID: 22522938; PubMed Central PMCID: PMC3338929.

Giannakopoulos P, Hof PR, Bouras C. Alzheimer's disease with asymmetric atrophy of the cerebral hemispheres: Morphometric analysis of four cases. Acta Neuropathol 1994; 88: 440–7.

Giannini LAA, Irwin DJ, McMillan CT, Ash S, Rascovsky K, Wolk DA, Van Deerlin VM, Lee EB, Trojanowski JQ, Grossman M. Clinical marker for Alzheimer disease pathology in logopenic primary progressive aphasia. Neurology. 2017 Jun 13;88(24):2276-2284. doi: 10.1212/WNL.0000000000004034.

Gilman S, Koller M, Black RS, et al. Clinical effects of Abeta immunization (AN1792) in patients with AD in an interrupted trial. Neurology. 2005;64:1553–1562

Gorno-Tempini ML, Dronkers NF, Rankin KP, et al. Cognition and anatomy in three variants of primary progressive aphasia. Ann.Neurol. 2004; 55(3):335–346. [PubMed: 14991811]

Gorno-Tempini ML, Brambati SM, Ginex V, Ogar J, Dronkers NF, Marcone A, Perani D, Garibotto V, Cappa SF, Miller BL. The logopenic/phonological variant of primary progressive aphasia. Neurology. 2008 Oct 14;71(16):1227-34. doi: 10.1212/01.wnl.0000320506.79811.da. Epub 2008 Jul 16. PubMed PMID: 18633132; PubMed Central PMCID: PMC2676989.

Gorno-Tempini ML, Hillis AE, Weintraub S, Kertesz A, Mendez M, Cappa SF, Ogar JM, Rohrer JD, Black S, Boeve BF, Manes F, Dronkers NF, Vandenberghe R, Rascovsky K, Patterson K, Miller BL, Knopman DS, Hodges JR, Mesulam MM, Grossman M. Classification of primary progressive aphasia and its variants. Neurology. 2011 Mar 15;76(11):1006-14. doi: 10.1212/WNL.0b013e31821103e6. Epub 2011 Feb 16. PubMed PMID: 21325651; PubMed Central PMCID: PMC3059138.

Gmeindl L, Chiu Y-C, Esterman MS, Greenberg AS, Courtney SM, Yantis S. Tracking the will to attend: cortical activity indexes selfgenerated, voluntary shifts of attention. Atten Percept Psychophys 2016; 78: 2176–84.

Gottesman RF, Schneider AL, Zhou Y, et al. Association Between Midlife Vascular Risk Factors and Estimated Brain Amyloid Deposition. JAMA 2017; 317:1443.

Greenberg AS, Esterman M, Wilson D, Serences JT, Yantis S. Control of spatial and feature-based attention in frontoparietal cortex. J Neurosci 2010; 30: 14330–9

Gronenschild EHBM, Habets P, Jacobs HIL, Mengelers R, Rozendaal N, van Os J, et al. The effects of FreeSurfer version, workstation type, and Macintosh operating system version on anatomical volume and cortical thickness measurements. PLos One 2012; 7:e38234

Grossman M, Ash S. Primary Progressive Aphasia: A Review. Neurocase. 2004; 10(1):3–18. [PubMed: 15849155]

Guo JL, Lee VM. Cell-to-cell transmission of pathogenic proteins in neurodegenerative diseases. Nat Med. 2014 Feb;20(2):130-8. doi: 10.1038/nm.3457. Review. PubMed PMID: 24504409; PubMed Central PMCID: PMC4011661.

Han X, Jovicich J, Salat D, van der Kouwe A, Quinn B, Czanner S, et al. Reliability of MRI-derived measurements of human cerebral cortical thickness: the effects of field strength, scanner upgrade and manufacturer. NeuroImage 2006; 32: 180–94

Hassan A, Whitwell JL, Josephs KA. The corticobasal syndrome-Alzheimer's disease conundrum. Expert Rev Neurother. 2011 Nov;11(11):1569-78. doi: 10.1586/ern.11.153. Review. PubMed PMID: 22014136; PubMed Central PMCID:PMC3232678.

Henley D, May P, Dean R, et al. Development of semagacestat (LY450139), a functional γ-secretase inhibitor, for the treatment of Alzheimer's disease. Expert Opin Pharmacother. 2009;10:1657–1664

Herrero-San Martin A, Villarejo-Galende A, Rabano-Gutierrez A, Guerrero-Marquez C, Porta-Etessam J, Bermejo-Pareja F. Frontal-variant of Alzheimer's disease. Two pathologically confirmed cases and a literature review [in Spanish]. Rev Neurol 2013; 57: 542–8.

Howard R, Ballard C, O'Brien J, et al. Guidelines for the management of agitation in dementia. Int J Geriatr Psychiatry 2001;16(7):714–7.

Howard D and Patterson K. Pyramids and Palm Trees: A Test of Semantic Access from Pictures and Words. Bury St. Edmonds, UK: Thames Valley Test Company; 1992.

Hu WT, Rippon GW, Boeve BF, et al. Alzheimer's disease and corticobasal degeneration presenting as corticobasal syndrome. Mov Disord. 2009; 24(9):1375–1379.

Hu C, Hua X, Ying J, Thompson PM, Fakhri GE, Li Q. Localizing sources of brain disease progression with network diffusion model. IEEE J Sel Top Sig Process 2016; 10: 1214–25.

Iba M, Guo JL, McBride JD, et al. Synthetic tau fibrils mediate transmission of neurofibrillary tangles in a transgenic mouse model of Alzheimer's-like tauopathy. J Neurosci 2013; 33:1024.

Irwin DJ, Byrne MD, McMillan CT, Cooper F, Arnold SE, Lee EB, Van Deerlin VM, Xie SX, Lee VM, Grossman M, Trojanowski JQ. Semi-Automated Digital Image Analysis of Pick's Disease and TDP-43 Proteinopathy. J Histochem Cytochem. 2016 Jan;64(1):54-66. doi: 10.1369/0022155415614303. Epub 2015 Nov 4. PubMed PMID: 26538548; PubMed Central PMCID: PMC4810792.

Irwin DJ, Trojanowski JQ, Grossman M. Cerebrospinal fluid biomarkers for differentiation of frontotemporal lobar degeneration from Alzheimer's disease. Front Aging Neurosci. 2013;5. doi:10.3389/fnagi.2013.00006

Irwin DJ, McMillan CT, Toledo JB, Arnold SE, Shaw LM, Wang L-S, et al. Comparison of cerebrospinal fluid levels of tau and Ab 1–42 in Alzheimer disease and frontotemporal degeneration using 2 analytical platforms. Arch Neurol 2012; 69: 1018–25.

Isella V, Villa G, Mapelli C, et al. The neuropsychiatric profile of posterior cortical atrophy. J Geriatr Psychiatry Neurol 2014.

Iturria-Medina Y, Sotero RC, Toussaint PJ, Evans AC, Alzheimer's Disease Neuroimaging Initiative. Epidemic spreading model to characterize misfolded proteins propagation in aging and associated neurodegenerative disorders. PLoS Comput Biol 2014; 10: e1003956

Jack CR Jr, Bennett DA, Blennow K, Carrillo MC, Feldman HH, Frisoni GB, Hampel H, Jagust WJ, Johnson KA, Knopman DS, Petersen RC, Scheltens P, Sperling RA, Dubois B. A/T/N: An unbiased descriptive classification scheme for Alzheimer disease biomarkers. Neurology. 2016 Aug 2;87(5):539-47. doi: 10.1212/WNL.0000000000002923. Epub 2016 Jul 1.

Johnson DK, Barrow W, Anderson R, Harsha A, Honea R, Brooks WM, Burns JM. Diagnostic utility of cerebral white matter integrity in early Alzheimer's disease. Int J Neurosci. 2010 Aug;120(8):544-50. doi:10.3109/00207454.2010.494788.

Johnson JK, Head E, Kim R, Starr A, Cotman CW. Clinical and pathological evidence for a frontal-variant of Alzheimer disease. Arch Neurol 1999; 56: 1233–9

Jones BF, Barnes J, Uylings HB, et al. Differential regional atrophy of the cingulate gyrus in Alzheimer disease: a volumetric MRI study. Cereb Cortex. 2006; 16(12):1701–1708.

Josephs KA, Whitwell JL, Boeve BF, et al. Visual hallucinations in posterior cortical atrophy. Arch Neurol 2006a;63(10):1427–32

Josephs KA, Duffy JR, Strand EA, et al. Clinicopathological and imaging correlates of progressive aphasia and apraxia of speech. Brain. 2006b; 129(Pt 6):1385–1398. [PubMed: 16613895]

Ju YE, Lucey BP, Holtzman DM. Sleep and Alzheimer disease pathology—a bidirectional relationship. Nat Rev Neurol. 2014 Feb;10(2):115-9. doi: 10.1038/nrneurol.2013.269.

Kas A, de Souza LC, Samri D, et al. Neural correlates of cognitive impairment in posterior cortical atrophy. Brain 2011; 134: 1464–78

Kessing LV. Depression and the risk for dementia. Curr Opin Psychiatry 2012; 25(6):457–61.

Klein A, Tourville J. 101 labeled brain images and a consistent human cortical labeling protocol. Frontiers in Brain Imaging Methods. 2012;6:171. dx.doi.org/10.3389/fnins.2012.00171

Knopman DS, DeKosky ST, Cummings JL, et al. Practice parameter: diagnosis of dementia (an evidence-based review). Report of the Quality Standards Subcommittee of the American Academy of Neurology. Neurology 2001; 56:1143.

Koyama M, Yagishita A, Nakata Y, Hayashi M, Bandoh M, Mizutani T. Imaging of corticobasal degeneration syndrome. Neuroradiology. 2007; 49(11):905–912.

Kramer JH, Jurik J, Sha SJ, Rankin KP, Rosen HJ, Johnson JK, et al. Distinctive neuropsychological patterns in frontotemporal dementia, semantic dementia, and Alzheimer disease. Cogn Behav Neurol 2003; 16: 211–8

Laird NM, Ware JH. Random-effects models for longitudinal data. Biometrics. 1982 Dec;38(4):963-74. PubMed PMID: 7168798.

Lewis J, Dickson DW. Propagation of tau pathology: hypotheses, discoveries, and yet unresolved questions from experimental and human brain studies. Acta Neuropathol. 2016 Jan;131(1):27-48. doi: 10.1007/s00401-015-1507-z. Epub 2015 Nov 17. Review. PubMed PMID: 26576562.

Lehmann M, Crutch SJ, Ridgway GR, et al. Cortical thickness and voxel-based morphometry in posterior cortical atrophy and typical Alzheimer's disease. Neurobiol Aging 2011; 32: 1466–76

Lehmann M, Barnes J, Ridgway GR, Ryan NS, Warrington EK, Crutch SJ, et al. Global gray matter changes in posterior cortical atrophy: a serial imaging study. Alzheimer's Dement 2012; 8: 502–12

Lehmann M, Madison C, Ghosh PM, Miller ZA, Greicius MD, Kramer JH, et al. Loss of functional connectivity is greater outside the default mode network in nonfamilial early-onset Alzheimer's disease variants. Neurobiol Aging 2015; 36: 2678–86

Libon DJ, Bondi MW, Price CC, Lamar M, Eppig J, Wambach DM, Nieves C, Delano-Wood L, Giovannetti T, Lippa C, Kabasakalian A, Cosentino S, Swenson R, Penney DL. Verbal serial list learning in mild cognitive impairment: a profile analysis of interference, forgetting, and errors. J Int Neuropsychol Soc. 2011a Sep;17(5):905-14. doi: 10.1017/S1355617711000944. PubMed PMID: 21880171; PubMed Central PMCID: PMC3315271.

Libon DJ, Rascovsky K, Gross RG, White MT, Xie SX, Dreyfuss M, et al. The Philadelphia brief assessment of cognition (PBAC): a validated screening measure for dementia. Clin Neuropsychol 2011b; 25: 1314–30.

Ling H, O'Sullivan SS, Holton JL, et al. Does corticobasal degeneration exist? A clinicopathological re-evaluation. Brain. 2010; 133(Pt 7):2045–2057. Details that the pathological diagnosis associated with CBS are heterogeneous. [PubMed: 20584946]

Logovinsky V, Satlin A, Lai R, Swanson C, Kaplow J, Osswald G, Basun H, Lannfelt L. Safety and tolerability of BAN2401--a clinical study in Alzheimer's disease with a

protofibril selective Aβ antibody. Alzheimers Res Ther. 2016 Apr 6;8(1):14. doi: 10.1186/s13195-016-0181-2.

Markowitsch HJ, Staniloiu A. Amnesic disorders. Lancet 2012; 380:1429.

Massoud F, Léger GC. Pharmacological treatment of Alzheimer disease. Can J Psychiatry. 2011 Oct;56(10):579-88. Review.

Mattsson N, Schott JM, Hardy J, Turner MR, Zetterberg H. Selective vulnerability in neurodegeneration: Insights from clinical variants of Alzheimer's disease. J Neurol Neurosurg Psychiatry 2016; 87: 1000–4

McKhann GM, Knopman DS, Chertkow H, et al. The diagnosis of dementia due to Alzheimer's disease: recommendations from the National Institute on Aging-Alzheimer's Association workgroups on diagnostic guidelines for Alzheimer's disease. Alzheimers Dement 2011; 7:263.

McKhann G, Drachman D, Folstein M, et al. Clinical diagnosis of Alzheimer's disease: report of the NINCDS-ADRDA Work Group under the auspices of Department of Health and Human Services Task Force on Alzheimer's Disease. Neurology 1984; 34:939.

McMillan CT, Irwin DJ, Nasrallah I, Phillips JS, Spindler M, Rascovsky K, et al. Multimodal evaluation demonstrates in vivo 18F-AV-1451 uptake in autopsy-confirmed corticobasal degeneration. Acta Neuropathol 2016; 132: 935–37.

McMonagle P, Deering F, Berliner Y, et al. The cognitive profile of posterior cortical atrophy. Neurology 2006;66(3):331–8.

McShane R, Areosa Sastre A, Minakaran N. Memantine for dementia. Cochrane Database Syst Rev. 2006:CD003154.

Medaglia JD, Huang W, Segarra S, Olm C, Gee J, Grossman M, et al. Brain network efficiency is influenced by the pathologic source of corticobasal syndrome. Neurology 2017; 89: 1373–81.

Medina M, Avila J. The role of extracellular Tau in the spreading of neurofibrillary pathology. Front Cell Neurosci 2014; 8:113.

Mendez MF, Ghajarania M, Perryman KM. Posterior cortical atrophy: clinical characteristics and diff erences compared to Alzheimer's disease. Dement Geriatr Cogn Disord 2002; 14: 33–40

Mesulam MM. Primary progressive aphasia. Ann.Neurol. 2001; 49(4):425–432. [PubMed: 11310619]

Mesulam M, Wicklund A, Johnson N, et al. Alzheimer and frontotemporal pathology in subsets of primary progressive aphasia. Ann.Neurol. 2008; 63(6):709–719. [PubMed: 18412267]

Mesulam M, Wieneke C, Rogalski E, et al. Quantitative template for subtyping primary progressive aphasia. Arch.Neurol. 2009; 66(12):1545–1551. [PubMed: 20008661]

Mesulam MM, Rogalski EJ, Wieneke C, Hurley RS, Geula C, Bigio EH, Thompson CK, Weintraub S. Primary progressive aphasia and the evolving neurology of the language network. Nat Rev Neurol. 2014 Oct;10(10):554-69. doi: 10.1038/nrneurol.2014.159. Epub 2014a Sep 2. Review. PubMed PMID: 25179257; PubMed Central PMCID: PMC4201050.

Mesulam MM, Weintraub S, Rogalski EJ, Wieneke C, Geula C, Bigio EH. Asymmetry and heterogeneity of Alzheimer's and frontotemporal pathology in primary progressive aphasia. Brain. 2014b Apr;137(Pt 4):1176-92. doi: 10.1093/brain/awu024. Epub 2014 Feb 25. PubMed PMID: 24574501; PubMed Central PMCID: PMC3959558.

Mezias C, LoCastro E, Xia C, Raj A. Connectivity, not region-intrinsic properties, predicts regional vulnerability to progressive tau pathology in mouse models of disease. Acta Neuropathol Commun 2017; 5: 61

Migliaccio R, Agosta F, Rascovsky K, et al. Clinical syndromes associated with posterior atrophy: Early age at onset AD spectrum. Neurology. 2009; 73(19):1571–1578.

Migliaccio R, Agosta F, Toba MN, et al. Brain networks in posterior cortical atrophy: a single case tractography study and literature review. Cortex 2011; published online Oct 20, 2011. DOI:10.1016/j. cortex.2011.10.002

Montine TJ, Phelps CH, Beach TG, et al. National Institute on Aging-Alzheimer's Association guidelines for the neuropathologic assessment of Alzheimer's disease: a practical approach. Acta Neuropathol 2012; 123:1.

Möller C, Vrenken H, Jiskoot L, Versteeg A, Barkhof F, Scheltens P, et al. Different patterns of gray matter atrophy in early- and lateonset Alzheimer's disease. Neurobiol Aging 2013; 34: 2014–22.

Morris JC, Blennow K, Froelich L, et al. Harmonized diagnostic criteria for Alzheimer's disease: recommendations. J Intern Med 2014; 275:204.

Munoz DG, Woulfe J, Kertesz A. Argyrophilic thorny astrocyte clusters in association with Alzheimer's disease pathology in possible primary progressive aphasia. Acta Neuropathol 2007; 114: 347–57.

Murray ME, Graff-Radford NR, Ross OA, Petersen RC, Duara R, Dickson DW. Neuropathologically defined subtypes of Alzheimer's disease with distinct clinical characteristics: a retrospective study. The Lancet. Neurology, 2011. 10(9), 785--796. https://doi.org/10.1016/S1474-4422(11)70156-9

Nalivaeva NN, Turner AJ. Targeting amyloid clearance in Alzheimer's disease as a therapeutic strategy. Br J Pharmacol. 2019 Sep;176(18):3447-3463. doi: 10.1111/bph.14593. Epub 2019 Mar 11.

Nieuwenhuys R, Voogd J, Voogd J, van Huijzen C, van Huijzen C. The human central nervous system. 4th edn. Berlin: Springer; 2008.

Nwankwo T, Yoon SS, Burt V, Gu Q. Hypertension among adults in the United States: National Health and Nutrition Examination Survey, 2011-2012. NCHS Data Brief 2013; 133: 1–8.

Ossenkoppele R, Pijnenburg YA, Perry DC, Cohn-Sheehy BI, Scheltens NM, Vogel JW, Kramer JH, van der Vlies AE, La Joie R, Rosen HJ, van der Flier WM, Grinberg LT, Rozemuller AJ, Huang EJ, van Berckel BN, Miller BL, Barkhof F, Jagust WJ, Scheltens P, Seeley WW, Rabinovici GD. The frontal-variant of Alzheimer's disease: clinical, neuroimaging and pathological features. Brain. 2015a Sep;138(Pt 9):2732-49. doi: 10.1093/brain/awv191. Epub 2015 Jul 2.

Ossenkoppele R, Cohn-Sheehy BI, La Joie R, Vogel JW, Möller C, Lehmann M, van Berckel BN, Seeley WW, Pijnenburg YA, Gorno-Tempini ML, Kramer JH, Barkhof F, Rosen HJ, van der Flier WM, Jagust WJ, Miller BL, Scheltens P, Rabinovici GD. Atrophy patterns in early clinical stages across distinct phenotypes of Alzheimer's disease. Hum Brain Mapp. 2015b Nov;36(11):4421-37. doi: 10.1002/hbm.22927. Epub 2015 Aug 11. PubMed PMID: 26260856; PubMed Central PMCID: PMC4692964.

Ossenkoppele R, Pijnenburg YA, Perry DC, Cohn-Sheehy BI, Scheltens NM, Vogel JW, Kramer JH, van der Vlies AE, La Joie R, Rosen HJ, van der Flier WM, Grinberg LT, Rozemuller AJ, Huang EJ, van Berckel BN, Miller BL, Barkhof F, Jagust WJ, Scheltens P, Seeley WW, Rabinovici GD. The behavioural/dysexecutive variant of Alzheimer's disease: clinical, neuroimaging and pathological features. Brain. 2015c Sep;138(Pt 9):2732-49. doi: 10.1093/brain/awv191.

Osterrieth PA. Le test de copie d'une figure complexe; contribution à l'étude de la perception et de la mémoire. Archives de Psychologie 1944.

Ostrowitzki S, Lasser RA, Dorflinger E, Scheltens P, Barkhof F, Nikolcheva T, Ashford E, Retout S, Hofmann C, Delmar P, Klein G, Andjelkovic M, Dubois B, Boada M, Blennow K, Santarelli L, Fontoura P; SCarlet RoAD Investigators. A phase III randomized trial of gantenerumab in prodromal Alzheimer's disease. Alzheimers Res Ther. 2017 Dec 8;9(1):95. doi: 10.1186/s13195-017-0318-y.

Pa J, Boxer A, Chao LL, Gazzaley A, Freeman K, Kramer J, et al. Clinical-neuroimaging characteristics of dysexecutive mild cognitive impairment. Ann Neurol 2009; 65: 414–23

Panza F, Lozupone M, Solfrizzi V, Sardone R, Piccininni C, Dibello V, Stallone R, Giannelli G, Bellomo A, Greco A, Daniele A, Seripa D, Logroscino G, Imbimbo BP. BACE inhibitors in clinical development for the treatment of Alzheimer's disease. Expert Rev Neurother. 2018 Nov;18(11):847-857. doi:10.1080/14737175.2018.1531706. Epub 2018 Oct 24.

Parmera JB, Rodriguez RD, Studart Neto A, Nitrini R, Brucki SMD. Corticobasal syndrome: A diagnostic conundrum. Dement Neuropsychol. 2016;10(4):267–275. doi:10.1590/s1980-5764-2016dn1004003

Peter J, Abdulkadir A, Kaller C, Kümmerer D, Hüll M, Vach W, Klöppel S. Subgroups of Alzheimer's disease: stability of empirical clusters over time. J Alzheimers Dis. 2014;42(2):651-61. doi: 10.3233/JAD-140261.

Petersen RC, Smith GE, Waring SC, et al. Mild cognitive impairment: clinical characterization and outcome. Arch Neurol 1999; 56:303.

Phan KL, Wager T, Taylor SF, Liberzon I. Functional neuroanatomy of emotion: a meta-analysis of emotion activation studies in PET and fMRI. NeuroImage 2002; 16: 331–48.

Poulakis K, Pereira JB, Mecocci P, Vellas B, Tsolaki M, Kloszewska I, et al. Heterogeneous patterns of brain atrophy in Alzheimer's disease. Neurobiol Aging 2018; 65: 98–108.

Rabinovici GD, Rosen HJ, Alkalay A, et al. Amyloid vs FDG-PET in the differential diagnosis of AD and FTLD. Neurology 2011; 77:2034.

Rabinovici GD, Furst AJ, Alkalay A, et al. Increased metabolic vulnerability in early-onset Alzheimer's disease is not related to amyloid burden. Brain. 2010; 133(Pt 2):512–528.

Ramanan S, Bertoux M, Flanagan E, Irish M, Piguet O, Hodges JR, et al. Longitudinal executive function and episodic memory profiles in behavioral-variant frontotemporal dementia and Alzheimer's disease. J Int Neuropsychol Soc 2017; 23: 34–43.

Rascovsky K, Hodges JR, Knopman D, Mendez MF, Kramer JH, Neuhaus J, et al. Sensitivity of revised diagnostic criteria for the behavioural variant of frontotemporal dementia. Brain 2011; 134:2456–477.

Rascovsky K, Salmon DP, Hansen LA, Thal LJ, Galasko D. Disparate letter and semantic category fluency deficits in autopsyconfirmed frontotemporal dementia and Alzheimer's disease. Neuropsychology 2007; 21: 20–30

Raj A, Kuceyeski A, Weiner M. A network diffusion model of disease progression in dementia. Neuron 2012; 73: 1204–15.

Raj A, LoCastro E, Kuceyeski A, Tosun D, Relkin N, Weiner M. Network diffusion model of progression predicts longitudinal patterns of atrophy and metabolism in Alzheimer's disease. Cell Rep 2015; 10: 359–69

Rebeiz JJ, Kolodny EH, Richardson EP Jr. Corticodentatonigral degeneration with neuronal achromasia. Arch Neurol. 1968; 18(1):20–33.

Renner JA, Burns JM, Hou CE, McKeel DW Jr, Storandt M, Morris JC. Progressive posterior cortical dysfunction: a clinicopathologic series. Neurology 2004; 63: 1175–80.

Rey A. Rey-Osterrieth Complex Figure Test. Lutz, FL: Psychological Assessment Resources, 1944.

Rogalski E, Sridhar J, Rader B, Martersteck A, Chen K, Cobia D, et al. Aphasic variant of Alzheimer disease: clinical, anatomic, and genetic features. Neurology 2016; 87: 1337–43.

Rogalski E, Cobia D, Harrison TM, Wieneke C, Weintraub S, Mesulam M-M. Progression of language decline and cortical atrophy in subtypes of primary progressive aphasia. Neurology 2011; 76: 1804–10.

Rohrer JD, Warren JD. Phenomenology and anatomy of abnormal behaviours in primary progressive aphasia. J.Neurol.Sci. 2010; 293(1-2):35–38. [PubMed: 20400120]

Rohrer JD, Caso F, Mahoney C, Henry M, Rosen HJ, Rabinovici G, Rossor MN, Miller B, Warren JD, Fox NC, Ridgway GR, Gorno-Tempini ML. Patterns of longitudinal brain atrophy in the logopenic variant of primary progressive aphasia. Brain Lang. 2013 Nov;127(2):121-6. doi: 10.1016/j.bandl.2012.12.008. Epub 2013 Feb 8. PubMed PMID: 23395096; PubMed Central PMCID: PMC3880853.

Sabuncu MR, Desikan RS, Sepulcre J, Yeo BTT, Liu H, Schmansky NJ, et al. The dynamics of cortical and hippocampal atrophy in Alzheimer disease. Arch Neurol 2011; 68: 1040–8.

Schuff N, Tosun D, Insel PS, Chiang GC, Truran D, Aisen PS, et al. Nonlinear time course of brain volume loss in cognitively normal and impaired elders. Neurobiol Aging 2012; 33: 845–55.

Schwarz CG, Gunter JL, Wiste HJ, Przybelski SA, Weigand SD, Ward CP, et al. A large-scale comparison of cortical thickness and volume methods for measuring Alzheimer's disease severity. NeuroImage Clin 2016; 11: 802–12

Seeley WW. Anterior insula degeneration in frontotemporal dementia. Brain Struct Funct 2010; 214: 465–75.

Selkoe DJ. The molecular pathology of Alzheimer's disease. Neuron. 1991;6:487–498

Sevigny J, Chiao P, Bussière T, Weinreb PH, Williams L, Maier M, Dunstan R, Salloway S, Chen T, Ling Y, O'Gorman J, Qian F, Arastu M, Li M, Chollate S, Brennan MS, Quintero-Monzon O, Scannevin RH, Arnold HM, Engber T, Rhodes K, Ferrero J, Hang Y, Mikulskis A, Grimm J, Hock C, Nitsch RM, Sandrock A. The antibody aducanumab reduces Aβ plaques in Alzheimer's disease. Nature. 2016 Sep 1;537(7618):50-6. doi: 10.1038/nature19323.

Shakespeare TJ, Yong KX, Foxe D, et al. Pronounced impairment of everyday skills and self-care in posterior cortical atrophy. J Alzheimers Dis 2015;43(2): 381–4.

Shaw LM, Vanderstichele H, Knapik-Czajka M, Clark CM, Aisen PS, Petersen RC, et al. Cerebrospinal fluid biomarker signature in Alzheimer's disease neuroimaging initiative subjects. Ann Neurol 2009; 65: 403–13

Shelley BP, Hodges JR, Kipps CM, Xuereb JH, Bak TH. Is the pathology of corticobasal syndrome predictable in life? Mov Disord. 2009; 24(11):1593–1599. Details that the presence of memory impairment suggests CBS-AD.

Singer T. The neuronal basis and ontogeny of empathy and mind reading: review of literature and implications for future research. Neurosci Biobehav Rev 2006; 30: 855–63.

Sjobeck M, Elfgren C, Larsson EM, Brockstedt S, Latt J, Englund E, et al. Alzheimer's disease (AD) and executive dysfunction. A case-control study on the significance of frontal white matter changes detected by diffusion tensor imaging (DTI). Arch Gerontol Geriatr 2010; 50: 260–6.

Sled JG, Zijdenbos AP, Evans AC. A nonparametric method for automatic correction of intensity nonuniformity in MRI data. IEEE Trans Med Imaging. 1998 Feb;17(1):87-97. PubMed PMID: 9617910.

Snowden JS, Stopford CL, Julien CL, et al. Cognitive phenotypes in Alzheimer's disease and genetic risk. Cortex 2007;43:835–45

Sosa-Ortiz AL, Acosta-Castillo I, Prince MJ. Epidemiology of dementias and Alzheimer's disease. Arch Med Res 2012; 43:600.

Spreen O, and Strauss E. A compendium of neuropsychologial tests. In Administration, norms, and commentary. Oxford University Press Oxford; 1998.

Stella F, Radanovic M, Aprahamian I, et al. Neurobiological correlates of apathy in Alzheimer's disease and mild cognitive impairment: a critical review. J Alzheimers Dis 2014;39(3):633–48.

Stokholm J, Vogel A, Gade A, Waldemar G. Heterogeneity in executive impairment in patients with very mild Alzheimer's disease. Dement Geriatr Cogn Disord 2006; 22:54.

Suárez-González, A., Henley, S. M., Walton, J., & Crutch, S. J. Posterior Cortical Atrophy: An Atypical Variant of Alzheimer Disease. Psychiatric Clinics of North America. 2015; 38(2), 211--220. https://doi.org/10.1016/j.psc.2015.01.009

Tang J. Beta-secretase as target for amyloid-reduction therapy. Alzheimers Dement. 2009;5:P74–P74.

Tang-Wai DF, Graff-Radford NR, Boeve BF, et al. Clinical, genetic, and neuropathologic characteristics of posterior cortical atrophy. Neurology 2004;63(7): 1168–74.
Tannenbaum C, Paquette A, Hilmer S, et al. A systematic review of amnestic and non-amnestic mild cognitive impairment induced by anticholinergic, antihistamine, GABAergic and opioid drugs. Drugs Aging 2012; 29:639.

Teipel SJ, Bokde ALW, Meindl T, Amaro E, Soldner J, Reiser MF, et al. White matter microstructure underlying default mode network connectivity in the human brain. NeuroImage 2010; 49: 2021–32.

Toledo JB, Van Deerlin VM, Lee EB, Suh E, Baek Y, Robinson JL, Xie SX, McBride J, Wood EM, Schuck T, Irwin DJ, Gross RG, Hurtig H, McCluskey L, Elman L, Karlawish J, Schellenberg G, Chen-Plotkin A, Wolk D, Grossman M, Arnold SE, Shaw LM, Lee VM, Trojanowski JQ. A platform for discovery: The University of Pennsylvania Integrated

Neurodegenerative Disease Biobank. Alzheimers Dement. 2014 Jul;10(4):477-484.e1. doi: 10.1016/j.jalz.2013.06.003. Epub 2013 Aug 24. PubMed PMID: 23978324; PubMed Central PMCID: PMC3933464.

Tustison NJ, Avants BB. Explicit B-spline regularization in diffeomorphic image registration. Front Neuroinform 2013; 7: 39

Tustison NJ, Avants BB, Cook PA, et al. N4ITK: improved N3 bias correction. *IEEE Trans Med Imaging*. 2010;29(6):1310–1320. doi:10.1109/TMI.2010.2046908

Tustison NJ, Cook PA, Klein A, Song G, Das SR, Duda JT, et al. Large-scale evaluation of ANTs and FreeSurfer cortical thickness measurements. NeuroImage 2014; 99: 166–79

Tzourio-Mazoyer N, Landeau B, Papathanassiou D, Crivello F, Etard O, Delcroix N, et al. Automated anatomical labeling of activations in SPM using a macroscopic anatomical parcellation of the MNI MRI single-subject brain. NeuroImage 2002; 15: 273–89

Van Swieten J, Spillantini MG. Hereditary frontotemporal dementia caused by Tau gene mutations. Brain Pathology. 2007; 17(1):63–73.

Van Vliet D, de Vugt ME, Aalten P, et al. Prevalence of neuropsychiatric symptoms in young-onset compared to late-onset Alzheimer's disease - part 1: findings of the two-year longitudinal NeedYD-study. Dement Geriatr Cogn Disord 2012; 34(5–6):319–27

Vemuri P, et al. MRI and CSF biomarkers in normal, MCI, and AD subjects: predicting future clinical change. Neurology 2009;73:294–301.

Vos SJ, Verhey F, Frölich L, et al. Prevalence and prognosis of Alzheimer's disease at the mild cognitive impairment stage. Brain 2015; 138:1327.

Wang H, Suh JW, Das SR, Pluta J, Craige C, Yushkevich PA. MultiAtlas Segmentation with Joint Label Fusion. IEEE Trans Pattern Anal Mach Intell 2013; 35: 611–23

Warren JD, Fletcher PD, Golden HL. The paradox of syndromic diversity in Alzheimer disease. Nat Rev Neurol 2012; 8: 451–64.

Wechsler D. Wechsler Memory Scale–Revised. San Antonio: The Psychological Corporation; 1987.

Weintraub S, Salmon D, Mercaldo N, Ferris S, Graff-Radford NR, Chui H, Cummings J, DeCarli C, Foster NL, Galasko D, Peskind E, Dietrich W, Beekly DL, Kukull WA, Morris JC. The Alzheimer's Disease Centers' Uniform Data Set (UDS): the neuropsychologic test battery. Alzheimer Dis Assoc Disord. 2009 Apr-Jun;23(2):91-101. doi: 10.1097/WAD.0b013e318191c7dd.

Whitehouse PJ, Price DL, Struble RG, et al. Alzheimer's disease and senile dementia: loss of neurons in the basal forebrain. Science. 1982;215:1237–1239.

Whitwell JL, Jack CR Jr, Boeve BF, et al. Imaging correlates of pathology in corticobasal syndrome. Neurology. 2010; 75(21):1879–1887. Different patholgies associated with CBS show different patterns of atrophy.

Whitwell JL, Josephs KA, Murray ME, Kantarci K, Przybelski SA, Weigand SD, et al. MRI correlates of neurofibrillary tangle pathology at autopsy. Neurology 2008; 71: 743–49.

Whitwell JL, Dickson DW, Murray ME, Weigand SD, Tosakulwong N, Senjem ML, Knopman DS, Boeve BF, Parisi JE, Petersen RC, Jack CR Jr, Josephs KA. Neuroimaging correlates of pathologically defined subtypes of Alzheimer's disease: a case-control study. Lancet Neurol. 2012 Oct;11(10):868-77. doi: 10.1016/S1474-4422(12)70200-4. Epub 2012 Sep 3. PubMed PMID: 22951070; PubMed Central PMCID: PMC3490201.

Wilson SM, Henry ML, Besbris M, et al. Connected speech production in three variants of primary progressive aphasia. Brain. 2010;133(7):2069-2088. doi:10.1093/brain/awq129.

Wolk DA, Dickerson BC, Alzheimer's Disease Neuroimaging I. Apolipoprotein E (APOE) genotype has dissociable effects on memory and attentional-executive network function in Alzheimer's disease. Proc Nat Acad Sci 2010; 107: 10256–61.

Woodward MC, Rowe CC, Jones G, Villemagne VL, Varos TA. Differentiating the frontal presentation of Alzheimer's disease with FDG-PET. J Alzheimer Dis 2014; 44: 233–42.

Ju YE, Lucey BP, Holtzman DM. Sleep and Alzheimer disease pathology--a bidirectional relationship. Nat Rev Neurol 2014; 10:115.

Xia C, Makaretz SJ, Caso C, McGinnis S, Gomperts SN, Sepulcre J, et al. Association of In Vivo [18F]AV-1451 tau pet imaging results with cortical atrophy and symptoms in typical and atypical alzheimer disease. JAMA Neurol 2017; 74: 427–36

Yeh F-C, Panesar S, Fernandes D, Meola A, Yoshino M, FernandezMiranda JC, et al. Population-averaged atlas of the macroscale human structural connectome and its network topology. NeuroImage 2018; 178: 57–68.

Yuan Y, Gu ZX, Wei WS. Fluorodeoxyglucose-positron-emission tomography, single-photon emission tomography, and structural MR imaging for prediction of rapid conversion to Alzheimer disease in patients with mild cognitive impairment: a meta-analysis. Am J Neuroradiol 2009;30:404–410.

Yushkevich PA, Wang H, Pluta J, Das SR, Craige C, Avants BB, Weiner MW, Mueller S. Nearly automatic segmentation of hippocampal subfields in in vivo focal T2-weighted MRI. Neuroimage. 2010 Dec;53(4):1208-24. doi: 10.1016/j.neuroimage.2010.06.040. Epub 2010 Jun 30. PubMed PMID: 20600984; PubMed Central PMCID: PMC2939190.

Zeger SL, Liang KY, Albert PS. Models for longitudinal data: a generalized estimating equation approach. Biometrics. 1988 Dec;44(4):1049-60. Erratum in: Biometrics 1989 Mar;45(1):347. PubMed PMID: 3233245.

Acknowledgements

This work represents the end of a journey, and I'd like to thank all the people who walked with me along this path, even for just some step.

I thank my advisors from Philly, Murray Grossman and Jeffrey Phillips, who welcomed me in the FTD Center and taught me everything I learned during these years. I really hope we can continue to cooperate, you were such good supervisors. I would like to thank also my Italian supervisor, Prof. Carlo Ferrarese, who made it possible for me to live this amazing experience. I would like to aknowlege Prof. Guido Cavaletti and Prof. Valeria Isella as well, for the same reason, and Corey McMillan, the project co-authors, and the research fellows of the laboratory for the valuable feedbacks and shared time: every result described in this thesis was accomplished with their support.

Thank you, Mom, to show me the meaning of strength, everyday; thank you Dad, for being such an inspiring model; thank you Erika, for your constant support. Thanks to all the relatives as well, wherever they are.

How could not thank my second family? They are always with me, with their thoughts during my US internship, sometimes even for real (Matti in particular, rooting Philadelphia Eagles with me)
"...che è una cosa rara, che un oceano ci separa!"

Thank you, Silvia, because you were by my side along all the journey which brought me here and none of the studies of this work would have been possible for me without you... not even the idea of pursuing them.